# SURFACE WAVE PROPAGATION
# IN THE
# WESTERN UNITED STATES

Thesis

by

Shelton S. Alexander

In Partial Fulfillment of the Requirements

For the Degree of

Doctor of Philosophy

California Institute of Technology

Pasadena, California

1963

# ACKNOWLEDGMENTS

The author gratefully acknowledges the guidance and support of Dr. Frank Press throughout this study.

To his colleagues, particularly Dr. Don L. Anderson, Mr. David G. Harkrider, and Mr. Charles B. Archambeau, the author is indebted for many valuable discussions of various aspects of this research.

It is with pleasure that the author acknowledges Dr. John H. Healy of the U.S. Geological Survey (Crustal Studies Branch) for furnishing refraction results and other information in advance of publication.

Mr. Nafi Toksoz was of valuable assistance in the model experiment and Mr. Laszlo Lenches deserves special credit for preparing most of the figures.

This research was partially supported by contracts AF-AFOSR-25-63 and DA-ARO(D)-31-124-G216. During the period of this research the author held the Pan American Petroleum Company Fellowship, the Standard Oil Company of California Fellowship and a Woodrow Wilson Fellowship. The author is most grateful for the support from all these sources.

TABLE OF CONTENTS

PART I

CRUSTAL STRUCTURE IN THE WESTERN UNITED STATES FROM MULTI-MODE SURFACE WAVE DISPERSION



PART II

THE EFFECTS OF THE CONTINENTAL MARGIN IN SOUTHERN CALIFORNIA ON RAYLEIGH WAVE PROPAGATION



APPENDICES

# PART I

# CRUSTAL STRUCTURE IN THE WESTERN UNITED STATES FROM MULTI-MODE SURFACE WAVE DISPERSION

## ABSTRACT

Multi-mode group velocity dispersion of both Rayleigh and Love waves was measured for a number of paths in the Western United States by means of a technique developed for separating the modes. Results for each region studied are interpreted in terms of a crustal structure which produces simultaneous agreement with all the modes observed, as well as available body wave data. Certain diagnostic features of group velocity dispersion curves were noted and used to advantage in this study.

The analysis techniques developed have rather broad geophysical applications, for example in studies of source properties, interference phenomena, and noise properties.

# PART I

# CRUSTAL STRUCTURE IN THE WESTERN UNITED STATES FROM MULTI-MODE SURFACE WAVE DISPERSION

## INTRODUCTION

It is important to realize the contribution surface wave dispersion studies of the type to be presented here can make in determining earth properties. In particular, what can be learned from such dispersion studies that cannot be learned as easily by another technique, such as refraction, and what are the advantages of using surface waves.

Perhaps the most important role of surface waves is in determining the shear velocity distribution, since little body wave data exists for this distribution in the crust and upper mantle. With few exceptions the crustal shear velocity has always been inferred from reflection and refraction data by assuming Poisson's ratio, because direct measurement of shear velocity by these methods has proved difficult in practice. Such body wave models rarely, if ever, have accounted for observed surface wave dispersion. Structures derived from gravity measurements are even less adequate in this regard. These discrepancies are due, among other things, to the existence of Poisson ratios different from those assumed. This means that these techniques alone do not provide a sufficiently complete description of the existing structure, inasmuch as the true structure must produce simultaneous agreement among body wave, gravity, and surface wave results. Surface wave dispersion, which is controlled largely by the

shear velocity structure, provides an independent means of inferring the existing shear velocity distribution; hence the distribution of Poisson's ratio. One of the most important results of this study, therefore, is the determination of the average shear velocity structure for the paths investigated.

The existence of vertical velocity gradients is also difficult to establish by reflection or refraction methods. One can discern such features by use of surface waves, as will be demonstrated later in this discussion.

The presence of masked layers (those which do not produce first arrivals on refraction profiles) can be detected by surface wave analysis. This includes low velocity layers at depth, which are not ever detectable by refraction methods. This use of dispersion is particularly important for depths greater than 20 or 30 kilometers where existing reflection and refraction methods begin to fail.

Surface waves have the simple advantage that they arrive with much greater amplitudes than body waves, both because the dependence of amplitude with distance is different from body waves and because more energy initially is partitioned into surface waves. Hence, surface waves can be detected and accurately measured to relatively large distances, so that even aseismic regions where only small events occur can be investigated. In addition, surface waves represent a sampling of the entire structure rather than just portions having high velocity contrast.

Moreover, whole regions may be investigated very expeditiously and economically with surface waves by only one person with a minimum of a single instrument, whereas body wave surveys require much more gear and manpower. Furthermore, regions that are inaccessible and virtually uninhabitable can readily be investigated, since only measurements exterior to such regions are required.

Aside from deducing earth structure from surface wave dispersion, the dispersion is important in itself in order to provide a description of the transfer function of the earth. Only after accurately correcting for propagational effects can source properties be deduced. Ideally, then, one would like to construct a world wide "map" of the earth's transfer function in as great detail as possible. To this end any data is valuable. The important problem of distinguishing underground nuclear explosions from earthquakes illustrates the need for knowing the transfer function of the earth.

Among the more significant contributions of the present investigation are (1) the first estimate from combined body wave, Love wave, and Rayleigh wave data of the vertical distribution of shear velocity and Poisson's ratio in the crust of the regions studied; (2) establishment of the general character of the important transition zone from crust to upper mantle (25 - 100 km depth) in the Western United States; (3) a comparison of similarities and differences in crustal

structure from one geologic province to another which may provide important clues to the geologic history of the Western United States; (4) the development of a systematic method for delineating normal modes of surface waves; (5) the determination of certain general structural properties which account for salient features of group velocity dispersion curves, and (6) the programming for a digital computer of all the computations required for experimental dispersion measurements, so that comprehensive dispersion studies are now possible with a minimum of tedious hand calculations.

The use of surface wave dispersion to determine crustal structure is now widespread and the basic ideas involved have been published in the literature.

Until recently dispersion over only a limited period range for one or two modes, usually the fundamental mode of Rayleigh waves, could be measured sufficiently well to allow an interpretation in terms of crustal structure. The structures derived from such data are far from unique, and detailed features of the structure are impossible to determine. This is not to say, however, that surface wave dispersion is not a sensitive measure of crustal properties, for its sensitivity can be demonstrated. Two recourses exist for improving the usefulness of surface wave dispersion to discern structural detail. One is to extend the observation range for a single mode to periods long enough so that shallow crustal features have little effect on the dispersion and to periods so short that only the very shallow structure controls their

dispersion. The other is to measure several modes in a restricted period range and take advantage of the different way each mode samples the structure. Ideally one would like to do both.

Therefore, if the fundamental Rayleigh and Love modes and two or three higher modes of each can be measured over a broad period range, a very restrictive structure is required to fit all the data. While this derived structure, too, will not be unique, it should be reasonably close to the true situation, because of the additional constraints imposed by the higher modes and the required fit over a large period range.

In this study an attempt was made to extend the period range of observations and to delineate as many modes as possible. Higher modes have previously been used for studying crustal structure by Oliver, Press, Brune, and others for a few events where it was possible to readily delineate portions of the higher mode dispersion curves by visual methods. For the most part, however, the valuable higher mode information has not been fully used in surface wave studies of crustal structure due to their complicated appearance on the seismograms and the resulting difficulty in making reliable measurements of their dispersion.

A method for systematically delineating the various modes was developed and used to great advantage in this study. The technique involves a combination of group velocity windows and band pass filtering so that a record containing only

energy from an arbitrary region in the group velocity - period plane can be obtained. Each region can be chosen such that it contains only one mode. In effect, then, the technique allows separation of superposed signals so long as no two energy arrivals of the same frequency occur simultaneously.

Several paths in the Western United States were investigated using group velocity dispersion obtained for the fundamental Love and Rayleigh modes with periods extending to 50 seconds and for the first two higher modes in the period range 2 to 15 seconds. Fundamental mode Rayleigh wave phase velocity was also measured over one large net in the southern part of the Basin and Range province.

The path lengths involved are all of the order of 1000 kilometers. Therefore, the assumption must be made that the structure does not have strong lateral variations over these individual paths so that the average structure derived from the observations is representative of the structure over the region traversed. The paths were chosen such that each was confined as nearly as possible to a single structural province, such as the Basin and Range, Sierra Nevadas, or coastal region of California. The refraction data available at various locations along these paths indicate that, in fact, no strong lateral variations in crustal structure exist along the individual paths. However, from region to region the "average" structure is significantly different. Hence, it is considered legitimate to interpret the observed dispersion in

terms of an average structure between the source and stations.

The average structure along each path was obtained by comparing the observed data with theoretical dispersion* for various assumed models of the structure, respecting any available refraction data, and adjusting the elastic parameters of these models until the best over-all fit to the data was achieved.

Regardless of any such structural models deduced to fit the data, however, comparison of the observed data between regions in itself is sufficient to indicate the nature of the differences which exist between the regions.

It was found that one of the most diagnostic features of a group velocity curve is its shape. For example, one can use the shape to deduce the existence of thick uniform layers as well as to ascertain whether any sharp velocity contrasts exist at depth. This is why one should span a large period range whenever possible.

---

*The dispersion programs of Harkrider and Anderson (1962) and Press, Harkrider, and Seafeldt (1961) were used for the theoretical calculations.

METHODS OF ANALYSIS

A glance at the surface wave portion of typical seismograms for continental travel paths, such as those shown in Figures 4 and 5, is sufficient for one to appreciate the difficulty in obtaining reliable group (and phase) velocity dispersion measurements using standard visual techniques, since precise period vs. arrival time curves are required. The problem is that appreciable energy at several different frequencies arrives simultaneously and the resulting seismogram appears very complicated. This is always to be expected where more than one mode is present and when any mode has an inverse branch of group velocity dispersion.

To get an idea of the type of complications to expect when several modes are present, consider Figure 3, which shows typical group velocity dispersion curves for three modes of continental Rayleigh waves. If this were the prevailing dispersion, one would observe within the group velocity window from 3.8 - 3.5 km/sec on the seismogram a long period wave ($M_{11}$) decreasing in period from about 45 seconds to 30 seconds. Riding on this wave would be two shorter period waves, one decreasing in period from about 10 seconds to 9 seconds ($M_{21}$) and one decreasing in period from 7 seconds to 6 seconds ($M_{12}$). Obviously inclusion of more modes and a broader period range would make the seismogram still more complex.

Therefore, one of the first tasks in this study was to devise a method for separating the modes such that the dispersion of each mode could be reliably obtained.

Two workable methods were developed. One is based primarily on the definition of group velocity. The other is based on the fact that individual modes are sufficiently separate in most of the group velocity-period plane that they may be isolated in the time domain. Each mode so isolated may then be analyzed independently, as if only that mode were present.

These methods are discussed in detail in Appendix F. Therefore, only a summary of how they work will be included here.

To make use of either method the seismogram must first be digitized at intervals sufficiently small that the Nyquist frequency ( $\frac{1}{2\Delta t}$ ) is at least as great as the highest frequency visible on the record. Naturally this frequency must also be greater than any frequency of interest in the study.

Then, to apply the first method (Method A) one numerically band-pass filters the digitized seismogram, allowing only a very narrow band of frequencies ($\Delta\omega$) about some center frequency ($\omega_0$) to contribute to the filtered seismogram. This filtering operation is done such that no phase shift is introduced for any frequency (see Appendix G). The group arrival for the frequency $\omega_0$ occurs where the harmonic components about $\omega_0$ add together in phase. Thus, peaks in the envelope of the narrow band-pass filtered seismogram correspond to group arrivals for frequency $\omega_0$. Each of these group arrivals in turn belongs to a particular mode. The bottom trace in Figure 8 illustrates such group arrivals,

corresponding to the modes $M_{21}$, $M_{12}$, and $M_{11}$, for a band-pass centered at a period of about 6 seconds. By repeating this procedure for a succession of center frequencies spanning the period range of interest, the complete set of dispersion curves for all the modes present can be obtained.

It should be noted in passing that this method also permits an estimate of the relative excitation of the various modes with frequency. These relative excitations are strongly controlled by source depth and source type, so that this method may prove very useful for future investigations of source phenomena.

In principle a time record containing only contributions from an arbitrarily chosen region of the group velocity - period (U-T) plane can be obtained using a combination of group velocity windows and numerical band-pass filtering.

To illustrate, consider the region R in the U-T plane shown in the diagram at the right. Approximate this region by N blocks (dashed in the diagram) each of which is specified by a minimum ($T_{i1}$) and maximum period ($T_{i2}$) and a maximum ($U_i$) and minimum ($U_{i+1}$) group velocity. Therefore, if one band-pass filters the seismogram such that for the time interval $\Delta/U_i \leq t \leq \Delta/U_{i+1}$ only periods in the range $T_{i1} \leq T \leq T_{i2}$ can contribute with sizable amplitude, the resultant total record from $\frac{\Delta}{U_1} \leq t \leq \frac{\Delta}{U_N}$

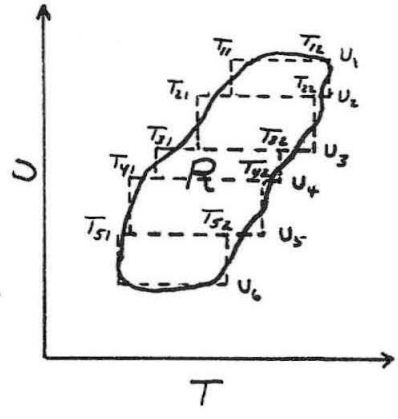

represents the signal from R.

The second method (Method B) is an application of this concept where one chooses R such that each group arrival from R is a single valued function of T. The resulting record, therefore, can be analyzed by simple conventional methods to define whatever dispersion curve(s) lies within R. Examining a number of adjacent or overlapping regions in this fashion allows one to construct the continuous dispersion curve for each mode over a wide period interval. The adjacent shaded and unshaded portions of Figure 2 above 6 seconds period illustrate the simplest types of acceptable regions.

A graphic example of how well this technique works is provided by a comparison of Figure 6, which shows the Benioff 1-90Z seismograms of a Montana aftershock recorded at three stations in Southern California, and Figure 7, which shows these same records after band-pass filtering to obtain the longer period fundamental mode ($M_{11}$).

This technique was so effective that fundamental mode phase velocity measurements could also be made over arrays in Southern California using records as complicated as those shown in Figures 4 and 6.

As another illustration of this method, Figure 8 shows the result of three band passes on the Riverside seismogram shown in Figure 6. Each pass shown permits one to accurately define a portion of the group velocity dispersion curve of one or more modes.

In applying Method B there exists the problem of selecting regions in the U-T plane which contain only a single mode, or at least contain no two modes overlapping in group velocity. As a practical matter, therefore, it is best to use method B only after the approximate location of the modes in the U-T plane is established, since trial and error in choosing the regions is very time consuming. However, the problem is not as acute as it might at first appear, even for the worst situation; namely, when the only data available is the seismogram for an event of known epicentral distance and origin time. It is not so acute, because a rough scanning of the seismogram (in a fashion to be discussed presently) quickly establishes approximately where the energy (hence one or more modes) is located in the U-T plane.

One way to quickly scan the record for this purpose is to successively apply Method A for a set of rather widely spaced center frequencies in the range of interest. Correlating group arrivals from one such pass to the next and interpolating between them outlines the regions of interest.

Another is to compute the Fourier transform for each of several short record segments, defined by narrow group velocity windows in the group velocity interval of interest. Relative maxima in the Fourier spectrum of any such segment will occur for those frequencies whose group arrivals lie within the group velocity window defining that segment. This procedure may be termed the "transform" of Method A, since

it works essentially the same as Method A with the roles of frequency and group velocity interchanged.

As an illustrative example, consider the velocity window 4.3 km/sec to 3.54 km/sec defined by the unshaded portion in Figure 3. If the dispersion shown there prevailed, the Fourier spectrum of the seismogram for that window would exhibit three peaks, one at about 7 seconds period, corresponding to the second higher mode ($M_{12}$), one at about 12 seconds period, corresponding to the first higher mode ($M_{21}$), and another at a period greater than 30 seconds corresponding to the fundamental mode ($M_{11}$). With no prior knowledge whatsoever of the dispersion, these peaks would be sufficient to infer the approximate location of these three modes in the group velocity interval from 4.3 km/sec to 3.54 km/sec. As the velocity window is changed, each of these peaks migrates along a path in the U-T plane which defines the locus of a zone of energy concentration, corresponding to one or more modes.

The results of one of the earliest attempts to use this idea on a seismogram are shown in Figure 9, where the group velocity window extended from approximately 4.4 km/sec to 3.0 km/sec. While this window was much too large to separate the higher modes in detail, the resulting peaks (each labeled with its period in Figure 9) were sufficient to indicate where most of the higher mode energy was located (6-10 seconds period) within this window. The prominent peak at a period of about 27.8 seconds in Figure 9 is due to the

fundamental mode. Therefore, these results provided a sound starting point for the more detailed analysis, as is evident from the location (above 3.0 km/sec) of the precisely determined experimental dispersion shown in Figures 14 and 16.

In addition to the uses of these methods in dispersion and source studies, numerous other important applications exist. For example, in detailed earth noise studies Method A would provide essentially a pointwise (in time) Fourier analysis of the records. The advantages of this are obvious, since the duration of coherent sections of a noise record suitable for correlation over a horizontal or vertical array is usually very short. Two other very important applications of these methods may be made in refraction work. First of all they can be used to pick secondary refracted arrivals, particularly when the predominant frequency for separate refracted arrivals varies. Secondly, the spectrum of amplitude attenuation with distance for each arrival can be obtained, again by using Method A to provide nearly pointwise time domain Fourier analysis. Thus a valuable body of additional information can be obtained routinely for every refraction profile.

These methods, Method B especially, can also be used to advantage in studies of interference phenomena, where it is desirable to decompose records containing beats into simpler wave trains with no beats. These simpler wave trains, taken together, will reproduce the interference phenomena and, taken separately, may provide clues to the physical con-

ditions causing interference.

Actually Method B is applicable to almost any problem requiring separation of superposed wave trains, and Method A is applicable to any problem requiring dynamic Fourier analysis.

Both of the above methods were programmed for the IBM 7090 computer, so that given the origin time, the epicentral distance, and the digitized seismogram, any number of passes with different combinations of velocity windows and band-pass filtering can be made. The filtered seismogram is plotted and the dispersion computed and plotted automatically for each pass on the data. Optionally, the Fourier transform can also be computed and plotted for each pass. Therefore, these techniques may now be used routinely for any of the applications discussed above.

The methods presented here constitute the first systematic means of delineating higher mode dispersion curves on a routine basis.

## EXPERIMENTAL RESULTS AND INTERPRETATION

In this study an attempt was made to define experimentally as many modes of Rayleigh and Love waves as possible over a broad frequency band and to include any available body wave and gravity information, so that the best possible approximation to the existing structure in each region could be obtained. This preferred structure was obtained by adjusting the elastic parameters of assumed structures until the best over-all fit between the theoretical and experimental dispersion was achieved.

It is worthwhile at this point to digress long enough to state why the structure so derived should be a reasonable approximation of the existing structure. Any given structure is sampled in a characteristically different (linearly independent) fashion by each frequency of each mode of Love and Rayleigh waves. For example, Figure 10 illustrates approximately how the structure shown there is sampled by the vertical component of the first three Rayleigh modes at periods of 10.2 seconds and 6.0 seconds.

Therefore, for infinitely precise multi-mode dispersion over an arbitrarily large frequency interval, it follows that one and only one structure can be found which will produce an exact fit to all the data. In practice, however, the accuracy of measurement, the number of modes defined, and the frequency interval are all limited, so one cannot hope to define a completely unique structure.

However, the permissible structures which explain all the observations equally well, can be expected to converge to the true structure as the data become more complete and accurate. The class of structures which simultaneously explains the observed multi-mode Rayleigh and Love wave dispersion, as well as refraction and gravity data, will be far more restrictive than the class which explains the data of a single mode. The existing structure will be between the narrower limits of this more restrictive class.

As the result of investigating many assumed models during the course of this study, it became apparent that salient features in the shape of group velocity curves are diagnostic of certain important properties of the structure.

The existence of an Airy phase (i.e. a stationary value of group velocity) for example, indicates that a section of relatively uniform velocity exists at depth. The separation in frequency (wave length) between adjacent Airy phases is a measure of the thickness of such a section, and the difference in group velocity of the adjacent Airy phases is a measure of the velocity contrast at the bottom of the uniform section. Figure 12 shows a test of these effects where several cases for one model were computed varying only the thickness of the "granite" layer, as indicated.

From this Figure it can be seen that as the thickness of the uniform layer increases from 19 km to 21 km to 24 km (curves 2, 3, and 5 respectively), the separation between the maximum Airy phase at about 8 seconds period and the adjacent minimum at longer periods systematically increases from 6 seconds to 7 seconds to 8.5 seconds (about .5 seconds per km increase in thickness). The curve for 12 km thickness (curve 4) conforms to this pattern also, if the interval between its points of maximum curvature (Airy phases are also such points) are used to define the separation. These Airy phases disappear as the structure approaches a linear velocity increase with depth. The usefulness of this result in crustal studies is apparent, inasmuch as one can, merely by looking at the dispersion curve for a region, or just the seismogram, infer whether the underlying structure has thick uniform sections or increases in velocity gradually with depth. In this regard dispersion also complements refraction data by indicating whether velocity gradients exist between the velocity discontinuities inferred from the travel time curves; that is, whether or not it is legitimate to approximate the refraction travel time curve by the particular straight line segments selected.

Therefore, if a thick uniform section does exist, one can tell how its thickness changes from one area to

to another by comparing the period interval between the adjacent Airy phases on the dispersion curves or just on the seismograms, for each region.

Figure 12 also illustrates how a change in the effective velocity contrast at the bottom of the uniform layer affects the difference in group velocity between the adjacent Airy phases. For curve 1 the average velocity gradient below the thick layer was made slightly greater than for the corresponding curve 3. This increased the difference in group velocity between the adjacent Airy phases as shown in Figure 12 (compare curves 1 and 3). Note that this did not alter the separation between the Airy phases, as the thickness of the uniform layer was kept fixed at 21 km for both curves. Thus, comparison of the "depth" of an Airy phase minimum from region to region will indicate how the effective velocity contrast at the base of a uniform section changes.

These same effects occur for the higher modes and are still more pronounced, since the higher modes are more sensitive to structural details. Therefore, higher mode dispersion can be used to great advantage in determining the sharpness of velocity gradients and discontinuities as well as to detect thinner uniform portions of the structure.

The point of the foregoing discussion is that when

one finds a structure which produces agreement in shape but not absolute value between theoretical and observed dispersion, it means that the relative velocity relationships with depth are nearly correct, so that this structure has only to be scaled uniformly to produce good agreement with the data.

In the discussion to follow it will be instructive to keep the foregoing statements regarding the significance of the shape of dispersion curves in mind, especially when examining the experimental and theoretical curves for the areas investigated.

The events analyzed were chosen such that their travel paths to the recording stations in Southern California were confined as nearly as possible to single geologic provinces. The lines emanating from Pasadena on the map shown in Figure 1 indicate the principal paths investigated. Data for the slightly different paths between other stations in Southern California and each of the epicenters listed in Table 2 were included whenever possible, since the dispersion for these perturbed paths was the same within the precision in measurement.

The data for the Basin and Range are the most complete, in that the dispersion was measured for more paths and more events in this region, and in that extensive portions of this province have been explored by

refraction and gravity methods. The permissible crustal structures which produce equally good agreement with all the available data in this region can vary only in detail.

Figures 14, 15, and 16 summarize the experimental group velocity dispersion measurements obtained for paths in the Basin and Range Province. By comparison of these figures it can be seen that the data are essentially the same for different distances along slightly different paths. This, to an extent, validates the assumption that the structure in the Basin and Range is undergoing no strong lateral variations.

From these Figures one can see that it was possible to delineate the fundamental Rayleigh and Love modes in the period range from about 6 seconds to 50 seconds as well as the first two higher modes of both Rayleigh and Love waves in the period range from 2 to about 12 seconds. A few points which may belong to the third higher mode were also obtained.

Figure 14 represents data from the larger events in aftershock sequence of the Montana earthquake of August 17, 1959. Figures 15 and 16 represent data from a pair of earthquakes on the Utah-Idaho border in 1962. Table 2 gives the location, origin time, magnitude, and approximate depth for each of these events.

These events from Utah offered a unique opportunity to investigate Love waves, since the Caltech digital

seismograph was oriented such that one component was normal to the geodesic path of propagation to within one degree.

Theoretical dispersion curves were computed for numerous structures based on the available compressional velocity refraction models. None of these produced agreement with the observed dispersion when the shear velocity was inferred* using a constant Poissons ratio of .25. Some of these cases which do not fit the data well are shown in Figures 19-23.

Among other things, the poor agreement of these structures with the data indicates that if the layer thickness and compressional velocities are correct, Poisson's ratio is not constant at .25 in this region. In addition, these examples point up the value of obtaining data over as large a period range as possible. That is, several of these cases produce reasonable agreement with the data over a restricted period range, but seriously depart from it elsewhere. Only when the over-all shape of theoretical and experimental curves agree has a good approximation to the true structure been obtained.

---

*The shear velocity ($\beta$) and compressional velocity ($\alpha$) are related by the expression $\alpha^2 = \beta^2\left(1 + \frac{1}{1-2\sigma}\right)$ where $\sigma$ is Poisson's ratio. Figure 31 gives a convenient plot of compressional velocity versus shear velocity for various Poisson ratios.

When Poisson's ratio was allowed to vary within reasonable limits (.22-.30), it was possible, after numerous trials, to arrive at a structure which simultaneously produced satisfactory agreement among all the data, including refraction. That structure is shown in Figure 17. Basically this is a rather simple structure consisting of about 2-3 km of "sedimentary" material overlying a rather uniform section of "granitic" material about 23 km thick, which in turn overlies an intermediate section about 25 km thick which will be designated section X.

Next, a maximum in velocity occurs at a depth of about 50 km with a gradual decrease in velocity at greater depth corresponding to the beginning of the Gutenberg low-velocity zone centered at a depth of around 125-150 km.

The theoretical dispersion for this structure is compared with the data in Figures 14, 15, and 16. The over-all agreement for the fundamental mode Love and Rayleigh waves, the higher Love modes, and the second higher Rayleigh mode is considered good. The first higher Rayleigh mode agrees satisfactorily in shape but not in absolute value between 6 and 10 seconds period. A correction for curvature of the earth would bring the theoretical and experimental results for the higher modes into even better agreement at the longer periods

(7-12 seconds) without altering the results at the shorter periods. Below 50 seconds the curvature effect on the fundamental Love and Rayleigh modes is smaller than the scatter of the data.

The other theoretical curve shown in Figure 14 (Case 5EEBM3) gives as good a fit as Case 35CM2 at the longer periods for all the modes except $M_{21}$. The structure for this case is given in Figure 18. It is important to note that the only significant difference in the shear velocity structure of this case and Case 35CM2 is the presence of a thin (6 km) high velocity layer at a depth of about 25 km in this model. The compressional velocity structure at 25 km has a corresponding high velocity layer formed by reducing the compressional velocity from 7.7 km/sec to 7.0 km/sec between 30 and 50 km depth.

The observed data for the first higher mode ($M_{21}$) decidedly rules out model 5EEBM3 in favor of model 35CM2 and indicates that no such high velocity layer persists in the Basin and Range. The reason $M_{21}$ is so diagnostic is that in the period range from 4-10 seconds, it is controlled mainly by that portion of the structure containing the high velocity layer. The second higher mode ($M_{12}$) has a node in vertical displacement in this depth range for the periods involved, as can be seen from Figure 10, and the fundamental mode averages the

structure so uniformly that it is not very sensitive to such fine structural details at depth. In contrast, $M_{21}$ has its maximum vertical displacement in the depth range of the high velocity layer (see Figure 10) and is, therefore, very sensitive to that portion of the structure.*

It is important to point out which features of this best structure (35CM2) are definite and which are questionable.

The location of the fundamental mode maximum at about 10 seconds period and the steep drop to low velocities for periods under 10 seconds (see Figure 14) requires an appreciable surface "sedimentary" layer approximately 2-3 km thick with a very strong velocity contrast between this surficial layer and the "granite" layer. A thickness of this order is necessary to move the Airy phase maximum to a period as high as 10 seconds. This surficial layer probably is not uniform in velocity or composition over this area, but it varies within limits which do not materially affect this relationship. One can, as a matter of fact, note some difference in both the Love wave and Rayleigh wave dispersion for

---

*The close correspondence between the amplitude of vertical displacement with depth and the contribution to the group velocity from each portion of the structure is discussed in Section II of Appendix G.

periods below 10 seconds for different stations and events (Figures 14, 15, and 16).

The distinctive inverse branch of dispersion in the fundamental mode from 10 seconds period to 17 seconds period (see Figure 14) requires the uniform "granitic" layer. The interval between these Airy phases requires the thickness of this uniform section to be very close (within about 2 km) to 23 km in thickness. The average thickness of this layer cannot be as great as 30 km.

The inverse branch of the higher mode dispersion, beginning at about two seconds with a velocity of about 3.55 km/sec (Lg), is the analog of the inverse branch of the fundamental Rayleigh mode dispersion curve between 10 and 17 seconds period and similar remarks can be made for the interval between 2 and 4.5 seconds. The value 3.55 km/sec represents a lower bound on the average shear velocity in the "granite" layer. The higher the mode the closer this Airy phase maximum approaches the shear velocity in the "granitic" layer. For any model to fit the shorter period dispersion data even reasonably well, an average shear velocity between 3.6 and 3.65 km/sec was required in this upper layer.

A nearly constant compressional velocity of 6.1 ± .1 km/sec for the top of this section has been definitely established over much of the Basin and Range by the

extensive refraction work of the Crustal Studies Branch of the United States Geological Survey. From the work of Birch (1958, 1960) it is reasonable that this velocity may increase slightly ($\sim$.2 km/sec) with depth, but not sufficiently to destroy the relative uniformity of this layer. Thus, the compressional velocity in this section was not allowed to vary beyond the limits just stated.

The structure just below the "granitic" layer (Section X) which has a shear velocity of 4.1 km/sec and a compressional velocity of 7.7 km/sec in model 35CM2 is highly controversial and requires some discussion. The fact that a layer with a compressional velocity between 7.7 km/sec and 7.85 km/sec persists over large portions of the Basin and Range has been established by the recent refraction work of the USGS.

Keeping the compressional velocity of section X fixed at 7.7 km/sec, a shear velocity of about 4.1 km/sec (corresponding to a Poisson ratio of about .3) was required to fit the observed dispersion in the intermediate period ranges. However, a zone of higher shear velocity ($\sim$4.6 km/sec) is required at a depth of about 50 km in order to fit the fundamental Rayleigh and Love modes near 50 seconds period. It was not possible to determine the sharpness of the boundaries of this higher velocity zone, although of the models investigated, the

ones with the sharper contrast seemed to fit the data better. The possibility that the velocity gradually increases from 4.1 km/sec to about 4.6 km/sec in lower portions of section X cannot be conclusively ruled out.

The value of Poisson's ratio (.3) required in the upper part of section X to simultaneously satisfy the refraction and dispersion data is unusually high, although not unreasonable. Values approaching .3 have been observed in tectonically active regions of Japan, for example. Observed values at the base of the crust in Southern California and Eastern New Mexico are about .28.

At the present time, however, considerable evidence is accumulating for the presence of a masked layer at the top of section X with a compressional velocity of about 7.0 km/sec and thickness of about 10 km. If this is the case, then a more ordinary Poisson's ratio between 25 and 50 km depth can be inferred. However, in either case the dispersion requires that the average shear velocity in section X cannot be changed greatly from 4.1 km/sec. Such a layer will not appreciably affect the dispersion results if only the compressional velocity is involved, since variations in compressional velocity alone do not have a strong effect.

All the models (including 35CM2) which agree with the higher mode dispersion have a low velocity zone

in the upper mantle. None of the other models investigated could be made to agree well in shape or numerical values with the observed longer period (7-12 seconds) higher mode dispersion.

A thick layer ($\sim$100 km) of constant shear velocity in the mantle also gives poor agreement. A half space with constant velocity below 50 km depth produces a very poor fit for the longer period higher modes, which are influenced strongly by the structure below that depth. Hence a low velocity zone at depth produces a better overall result and is decidedly the preferred interpretation of the observed data. The fundamental Rayleigh and Love modes below 50 seconds in period are not very sensitive to this deeper ($H \gtrsim 65$ km) structure and do not furnish any evidence on the structure below 65 km.

An attempt was made to find other evidence for the presence or absence of an increased compressional wave velocity around 50 km depth corresponding to that required in shear velocity by the dispersion.

First of all, if the compressional velocity structure of Case 35CM2 is approximately correct, one would observe the change in the slope of refraction travel time curves from 7.7 km/sec to about 8.1 km/sec at a distance of about 500-600 km, corresponding to the arrival from the high velocity layer at 50 km depth. Travel time curves for paths in the Basin and Range were

constructed for several of the larger nuclear shots in Nevada to try to observe such an arrival. While there was a suggestion that the slope changed in that distance range, the scatter of the points was so great that no definite conclusions could be drawn.

One other piece of evidence was found, however, which is suggestive that such an arrival is present in this distance range. It comes from the amplitude attenuation data for refracted waves from nuclear explosions given in a recent publication by Werth and Herbst (1963), in which a pronounced jump in the amplitude of the first half cycle of motion was observed in the distance range 500-700 km. They suggested that this may represent a new arrival, but did not identify it with any particular part of the structure. This feature is explained very well by the structure in Case 35CM2. Even the more rapid apparent attenuation with distance for this arrival is consistent with Case 35CM2, since a refracted wave in this thin layer would leak energy into the low velocity section below and give rise to rapid apparent attenuation with distance.

One additional test of this model was possible using phase velocity dispersion for the fundamental Rayleigh mode. Figure 24 shows the comparison between Case 35CM2 and phase velocity dispersion measured for the tripartite array of Pasadena, California; Ruth, Nevada;

and Albuquerque, New Mexico for the Russian nuclear series at Novaya Zemlya. The agreement in shape over the whole range of values is excellent. Uniformly increasing the over-all crustal thickness in the Case 35CM2 by about 10 km will produce excellent agreement with these observed phase velocity values. This means that the velocity relationships among layers in Case 35CM2 are nearly correct. This array covered an area including, but mostly southeast of, the paths studied from Utah and Montana. Other evidence exists which suggests that the crustal thickness is in fact somewhat greater in this region. This evidence consists of refraction profiles and the additional group velocity dispersion data shown in Figure 25, which also indicate that this region is uniformly thicker than the central Basin and Range, but has the same velocity relationships between layers.

So far there has been no discussion of the density structure in the various models used, Case 35CM2, in particular. The density structure was always kept consistent with the compressional velocity structure using the results of Birch (1961), Woollard (1959), and Nafe and Drake (Talwani et al, 1959) concerning the relationship between compressional wave velocity and density. Since surface wave dispersion is not very sensitive to density variations, the density of Case 35CM2 is not

necessarily very close to the true density structure in the Basin and Range. For example, the effect of decreasing the density from 2.92 to 2.71 $g/cm^3$ in a section 18 km thick in the crust is shown in Figure 13 for the fundamental Rayleigh mode. It can be seen that the change in dispersion was not great. The density structure of Case 35CM2 is, however, a reasonable one.

The most significant contributions to our knowledge of the Basin and Range provided by this study then are (1) the first direct determination of the complete shear velocity structure which prevails there, (2) the first estimates of the distribution of Poisson's ratio in the Basin and Range from combined multi-mode dispersion and refraction data, establishing that Poisson's ratio departs significantly (particularly between 25 and 50 km depth) from the value of .25 usually assumed in the crust, and (3) the inference that a thin (~15 km) high velocity zone exists at a depth of around 50 km with a subsequent decrease into a mantle low velocity zone.

These results are all pertinent to a discussion of isostasy in this region. First of all, the lateral variations of compressional velocity in the deeper part

of the crust* (25-50 km) indicated by refraction and the inference from this study of a low velocity zone at greater depth points up a very important point regarding isostatic compensation in general and this region in particular. The assumption of isostatic compensation implies that there exists a level in the earth (at depth H below sea level) above which the mass is constant; that is, $\int_0^{H+h} \rho(z)\,dz$ = constant, where h is the surface elevation above sea level and $\rho(z)$ is the density at an elevation z above the level of compensation. It is most reasonable to expect that if such a level exists, it will be in or below any zone of weakness, where dynamic processes (such as plastic flow) leading to a redistribution of mass, can most readily occur. The mantle low velocity zone quite probably corresponds to such a zone of weakness.

Therefore, the common assumption in the literature that the level of compensation is at the Mohorovicic discontinuity does not seem reasonable, since the rigidity (and presumably the strength have a maximum there. In separate investigations using different assumptions, Hayford (1909) and Bowie (1917) both concluded that the most probable depth of the level of compensation in the

---

*There is considerable controversy as to whether this zone legitimately belongs to the crust or the mantle. The USGS has adopted this zone as the beginning of the mantle. The view taken in this study, however, is that this zone should be included as part of the crust.

United States is around 100 km. These results add additional weight to the statements made above.

Moreover, the strongest lateral variations in crustal velocities between provinces in the Western United States seem to occur below a depth of 25 km. Therefore, if the density varies laterally with these velocities (as is probable), then the level of compensation must be at depth of the order of 100 km at least. Pakiser (1963) used the available refraction data in the Western United States along with velocity-density relations of Nafe and Drake, and Birch to compute the depth of compensation such that the Basin and Range province would be in isostatic equilibrium with the Great Plains province. The resulting depth was about 80 km when a constant velocity (and density) was assumed below the Mohorovicic discontinuity.

The inference in this study of a thin high velocity zone near 50 km depth with an attendant low velocity zone in the deeper mantle materially relates to the existing density structure in the lower crust and upper mantle of the Basin and Range province, assuming that this region is in isostatic equilibrium with adjacent provinces. If the density structure below this high velocity zone is laterally uniform from province to province, then the usual relation between velocity and density cannot hold for the intermediate zone above,

since the density could not have strong lateral variations. On the other hand, if the velocity-density relation holds, then lateral variations in the density distribution must occur for depths well into the mantle, perhaps to depths approaching 150 km. The latter interpretation is preferred, since it appears that the entire upper mantle has been involved in the relatively recent tectonic activity in the Basin and Range.

The value of .3 for Poisson's ratio in the anomalous 7.7 km/sec section X as suggested by the combined surface wave and refraction data, greatly reduces the number of possible materials which may constitute that zone since the limited data which exist (Molotova and Vassil'ev, 1960) indicate that only a few rock types exhibit such high Poisson ratios (gabbro is one). Therefore, a more detailed determination of Poisson's ratio in this zone, as well as laboratory measurements of Poisson's ratio for various rock types under appropriate conditions of pressure and temperature may provide important clues as to the composition of this zone. The same is true for other parts of the structure as well.

The existence of the high velocity zone at about 50 km depth has at least two possible explanations in terms of tectonic history. It could be a remnant feature indicating where the Mohorovicic discontinuity once was, if the ensuing tectonic activity in this region served only to redistribute the upper mantle materials

into the lower part of the crust. In this case, the top of the 7.7 km/sec layer should be considered the Mohorovicic discontinuity at present.

If, on the other hand, the physical location of this zone is controlled by the prevailing pressure-temperature conditions, it may be that this high velocity zone once was located at the top of the now 7.7 km/sec section and migrated downward to its present depth during the recent period of tectonic activity and associated vulcanism. In this case, the 7.7 km/sec layer would now represent a vestige of a pre-existing crust-mantle interface.

A comparison of the dispersion results in this region with the more limited data for other paths in the Western United States was made in order to infer how the structure changes laterally from one geologic region to another.

Figure 24 shows experimental phase velocity for the tripartite array of Pasadena, California; Ruth, Nevada; and Albuquerque, New Mexico obtained from the Russian nuclear explosions at Novaya Zemlya. The solid line shows the phase velocity for Case 35CM2, the best structure for the Basin and Range paths just discussed (see Figure 17). One sees that the experimental and theoretical curves agree very well in shape, but not in absolute value. This means that the relative velocity

relationships for the crustal layers in Case 35CM2 are very nearly correct for this region also, but that the over-all thickness is approximately 10 km too small in Case 35CM2.

Figure 25 compares observed fundamental mode Love and Rayleigh wave dispersion for a path from Oklahoma to Pasadena (see Figure 1) with the data for paths from Montana and Utah to Pasadena. This comparison also indicates a rather uniform increase in average crustal thickness for this path compared to the paths confined strictly to the central Basin and Range.

There is also a strong suggestion that the basic shear velocity distribution of Case 35CM2 (see Figure 17) persists southward as far as the southern part of Mexico. Figure 26 shows the experimental dispersion for an earthquake in the southern part of Mexico at a depth of 100 km. All the measurements shown in this Figure were made by visual methods, which accounts for the greater scatter in the data. Nonetheless, the agreement of Case 35CM2 with this data is remarkable. This suggests that the velocity structure along this path is not appreciably different from that measured in the Basin and Range. The temptation, then, is to suggest that Basin and Range type structure persists as a geologic unit at least to Southern Mexico.

One additional fragment of evidence exists for this

assertion. For several earthquakes in Mexico, Gutenberg and Richter (1940) measured apparent velocities of body waves between stations within the Basin and Range region having significantly different azimuths from the source. The distances involved were appropriate for section X first arrivals. Surprisingly enough, these apparent velocities were consistently about 7.8 km/sec, which agrees with the recent detailed refraction results in the Basin and Range.

The inference from this is that at least within the region defined by the various azimuths from these events to the recording stations, the crustal velocity to the south of the Basin and Range is laterally uniform.

The experimental dispersion points between 10 and 30 seconds period with velocities above 4.0 km/sec shown in Figure 26 constitute one of the first experimental measurements of mantle higher mode dispersion for a continental path. It is reasonable that this event in Mexico would excite mantle modes, because the depth of source was about 100 km, which is favorable for long period higher mode excitation. The dashed curves shown are for a Gutenberg-Birch earth model computed by Kovach (1963). The important feature of that model is its mantle low velocity zone, which produces the minima shown in the period range 10-30 seconds. Models without a mantle low velocity zone do not produce such pronounced

minima in this range. Since the data indicate even more pronounced minima than exist for this model, it is suggested that a mantle low velocity zone definitely exists along this path. A more precise determination of the dispersion in this period range, however, is necessary before drawing further conclusions about the details of such a mantle low velocity zone under this continental region.

Figure 27 shows a comparison of fundamental Rayleigh and Love mode dispersion for the paths in the Basin and Range with that for a path along the Sierra Nevada range from Vancouver, British Columbia to Southern California and for a path along the coastal region of California from a source off Oregon. These paths are shown in Figure 1.

It is evident from this comparison that the prevailing structure in the Sierra Nevada is strikingly different from that in the Basin and Range and the California coastal regions. From this comparison one can conclude, first of all, that the same velocity relationships do not exist in the Sierras that exist in the crust of the Basin and Range. In particular there appears to be no "sedimentary" layer of any consequence in the Sierras, nor any thick, uniform layer of material near the top of the section, as exists in the Basin and Range. Instead, the velocity in the shallower portion

seems to increase gradually with depth, attaining an intermediate shear velocity (~4.2 km/sec) at a moderate depth (~25 km). The broad plateau in the Rayleigh wave dispersion between 25 and 40 seconds and for Love wave between 28 and 35 seconds indicates the presence of a very thick section (~40 km) of intermediate velocity material in the lower portion of the crust. This thick section is also responsible for the kinks observed in the first two higher Rayleigh modes between 6 and 10 seconds period.

At present, a model which agrees well with all the data for the Sierras has not been found. However, some structures which are reasonably acceptable are given in Table 4. These are shown in comparison to the data in Figure 28. The high shear velocity (4.6 km/sec) is required at the base of the thick section in order to produce the observed plateau in both Rayleigh and Love waves.

The theoretical curves for the higher modes, while agreeing in shape, are too high compared with the data. Insertion of a mantle low velocity zone would improve the fit at the longer periods without seriously altering the shape in this region.

Therefore, the results of this study give another indication that a "root" exists under the Sierra Nevadas extending to a depth of the order of 70 km, where it is

terminated by high velocity mantle material. Moreover, these dispersion results establish that this "root" is a result of an increase in thickness of the intermediate crustal layer rather than in the "granitic" layer at the top. However, instead of two distinct crustal units separated by a strong velocity discontinuity, there seems to be a gradual transition from one zone to the other.

The last path investigated was along the California coast as seen in Figure 1. Figure 27 shows the comparison of this data with that from the Sierras and the Basin and Range. It is clear from this comparison that this path has a thinner crust than those in the Basin and Range or the Sierras. A long reversed refraction profile between Los Angeles and San Francisco has been studied by the USGS, (Healy, 1962) which nearly duplicates the path for this event. In Figure 29 the experimental dispersion is compared to the dispersion curves for a set of models all of which are consistent with the refraction data for this path, assuming a Poisson's ratio of .25. These models are shown in Figure 30. None of these produces good agreement in shape with the observed dispersion. It appears, therefore, that in order to fit both the dispersion and refraction data, Poisson's ratio must be allowed to vary from a value less than .25 in the upper part of

the crust to a value greater than .25 in the deeper structure.

## CONCLUSIONS

The conclusions one can draw from this study regarding crustal structure in the Western United States may be summarized as follows:

Throughout the Basin and Range province the crustal structure is very close to that shown in Figure 17. The high Poisson's ratio in the zone from 25-50 km depth, the thin high velocity layer at about 50 km depth, and the mantle low velocity zone are noteworthy features of this structure.

The velocity relationships of this model persist to the southwest of the Basin and Range with an increase in over-all crustal thickness of about 10 km. There is also a strong indication that this basic velocity structure, including the mantle low velocity zone, persists southward all the way to the southern part of Mexico.

A very different type of crustal structure exists in the Sierra Nevada region. Here there is a very thick intermediate crustal layer extending to a depth of around 70 km, accounting for the "root" of the Sierras. No "sedimentary" layer of importance persists in this region, and the velocity in the "granitic" layer increases with depth to where it joins the intermediate layer at a depth of about 25 km. The

coastal region of California was concluded to have a shallower crust with Poisson's ratio increasing with depth.

Considerable variation in Poisson's ratio was found to occur in the crust in the Western United States. This means that the common practice of assuming a Poisson's ratio of .25 to infer crustal shear velocity from compressional velocity should be abandoned.

# PART II

# THE EFFECTS OF THE CONTINENTAL MARGIN IN SOUTHERN CALIFORNIA ON RAYLEIGH WAVE PROPAGATION

ABSTRACT

The effects of the transition zone at the continental margin of Southern California on Rayleigh wave propagation have been investigated. Among the anomalous effects discovered are a minimum in phase velocity between 20 and 35 seconds period, different phase velocities on reversed paths across the same array, and systematic lateral refraction at the continental boundary. These anomalous effects can be attributed largely to the slope and curvature of the Mohorovičić discontinuity across this region. An ultrasonic model was constructed to aid in interpreting these results.

Interpretation of the dispersion for periods below 20 seconds indicates that the crust thickens toward the continent with a slope of about $5^{o}$ attaining a thickness of approximately 35 km under Southern California.

# PART II

# THE EFFECTS OF THE CONTINENTAL MARGIN IN SOUTHERN CALIFORNIA ON RAYLEIGH WAVE PROPAGATION

## INTRODUCTION

The purpose of this investigation was to observe the effects of a transition zone, such as a continental margin, on Rayleigh wave propagation, and to identify, if possible, the structural features which produce these effects, and to determine which effects may be used as diagnostic aids for studying other transition zones.

This represents a controlled experiment in that some gravity and refraction data exist for the structure in the continental margin region of Southern California.

Dispersion, amplitude attenuation, and direction of propagation are the parameters which completely describe surface wave propagation across an array, so that effects on each of these parameters are relevant.

It is to be expected that the results cannot be interpreted solely using simple, plane parallel layered structure models at a continental margin where lateral changes are appreciable. To aid in interpreting the results for which only rudimentary theory exists, an ultrasonic model was constructed and used as an analog device in this study.

In such a transition zone effects on amplitude and direction of propagation of Rayleigh waves become more pronounced, and these may be diagnostic of certain of the lateral changes, in contrast to the simple layered structures where dispersion is the only diagnostic surface wave parameter.

Therefore, combined measurements of dispersion, direction of propagation, and amplitude attenuation of Rayleigh waves should be used whenever possible for studying transition zones.

While phase velocity dispersion across such a zone is not so easily interpreted as for laterally homogeneous areas, it remains a sensitive measure of crustal structure when used properly. For this reason strong emphasis was placed on investigation of effects on phase velocity dispersion during this study.

One important side result of this research was the programming of experimental phase velocity methods for a digital computer so that phase velocity dispersion can be computed rapidly and routinely in the future.

METHODS OF ANALYSIS

The most important experimental methods for measuring phase velocity and direction of propagation are summarized in Figures 33, 34, and 35. The least squares technique is the most general and the others can be derived from it. The relative merits of these and other methods, as well as detailed requirements for the use of each, are discussed in Appendix A.

For most of the dispersion measurements time domain methods were used. However, frequency domain methods were used to check the time domain results in a few instances, as well as to measure most of the dispersion for the ultrasonic model. For a more complete discussion of the methods used for the model experiment, refer to Appendix D.

Computer programs for these methods were written for the Bendix G-15 and IBM 7090 digital computers. These programs, described in detail in Appendix H, allow routine computation of phase velocity dispersion and direction of propagation, as well as the auxiliary distance and azimuth information required. Table 3 gives the distances and azimuths between stations in the Southern California network using these programs.

For the continental sources there exists the problem of separating the long period fundamental mode Rayleigh waves from the higher modes so that reliable time domain

correlation among the stations could be achieved. A method involving a combination of numerical band pass filtering and velocity windows was developed for separating the modes. A detailed discussion of this method can be found in Appendix F and Part I of this thesis. An example of the great effectiveness of this method is given by a comparison of Figures 6 and 7. Figure 6 shows seismograms from a single event recorded at three stations in the Southern California network. Figure 7 shows the same seismograms after applying the mode delineation method. Its effectiveness is apparent. This method proved invaluable in obtaining reliable results from the continental sources.

Amplitude spectrum measurements were made by numerically computing the Fourier transform of the digitized wave train using a computer program written for this purpose. Appendix H also contains a description of this program and the integration methods which can be used with it.

Theoretical dispersion curves for various structural models were computed by means of existing computer programs previously described in the literature (Press, Harkrider and Seafeldt, 1960; Harkrider and Anderson, 1961).

## EXPERIMENTAL RESULTS AND INTERPRETATION

Figure 32 shows the locations of stations (solid dots) available for this study. Records from Benioff 1-90 long period vertical seismometers at each station were used in the analysis. These instruments were suitably matched in phase response (see Appendix E) so that reliable correlation of each wave train across the array could be achieved.

A number of earthquakes located in the South Pacific were used to investigate propagation from the ocean to continent. Table 1 lists pertinent epicenter information about these events. Table 2 gives similar data for the continental shocks used to investigate continent to ocean propagation over the same array of stations.

Composite curves showing the average phase velocity dispersion measured for various coastal tripartite arrays are shown in Figure 37 where Press's "standard" curves (Press, 1956) are shown as a frame of reference. The values shown represent the mean of the values obtained from all the events from the South Pacific. The standard deviation of the mean is about .5 percent for periods below 22 seconds and about 1 percent at the longer periods. Figure 38 shows a representative set of curves from the use of least squares for reversed propagation over the array. The length of the vertical symbol in the case where all stations were simultaneously used represents the standard deviation of the mean.

For periods under 22 seconds, the values for both directions have standard deviations around .5 percent and many for ocean to continent propagation were under .3 percent.

Several features are evident from examination of these two figures. First, for periods below about 22 seconds the dispersion is typical and indicates a systematic change (thickening) in crustal structure with distance inland. That is, for arrays where the average thickness of the crust is shallow, the phase velocity dispersion is consistently higher than for arrays under which the average crustal thickness is greater. Figure 39 shows the comparison of the published results of Shor and Raitt from refraction in the offshore region of Southern California and the values of thickness inferred from phase velocity dispersion using Press's standard curves. While the absolute values of thicknesses inferred from the dispersion are from 5 to 8 km greater than those inferred from refraction, the agreement in the slope of the crust-mantle interface derived from the two techniques is good.* The slope inferred from the dispersion is somewhat greater, however.

*The validity of using these curves to interpret the observed dispersion in terms of absolute crustal thickness is open to question, since the assumption of a plane parallel-layered structure is clearly violated in this region. On the other hand, changes in thickness can be estimated rather well using adjacent arrays, since $\left[\frac{\partial C(H,T)}{\partial H}\right]_T$ is a slowly varying function of the total crustal thickness, H. Appendix I discusses a modified approach for using the plane-parallel layer theory to interpret results in regions where the thickness changes laterally.

Secondly, from Figure 38 one can see that the velocity of propagation from continent to ocean is higher than for propagation from ocean to continent over the same network in Southern California. This effect is more pronounced when the individual tripartite arrays near the coast are used. These results are analogous to refraction results over dipping layers in that the apparent velocity updip is greater than that for propagation downdip across a fixed array of receivers.

The mean of the phase velocities obtained for these reversed directions gives an average crustal thickness about 2 km less than the values inferred only from ocean to continent propagation. This adjustment would bring the values of thickness determined from refraction and phase velocity shown in Figure 39 into better agreement without appreciably changing the slope of the base of the crust.

Figure 40 shows two Bouguer anomaly profiles, derived from Emery's published results (Emery, 1959), across two portions of the region studied. The profiles are defined by the co-ordinates of latitude and longitude they transverse. These also indicate a gradual (almost linear) increase in crustal thickness from the continental slope to the coast of California.

Theoretical dispersion for the refraction structure of

Shor and Raitt, assuming a Poisson's ratio of .25, gave results which agreed reasonably well in shape with the observed dispersion below 22 seconds period, but which were consistently above the observed dispersion. Uniformly increasing the layer thicknesses of their refraction model, inserting a thin (5 km) crustal low velocity layer, or increasing Poisson's ratio in the crust will each bring the refraction and dispersion results into reasonably close agreement. At the present time there is little to choose among these alternatives, although crustal low velocity layers do not appear to be present further inland.

In this regard, shear velocity refraction measurements would be most useful for resolving the discrepancies between surface wave and body wave crustal models, since the practice of inferring shear velocity from compressional velocity, assuming a Poisson's ratio of .25 almost never leads to satisfactory agreement between refraction and dispersion results.

The results discussed above are all consistent in that they indicate a gradual, almost linear, thickening of the crust from 300 km offshore to the coastal region of Southern California. There the slope of the crust-mantle interface decreases and the crustal thickness is slowly varying as one goes further inland.

The third striking feature of the observed data is a

phase velocity minimum, or certainly a knee in the experimental dispersion, which occurs in the period range 20-35 seconds, as shown in Figures 37 and 38. This feature becomes less pronounced for arrays away from the coast. Similar features for both the Pacific and Atlantic continental margins can also be observed in this period range in the experimental phase velocity dispersion curves previously published by Press and Ewing (1959). In their results, too, this perturbation becomes less pronounced for arrays further inland, where the structure is presumably laterally more uniform.

Frequency domain determinations of the phase velocity gave results consistent with time domain measurements in the period range of this anomalous feature, as can be seen in Figure 37.

Experimental errors (Appendix C) are not nearly large enough to remove this anomalous feature. Moreover, no prominent "holes" occur in the spectrum of the Rayleigh waves in this period range, as can be seen from Figure 42, where typical spectra for events from the South Pacific are shown. The reason this point is important is that peculiar phase velocities have often been observed for periods corresponding to minima in the amplitude spectrum, particularly when these minima result from interference. (Pilant, 1962).

Therefore, it was concluded that this anomalous feature in the dispersion was real. This naturally brings up the question of how to explain this curious result.

First of all, the theory for plane parallel layer structure does not predict a minimum in phase velocity dispersion; at most a flat plateau can occur. Therefore, the existence of this minimum indirectly indicates that lateral changes in crustal thickness are at least partly responsible for this feature. The fact that, for arrays progressively further inland (where the crustal thickness becomes laterally uniform), this feature becomes less pronounced gives another indication that the rapid lateral changes of the crust at the continental margins are responsible for the anomalous dispersion.

No adequate theory exists at present which gives the Rayleigh wave dispersion for geometries other than flat lying layers. These problems are exceedingly difficult to solve exactly (or approximately) even for the simplest case of a lateral linear increase in crustal thickness.

Therefore, it was concluded that the study of an analog model would be the most fruitful approach to explaining these anomalous features. Using the available refraction, gravity, and surface wave data for a guide, an ultrasonic model was constructed which approximates the geometry, as well as the ratio between the mean crustal velocity and the

mantle velocity, for this region. The shape of this model is shown at the bottom of Figure 45. This is the analog of a crust which thickens with a constant (5 degree) slope from a thickness of 10 km to 40 km. In this particular analog model the period in microseconds corresponds directly to the period in seconds in the earth. For a detailed account of how this model was constructed and how the results were obtained refer to Appendix D. Figure 45 summarizes the dispersion results for this model, for various station arrays on the model. The solid curves are the plane-layer theory for a layer over a halfspace where only the thickness of the layer is changed.

The agreement between the measured and theoretical values outside the transition zone is very good as shown for the curves H=.25 and H=1.0 in this figure. For profiles entirely within, or partly within, this transition, however, certain important departures from the theory were observed.

First of all for arrays completely in the transition zone (where the underlying slope is linear) the velocity of propagation updip was higher than for propagation downdip. At the shorter periods the mean of these velocities fell on the theoretical curve appropriate for the mean thickness beneath the array. (Profiles 22-27 in Figure 45, for example).

When the array was partly in and partly out of the transition zone (that is, when it spanned the section where the slope changed) certain anomolous results were obtained at the longer periods ( > 20 $\mu$sec). In these instances there was a pronounced flattening in the dispersion curves between periods of 20 and 40 micro-seconds for both directions of propagation and in one or two cases a slight minimum occurred. (Profiles 25-29, 26-29 in Figure 45, for example.)

Below 20 $\mu$seconds period the dispersion followed the typical pattern of decreasing uniformly as the mean thickness over the array increased. This was true even when the mean thickness was only slightly different (Profiles 23-29, 25-29, and 26-29 in Figure 45). Below 20 $\mu$seconds the velocity was different over reversed profiles, but not so pronounced as when the profile was completely inside the transition zone (Profile 25-29 in Figure 45, for example).

These results are highly suggestive that the different phase velocities observed on a reversed path in Southern California are a result of the slope of the crust-mantle interface and that the anomalous dispersion beyond 22 seconds period is due to changes in the slope of this interface beneath the arrays in Southern California. This would explain why these anomolous effects are less pronounced or absent away from the continental margins in laterally more homogeneous areas. In the model this effect

is most pronounced for wave lengths from 3 to 5 times the mean depth of the layer-halfspace interface. By analogy, the same features should be observed for approximately this range of wave lengths in the earth. The ranges of wave lengths where the anomaly occurs in Southern California is from about 80 to 150 km, which is approximately the range of 3-5 times the mean crustal thickness in this region.

It is clear that only the shorter period ( $\leq$ 22 seconds in Southern California) phase velocity dispersion gives a reliable indication of how the crust is changing in a transition zone when conventional interpretation is used. In both the experimental results and the model results the dispersion in this shorter period range, without exception, reflected the systematic increase in crustal thickness by a corresponding decrease in phase velocity.

However, if the foregoing conclusions concerning the anomalous features of the dispersion in this transition zone are correct, it means that it will also be possible to use these peculiarities of phase velocity dispersion to detect the presence of a tapering crust, to locate sections where the slope of the crust-mantle interface changes, and to determine the approximate depth at which these perturbations in crustal thickness occur.

Therefore, phase velocity dispersion should be a very practical means of studying lateral changes of the crust

at the continental margins of other areas. One could then determine the similarities and differences in the continent to ocean transition zone from one area to another. Such studies might furnish important clues to the geologic processes which lead to the formation of continents as well as those which maintain the continents in their present position.

In addition to dispersion, one other aspect of surface wave propagation is useful in investigating transition zones. That feature is lateral refraction of surface waves for oblique incidence on a velocity boundary. This refraction follows Snell's law and is controlled by the phase velocity in the two regions. A more complete discussion of lateral refraction of surface waves is given in Appendix B.

Because direction of propagation is computed as a by-product of phase velocity measurements, the refraction as a function of frequency can be experimentally measured simultaneously with the phase velocity, provided the direction of propagation of the incident wave can be determined.

In the present study limited use of lateral refraction could be made since the angles of incidence were small ($< 20$ degrees), and there was no sure way of determining the exact angle of incidence on the boundary. It could only be assumed that every frequency in the wave train had

the identical angle of incidence on the boundary and that this direction corresponded to the geodesic direction back to the source.

An attempt was made to check the validity of this assumption by examining the group velocity data for the Pacific which was recently published by Santo and Båth (1963). Their data indicates that over the entire range of geodesic paths to Southern California used in this study, the oceanic crust is relatively uniform and has high group velocity compared to adjacent regions. This means that the least time path should correspond rather closely to the geodesic path for the events used in this study. The group velocity of one of the events used is shown in Figure 43. The lines bracketing the data in this figure represent the limits of group velocity for the range of possible paths to the United States from the source region of interest here. These limiting curves aretaken from the results of Santo and Båth (1963), just mentioned.

Therefore, the angle of incidence at any point on the continental boundary can be expected to coincide reasonably closely to the geodesic direction back to the source for all the events used in this study.

In spite of these possible uncertainties, the observed direction of propagation showed a systematic variation such that for propagation from ocean to continent the waves always

appeared to come more nearly from the normal to the continental boundary. There was some dispersion in this systematic refraction, in that waves of about 40 seconds period and above were essentially unrefracted, as were waves at about 15 or 16 seconds period, while intermediate periods were refracted several degrees depending on the angle of incidence at the boundary.

The fact that periods above 40 seconds were hardly refracted at the boundary implies that the sharp differences in velocity between oceans and continents are superficial, since with increasing period, the waves are sampling the structure to progressively greater depths. The lateral differences in velocity between oceanic and continental structure are a maximum at the intermediate depths (10-50 km), since the intermediate periods which "feel" the velocity at these depths most strongly, are refracted most in traversing the continental boundary.

However, the vanishing refraction around 15 seconds period (indicating no velocity contrast) points up the danger of associating velocity with composition in the earth. Clearly the shallow (top 10-20 km) material in the oceans is vastly different from that in the continent. Yet for certain periods (in this case around 15 seconds) the average velocity which the wave "sees" is the same for both oceanic and continental propagation.

Similar refraction effects were observed for events propagating from the continent to the ocean, except that the refraction was away from the normal to the boundary, as expected for an average crustal velocity increase toward the ocean.

A method for using the lateral refraction of surface waves to experimentally determine the strike of linear features was developed. Basically, it takes advantage of the fact that the smaller the angle of incidence, the smaller the deflection from the incident direction of propagation. This method is described in detail in Appendix B and summarized in Figure 44. When applied in Southern California, the strike of the velocity boundary between continent and ocean was found to be about N30W, which agrees reasonably well with the strike of the continental slope, shown dotted in Figure 32.

CONCLUSIONS

It may be concluded from this study that the crust at the continental margin of Southern California increases in thickness toward the continent with a slope of about 5 degrees, achieving a thickness of approximately 35 km under Southern California proper.

Over transition zones where the crustal thickness varies rapidly, only the shorter period ($\leq$ 20 seconds) portion of the dispersion curve can be used reliably to determine lateral changes in crustal thickness, using conventional interpretations of dispersion data.

The anomalous feature of the observed dispersion, that the phase velocity in opposite directions over a fixed array is different, may be attributed to a sloping crustal-mantle interface at the continental margin.

The pronounced minimum, or kink, in the observed dispersion in the period range 22-35 seconds may be attributed to changes in the slope of the Mohorovičić discontinuity under the coastal region of Southern California. This anomalous feature in the dispersion appears to occur for periods corresponding to wave lengths 3 to 5 times the mean depth of the perturbed interface.

Lateral refraction of surface waves at the continental margin indicates that the strong lateral variations in average velocity which occur in the transition from oceanic

to continental crust do not persist to great depth in the mantle under Southern California.

Lateral refraction of surface waves can be used to determine the strike of linear features in the earth. In Southern California the strike of the continental margin was found to be about N30W.

# REFERENCES


Aki, K., Study of earthquake mechanism by a method of phase
1960 equalization applied to Rayleigh and Love waves, J. Geophys. Research, 65, 729-741.

1961 Crustal structure of Japan from the phase velocity of Rayleigh waves, Bull. Earthquake Res. Inst., (Tokyo), 39, 249-277.

Anderson, D. L., Elastic wave propagation in layered
1961 anisotropic media, J. Geophys. Res., 66, 2953-2963.

1962 Surface wave dispersion in layered anisotropic media, Ph.D. Thesis, California Institute of Technology.

1963 Universal dispersion curves, (unpublished manuscript).

1963 Recent evidence concerning the structure and the composition of the earth's mantle, Physics and Chemistry of the Earth, 6, (in press).

Berg, J. W., K. L. Cook, H. D. Narans, Jr., and W. M.
1960 Dolan, Seismic investigation of crustal structure in the eastern part of the basin and range province, Bull. Seism. Soc. Am., 50, 511-535.

Biot, M. A. General theorems concerning the equivalence of
1957 group velocity and energy transport, Phys. Rev., 105, 1129-1139.

Biot, M. A., and I. Tolstoy, Formulation of wave propagation
1957 in infinite media by normal coordinates with an application to diffraction, J. Acoust. Soc. Am., 29, 381-391.

Birch, F., Elasticity and constitution of the earth's
1952 interior, J. Geophys. Research, 57, 227-286.

1960 The velocity of compressional waves in rocks to 10 kilobars, Part 1, J. Geophys. Res. 65, 1083-1102.

Birch, F., The velocity of compressional waves in rocks
1961 to 10 kilobars, Part II, J. Geophys. Res., 66, 2199-2224.

Blackman, R. B., and J. W. Tukey, The Measurement of Power
1958 Spectra, Dover Pub. Inc., New York.

Bolt, B., and J. Dorman, Phase and group velocities of
1961 Rayleigh waves in a spherical, gravitating earth, J. Geophys. Res., 66, 2965-2981.

Bomford, G., Geodesy, Oxford Univ. Press, 451 pp.
1952

Bowie, W., Investigations of gravity and isostasy, U.S.
1917 Dept. of Commerce Special Publication No. 40.

Brune, J., J. Nafe, and J. Oliver, A simplified method for
1960 the analysis and synthesis of dispersed wave trains, J. Geophys. Res., 65, 287-305.

Bullen, K. E., An Introduction to the Theory of Seismology,
1953 Cambridge Univ. Press, 296 pp.

Caloi, P., L'astenosfera come canale-guida dell'energia
1954 sismica, Ann. Geofis., 7, 491-501.

Cameron, J. B., Earthquakes in Northern California coastal
1961 region, Part I, Bull. Seism. Soc. Am., 51, 203-221.

1961 Earthquakes in Northern California coastal region, Part II, Bull. Seism. Soc. Am., 51, 337-354.

Diment, W. H., S. W. Stewart, and J. L. Roller, Crustal
1961 structure from the Nevada test site to Kingman, Arizona, from seismic and gravity observations, J. Geophys. Res., 66, 201-214.

Dorman, J., Period equation for waves of Rayleigh type on
1962 a layered, liquid-solid half space, Bull. Seism. Soc. Am., 52, 389-398.

Dorman, J., M. Ewing, and J. Oliver, Study of the shear
1960 velocity distribution in the upper mantle by mantle Rayleigh waves, Bull. Seism. Soc. Am., 50, 87-115.

Emery, K., The Sea Off Southern California, Wiley, New
1960 York, 366 pp.

Evernden, J. F., Direction of approach of Rayleigh waves
1953 and related problems, Part I, Bull. Seism. Soc. Am. 43, 335-374.

1954 Direction of approach of Rayleigh waves and related problems, Part II, Bull. Seism. Soc. Am., 44, 159-184.

Ewing, M., and F. Press, Determination of crustal structure
1959 from phase velocity of Rayleigh waves, Part III; the United States, Bull. Geol. Soc. Am., 70, 229-244.

Ewing, M., W. S. Jardetzky, and F. Press, Elastic Waves in
1957 Layered Media, McGraw-Hill Book Co., New York.

Gutenberg, B., The propagation of the longitudinal waves
1934 produced by the Long Beach earthquake, Ger. Beit. Z. Geophy., 41, 114-120.

1945 Variations in crustal layers, Am. J. of Sci., 243-A, Daly Volume, 285-312.

1945 Interpretation of records obtained from the New Mexico atom bomb test, Bull. Seism. Soc. Am., 36, 327-330.

1951 Revised travel times in Southern California, Bull. Seism. Soc. Am., 41, 143-163.

1951a Travel times from blasts in Southern California, Bull. Seism. Soc. Am., 41, 5-12.

1951b Revised travel times in Southern California, Bull. Seism. Soc. Am., 41, 143-163.

1952 Waves from blasts recorded in southern California, Trans. Am. Geophys. Union, 33, 427-431.

1955 Channel waves in the earth's crust, Geophysics, 20, 283-294.

1955 Wave velocities in the earth's crust, The Crust of the Earth, Sp. paper 62, Geol. Soc. Amer., 19-34.

Gutenberg, B., Physics of the Earth's Interior, Academic
1959 Press, New York and London, 240 pp.

Gutenberg, B., and C. F. Richter, Observed times of the
1938 Montana earthquakes, 1935, Bull. Seism. Soc. Am., 28, 85-87.

1946 Seismic waves from atomic bomb tests, Trans. Am. Geophys. Union, 27, 776.

Hagiwara, T., A Note on the theory of the electro-
1958 magnetic seismograph, Bull. Earthquake Res. Inst. (Tokyo), 36, 139-164.

Hales, A. L., and I. S. Sachs, Evidence for an intermediate
1959 layer from crustal structure studies in Eastern Transvaal, Geophys. J., 2, 15-33.

Harkrider, D. G., and D. L. Anderson, Computation of
1962 surface wave dispersion for multilayered anisotropic media, Bull. Seism. Soc. Am., 52, 321-332.

Harkrider, D. G., A. L. Hales, and F. Press, On detecting
1963 soft layers in the mantle with Rayleigh waves, Bull. Seism. Soc. Am., 53, 539-548.

Haskell, N. A., Dispersion of surface waves on multi-
1953 layered media, Bull. Seism. Soc. Am., 43, 17-34.

Hayford, J. F., The figure of the earth and isostasy from
1909 measurements in the United States, U.S. Dept. of Commerce, Special Publication No. 82.

Healy, J. H., Crustal structure along the coast of California
1962 from seismic refraction measurements, U.S.G.S. Crustal Studies Branch, Technical Letter, No. 5

Healy, J., and F. Press, Two-dimensional seismic models
1960 with continuously variable velocity-depth and density functions, Geophysics, 25, 987-997.

Herrin, E., and P. Minton, The velocity of Lg in the
1960 Southwestern United States and Mexico, Bull. Seism. Soc. Am., 50, 35-44.

1960 On the propagation of the Lg phase, Bull. Seism. Soc. Am., 50, 197-210.

Herrin, E., and J. Taggart, Regional variations in $P_n$
1962 velocity andttheir effect on the location of epicenters, Bull. Seism. Soc. Am., 52, 1037-1046.

Jeffreys, H., Small corrections in the theory of surface
1961 waves, Geophys. J. Roy. Astr. Soc., 6, 115-117.

Knopoff, L., On Rayleigh wave velocities, Bull. Seism.
1952 Soc. Am., 42, 307-308.

Knopoff, L., F. Gilbert, and W. L. Pilant, Wave prpagation
1960 in a medium with a single layer, J. Geoph. Res., 65, 265-278.

Knopoff, L., and F. Press, Study of the earth's crust in
1962 selected regions of the world, Final Report, U. of Calif. Inst. of Geophysics, Los Angeles, and CIT, Seismological Laboratory, Pasadena.

Kovach, R., and D. Anderson, Impulsive surface waves, Trans.
1963 Am. Geophys. Union, 44, 101.

Lambert, W. D., and C. H. Swick, Formulas and tables for
1935 the computation of geodetic positions on the international ellipsoid, U.S.C.G.S., Special Publication No. 200.

Lehmann, I., On the short period surface wave 'Lg' and
1953 crustal structure, Bul. d'Information, U.G.G.I., 2, 248-251.

1959 Velocities of longitudinal waves in the upper part of the earth's mantle, Ann. di Geophys. 15

1961 S and the structure of the upper mantle, Geophys. J. Roy. Astr. Soc., 4, 124-132.

Molotova and Vassilev, Velocity ratio of longitudinal and
1960 transverse waves in rocks, II., Izv. Geoph. Ser., 1097-1116.

Nafe, J. E., and C. L. Drake, Physical properties of crustal
1958 materials as related to compressional wave velocities, Abstr. in Geophysics, 23, 403.

Nagumo, S., Elastic wave propagation in a liquid layer over
1961 a sloping rigid bottom, Bull. Earth. Res. Inst. (Tokyo), 36, 189-197.

Oliver, J., A summary of observed seismic surface wave
1962 dispersion, Bull. Seism. Soc. Am., 52, 81-86.

Oliver, J., and M. Ewing, Higher modes of continental
1957 Rayleigh waves, Bull. Seism. Soc. Am., 47, 187-204.

1958 The effect of surficial sedimentary layers on continental surface waves, Bull. Seism. Soc. Am., 48, 339-354.

1958 Normal modes of continental surface waves, Bull. Seism. Soc. Am., 48, 33-49.

Oliver, J., J. Dorman, G. Sutton, The second shear mode
1959 of continental Rayleigh waves, Bull. Seism. Soc. Am., 49, 379-389.

Oliver, J., F. Press, and M. Ewing, Two-dimensional model
1954 seismology, Geophysics, 19, 202-219.

Oliver, J., R. Kovach, and J. Dorman, Crustal structure
1961 of the New York-Pennsylvania area, J. Geophys. Res., 66, 215-226.

Ormsby, J. F., Design of numerical filters with appli-
1961 cation to missile data processing, J. Assoc. Computing Mach., 8, 440-466.

Pakiser, L. C., Structure of the crust and upper mantle
1963 in the western United States, U.S.G.S., Technical Letter No. 8.

Pakiser, L. C., and D. P. Hill, Crustal structure in
1962 Nevada and Southern Idaho from nuclear explosions, U.S.G.S., Technical Letter No. 4.

Phinney, R. A., Propagation of leaking interface waves,
1961 Bull. Seism. Soc. Am., 51, 527-557.

Phinney, R. A., and S. W. Smith, Processing of seismic
1963 data from an automatic digital recorder, Bull. Seism. Soc. Am., 53, 549-562.

Pilant, W., Personal communication.
1962

Press, F., Velocity of Lg waves in California, Trans. Am.
1956 Geophys. Union, 37, 615-618.

Press, F., Determination of crustal structure from phase
1956 velocity of Rayleigh waves, Part I: Southern California, Bull. Geol. Soc. Am., 67, 1647-1658.

1957 Determination of crustal structure from phase velocity of Rayleigh waves, Part II: San Francisco Bay region, Bull. Seism. Soc. Am., 47, 87-88.

1960 Crustal structure in California-Nevada region, J. Geophys. Res., 65, 1039-1051.

Press, F., and M. Ewing, Two slow surface waves across
1952 North America, Bull. Seism. Soc. Am., 42, 219-228.

Press, F., M. Ewing, and J. Oliver, Crustal structure and
1956 surface wave dispersion in Africa, Bull. Seism. Soc. Am., 46, 97-103.

Press, F., D. G. Harkrider, and C. Seafeldt, A fast con-
1961 venient program for computation of surface wave dispersion curves in multi-layered media, Bull. Seism. Soc. Am., 51, 495-502.

Roller, J. C., and J. H. Healy, Seismic refraction measure-
1963 ments of coastal structure between Santa Monica Bay and Lake Mead, U.S.G.S., Technical Letter No. 7.

Romney, C., Amplitudes of seismic body waves from under-
1959 ground nuclear explosions, J. Geophys. Res., 64, 1489-1498.

Ryall, A., P waves, Bull. Seism. Soc. Am., 52, 235-273.
1962

Ryall, A., and D. Stuart, Travel times and amplitudes from
nuclear explosions: Nevada test site to Ordway,
1963 Colorado, U.S.G.S., Technical Letter No. 10.

Santo, T. A., and M. Båth, Crustal structure of the Pacific
1963 Ocean from dispersion of Rayleigh waves, Bull. Seism. Soc. Am., 53, 151-166.

Sato, R., Love waves propagated across a transitional zone,
1961 Japanese J. of Geophys., 2, 117-134.

Sato, Y., Analysis of dispersed surface waves by means of
1955 Fourier transform I, Bull. Earth. Res. Inst. (Tokyo) 33, 33-48.

Savarensky, E. F., On the determination of group and phase
1959 velocities from observations, Izvest, Akad. Nauk, SSSR, Geo. Ser., 11, 1550-1559.

Shor, G., Crustal structure and reflections from the
1954 Mohorovicic discontinuity in Southern California, Ph.D. Thesis, California Institute of Technology.

Shor, G., and R. W. Raitt, Seismic studies in the Southern
1958 California borderland, S 10 Reference 58-78, Marine Physical Lab., Scripps Inst. of Oceanography.

Smith, S. W., A reinterpretation of phase velocity data
1962 based on the GNOME travel time curves, Bull. Seism. Soc. Am., 52, 1031-1036.

Steinhart, J. S., and R. P. Mayer, Explosion studies of
1961 continental structure, Carnegie Inst. of Wash. Publication 622, Washington, D. C.

Stewart, S. W., and L. C. Pakiser, Crustal structure in
1962 eastern New Mexico interpreted from the GNOME explosion, Bull. Seism. Soc. Am., 52, 1017-1030.

Stoneley, R., On the apparent velocity of earthquake waves
1935 over the surface of the earth, Mon. Not. Roy. Astron. Soc. Geo. Suppl., 3, 262-271.

Sykes, L., M. Landisman, and Y. Sato, Mantle shear velocities
1962 determined from oceanic Love and Rayleigh wave dispersion, J. Geophys. Res., 67, 5257-5271.

Toksoz, M. N., and D. L. Anderson, Generalized two-dimension-
1963 al model seismology with application to anisotropic earth models, J. Geoph. Res., 68, 1121-1130.

Tolstoy, I., Dispersion and simple harmonic point sources
1955 in wave ducts, J. Acoust. Soc. Am., 27, 897-907.

1956 Resonant frequencies and high modes in layered wave guides, J. Acoust. Soc. Am., 28, 1183-1192.

1959 Modes, rays and travel times, J. Geophys. Res., 64, 815-823.

Tolstoy, I., and E. Usdin, Dispersive properties of strati-
1953 fied elastic and liquid media, a ray theory, Geophysics, 18, 844-870.

Tolstoy, I., and E. Usdin, Wave propagation in elastic
1957 plates: low and high mode dispersion, J. Acoust. Soc. Am., 29, 37-42.

Tranter, C., Integral Transforms in Mathematical Physics,
1956 Wiley and Sons, Inc., New York, 133 pp.

Tryggvason, E., Crustal structure of the Iceland region
1962 from dispersion of surface waves, Bull. Seism. Soc. Am., 52, 359-388.

Werth, G., and R. Herbst, Comparison of amplitudes of
1963 seismic waves from nuclear explosions in four mediums, J. Geophys. Res., 68, 1463-1476.

Woollard, G. P., Crustal structure from gravity and seismic
1959 measurements, J. Geophys. Res., 64, 1921-1944.

Yoshiyama, R., The ratio of P and S waves, Bull. Earthquake
1958 Res. Inst. (Tokyo), 35, 627-640.

# LIST OF TABLES

TABLE 1

SUMMARY OF OCEANIC SOURCES USED

| Date | Location | Lat. | Long. | Origin Time | Mag. |
|---|---|---|---|---|---|
| 1957 Dec 17 | E. Santa Cruz Is | 12 S | 167 E | 13:50:05 | 7 3/4 |
| 1958 May 31 | New Hebrides Is | 15 S | 169 E | 19:32:30 | 7½ |
| Aug 6 | W. Tonga Is | 17 S | 173 W | 21:09:09 | 6 3/4 |
| Aug 20 | New Hebrides Is | 14 S | 167 E | 09:40:07 | 6¼-6½ |
| Sept 22 | Kermadec Is | 33½S | 177½W | 19:05:44 | 6 3/4 |
| 1959 Apr 12 | Samoa Is | 15½S | 173 W | 20:54:00 | 6-6½ |
| May 31 | Solomon Is | 6½S | 155 E | 00:28:09 | 6½ |
| Aug 24 | Solomon Is | 10½S | 161 E | 21:30:46 | 7 |
| Sept 14 | Kermadec Is | 28½S | 177 W | 14:09:39 | 7 3/4 |
| Sept 29 | W. Kermadec Is | 29 S | 176½W | 15:31:57 | 6½-6 3/4 |
| 1960 Mar 8 | New Hebrides Is | 16½S | 168½E | 16:33:38 | 7-7¼ |
| 1961 July 6 | New Hebrides Is | 20 S | 169 E | 22:09:31.4 | 6½ |
| Aug 1 | Solomon Is | 9.8S | 160.5E | 05:39:53.2 | 6½-6 3/4 |

TABLE 2

SUMMARY OF CONTINENTAL SOURCES USED

| Date | Location | Lat(N) (Deg.) | Long(W) (Deg.) | Origin Time (GCT) | Mag. | Depth (km) |
|---|---|---|---|---|---|---|
| 1962 | | | | | | |
| Aug 30 | Utah | 41.8 | 111.8 | 13:35:28.7 | 5 3/4-6 | 37 |
| Sept 5 | Utah | 40.7 | 112.0 | 16:04:29.0 | 5.0 | 14 |
| 1959 | | | | | | |
| May 24 | Oaxaca, Mex | 17.5 | 97.0 | 19:17:40.0 | 6 3/4-7 | 100 |
| Aug 18 | Montana | 44.81 | 111.07 | 06:37:15.0 ±2.3 | 7.1 | 25 |
| Aug 18 | Montana | 45.0 | 111.0 | 07:56:18.0 | 6.5 | 25 |
| Aug 18 | Montana | 44.8 | 110.7 | 08:41:50.0 | 6.0 | 25 |
| Aug 18 | Montana | 44.8 | 111.1 | 11:03:52.0 | 5½-5 3/4 | 25 |
| Aug 18 | Montana | 44.88 | 110.73 | 15:26:06.5 | 6½ | 25 |
| Aug 19 | Montana | 44.9 | 111.63 | 04:04:03.0 | 6 | 25 |
| Sept 26 | Oregon Cst. | 43.5 | 128.5 | 08:20:51.0 | | |
| 1956 | | | | | | |
| June 28 | Vancouver Is. | 48.75 | 129.25 | 22:58:50.0 | 6¼-6½ | 25 |
| 1952 | | | | | | |
| April | Oklahoma | 35.38 | 97.78 | 16:29:34.4 | | |

TABLE 3

DISTANCES AND AZIMUTHS BETWEEN STATIONS
IN SOUTHERN CALIFORNIA

| STATION | LATITUDE(N) deg | min | sec | LONGITUDE(W) deg | min | sec | DISTANCE (Deg) | DISTANCE (km) | AZIMUTH (Deg) |
|---|---|---|---|---|---|---|---|---|---|
| Barrett | 32 | 40 | 48.0 | .116 | 40 | 18.0 | | | |
| St. Nicholas | 33 | 15 | 00.0 | .119 | 31 | 24.0 | 2.463 | 274.0 | 284.1 |
| Palos Verdes | 33 | 45 | 30.0 | .118 | 21 | 24.0 | 1.775 | 197.4 | 307.7 |
| Pasadena | 34 | 08 | 54.0 | .118 | 10 | 18.0 | 1.928 | 214.4 | 319.8 |
| Riverside | 33 | 59 | 36.0 | .117 | 22 | 30.0 | 1.436 | 159.7 | 336.0 |
| Palomar | 33 | 21 | 12.0 | .116 | 51 | 42.0 | .690 | 76.8 | 346.7 |
| Hayfield | 33 | 42 | 24.0 | .115 | 38 | 12.0 | | | |
| St. Nicholas | 33 | 15 | 00.0 | .119 | 31 | 24.0 | 3.280 | 364.8 | 263.1 |
| Pasadena | 34 | 08 | 54.0 | .118 | 10 | 18.0 | 2.153 | 239.5 | 282.5 |
| Riverside | 33 | 59 | 36.0 | .117 | 22 | 30.0 | 1.475 | 164.0 | 281.7 |
| Palomar | 33 | 21 | 12.0 | .116 | 51 | 42.0 | 1.082 | 120.4 | 251.3 |
| Barrett | 32 | 40 | 48.0 | .116 | 40 | 18.0 | 1.342 | 149.3 | 220.6 |
| Tinemaha | 37 | 03 | 18.0 | .118 | 13 | 42.0 | 3.955 | 439.8 | 328.4 |
| Palos Verdes | 33 | 45 | 30.0 | .118 | 21 | 24.0 | 2.267 | 252.1 | 272.1 |
| Palomar | 33 | 21 | 12.0 | .116 | 51 | 42.0 | | | |
| St. Nicholas | 33 | 15 | 00.0 | .119 | 31 | 24.0 | 2.231 | 248.2 | 268.1 |
| Palos Verdes | 33 | 45 | 30.0 | .118 | 21 | 24.0 | 1.312 | 145.9 | 288.3 |
| Pasadena | 34 | 08 | 54.0 | .118 | 10 | 18.0 | 1.349 | 150.0 | 306.4 |
| Riverside | 33 | 59 | 36.0 | .117 | 22 | 30.0 | .768 | 85.5 | 326.3 |
| Barrett | 32 | 40 | 48.0 | .116 | 40 | 18.0 | .690 | 76.8 | 166.6 |
| Tinemaha | 37 | 03 | 18.0 | .118 | 13 | 42.0 | 3.858 | 429.1 | 343.5 |
| Palos Verdes | 33 | 45 | 30.0 | .118 | 21 | 24.0 | | | |
| St. Nicholas | 33 | 15 | 00.0 | .119 | 31 | 24.0 | 1.098 | 122.2 | 242.8 |
| Pasadena | 34 | 08 | 54.0 | .118 | 10 | 18.0 | .418 | 46.5 | 21.5 |
| Riverside | 33 | 59 | 56.0 | .117 | 22 | 30.0 | .849 | 94.5 | 73.7 |
| Palomar | 33 | 21 | 12.0 | .116 | 51 | 42.0 | 1.312 | 145.9 | 107.5 |
| Barrett | 32 | 40 | 48.0 | .116 | 40 | 18.0 | 1.775 | 197.4 | 126.8 |
| Tinemaha | 37 | 03 | 18.0 | .118 | 13 | 42.0 | 3.290 | 365.9 | 1.8 |
| Pasadena | 34 | 08 | 54.0 | .118 | 10 | 18.0 | | | |
| St. Nicholas | 33 | 15 | 00.0 | .119 | 31 | 24.0 | 1.439 | 160.1 | 231.9 |
| Palos Verdes | 33 | 45 | 30.0 | .118 | 21 | 24.0 | .418 | 46.5 | 201.6 |
| Riverside | 33 | 59 | 36.0 | .117 | 22 | 30.0 | .679 | 75.5 | 102.9 |
| Palomar | 33 | 21 | 12.0 | .116 | 51 | 42.0 | 1.349 | 150.0 | 125.6 |
| Barrett | 32 | 40 | 48.0 | .116 | 40 | 18.0 | 1.928 | 214.4 | 139.0 |
| Tinemaha | 37 | 03 | 18.0 | .118 | 13 | 42.0 | 2.900 | 322.5 | 359.1 |

TABLE 3 (Cont.)

DISTANCES AND AZIMUTHS BETWEEN STATIONS
IN SOUTHERN CALIFORNIA

| STATION | LATITUDE(N) deg | min | sec | LONGITUDE(W) deg | min | sec | DISTANCE (Deg) | DISTANCE (km) | AZIMUTH (Deg) |
|---|---|---|---|---|---|---|---|---|---|
| Riverside | 33 | 59 | 36.0 | .117 | 22 | 30.0 | | | |
| St. Nicholas | 33 | 15 | 00.0 | .119 | 31 | 24.0 | 1.939 | 215.7 | 248.1 |
| Palos Verdes | 33 | 45 | 30.0 | .118 | 21 | 24.0 | .849 | 94.5 | 254.3 |
| Pasadena | 34 | 08 | 54.0 | .118 | 10 | 18.0 | .679 | 74.5 | 283.4 |
| Palomar | 33 | 21 | 12.0 | .116 | 51 | 42.0 | .768 | 85.5 | 146.0 |
| Barrett | 32 | 40 | 48.0 | .116 | 40 | 18.0 | 1.436 | 159.7 | 155.6 |
| Tinemaha | 37 | 03 | 18.0 | .118 | 13 | 42.0 | 3.133 | 348.4 | 347.4 |
| St. Nicholas | 33 | 15 | 00.0 | .119 | 31 | 24.0 | | | |
| Palos Verdes | 33 | 45 | 30.0 | .118 | 21 | 24.0 | 1.098 | 122.2 | 62.2 |
| Pasadena | 34 | 08 | 54.0 | .118 | 10 | 18.0 | 1.439 | 160.1 | 51.1 |
| Riverside | 33 | 59 | 36.0 | .117 | 22 | 30.0 | 1.939 | 215.7 | 66.9 |
| Palomar | 33 | 21 | 12.0 | .116 | 51 | 42.0 | 2.231 | 248.2 | 86.6 |
| Barrett | 32 | 40 | 48.0 | .116 | 40 | 18.0 | 2.463 | 274.0 | 102.6 |
| Tinemaha | 37 | 03 | 18.0 | .118 | 13 | 42.0 | 3.941 | 438.3 | 15.2 |
| Tinemaha | 37 | 03 | 18.0 | .118 | 13 | 42.0 | | | |
| St. Nicholas | 33 | 15 | 00.0 | .119 | 31 | 24.0 | 3.941 | 438.3 | 196.0 |
| Palos Verdes | 33 | 45 | 30.0 | .118 | 21 | 24.0 | 3.290 | 365.9 | 181.9 |
| Pasadena | 34 | 08 | 54.0 | .118 | 10 | 18.0 | 2.900 | 322.5 | 179.1 |
| Riverside | 33 | 59 | 36.0 | .117 | 22 | 30.0 | 3.133 | 348.4 | 166.9 |
| Palomar | 33 | 21 | 12.0 | .116 | 51 | 42.0 | 3.858 | 429.1 | 162.7 |
| Barrett | 32 | 40 | 48.0 | .116 | 40 | 18.0 | 4.548 | 505.8 | 163.2 |

TABLE 4

SIERRA STRUCTURES

Case S 70

| Layer Thickness D(km) | Compressional Velocity $\alpha$(km/sec) | Shear Velocity $\beta$(km/sec) | Density $\rho$(km/sec) |
|---|---|---|---|
| 4.0 | 5.10 | 3.00 | 2.50 |
| 4.0 | 5.73 | 3.40 | 2.67 |
| 5.5 | 5.93 | 3.60 | 2.72 |
| 7.0 | 6.33 | 3.70 | 2.78 |
| 3.0 | 6.33 | 3.85 | 2.85 |
| 16.0 | 7.40 | 4.10 | 3.20 |
| 16.0 | 7.40 | 4.10 | 3.20 |
| 15.0 | 7.40 | 4.10 | 3.20 |
| $\infty$ | 7.97 | 4.60 | 3.40 |

Case S 55

| Layer Thickness D(km) | Compressional Velocity $\alpha$(km/sec) | Shear Velocity $\beta$(km/sec) | Density $\rho$(km/sec) |
|---|---|---|---|
| 4.0 | 5.10 | 3.00 | 2.50 |
| 4.0 | 5.73 | 3.45 | 2.78 |
| 5.5 | 5.93 | 3.60 | 2.78 |
| 7.0 | 6.33 | 3.70 | 2.78 |
| 3.0 | 6.33 | 3.85 | 2.78 |
| 16.0 | 7.59 | 4.25 | 3.20 |
| 16.0 | 7.59 | 4.25 | 3.20 |
| 20.0 | 7.50 | 4.25 | 3.20 |
| $\infty$ | 8.10 | 4.65 | 3.47 |

Case S 10

| Layer Thickness D(km) | Compressional Velocity $\alpha$(km/sec) | Shear Velocity $\beta$(km/sec) | Density $\rho$(km/sec) |
|---|---|---|---|
| 3.0 | 5.10 | 2.94 | 2.60 |
| 15.0 | 5.95 | 3.44 | 2.67 |
| 10.0 | 6.40 | 3.65 | 2.70 |
| 25.0 | 6.93 | 4.02 | 3.00 |
| $\infty$ | 7.98 | 4.50 | 3.25 |

TABLE 5

INSTRUMENT CALIBRATION

GALVANOMETER (OR PENDULUM) DAMPING

$$\theta'(0) = A$$

$$\theta(0) = 0$$

$$\theta(t) = A e^{-h\omega_g t} \frac{\sinh\left(\sqrt{h^2-1}\,\omega_g t\right)}{\omega_g \sqrt{h^2-1}}$$

$$\max_t \left[\theta(t)\right] = \theta(t_m) \qquad t_m = \frac{\tanh^{-1}\left(\sqrt{h^2-1}/h\right)}{\sqrt{h^2-1}} \frac{T_g}{2\pi} = \alpha \frac{T_g}{2\pi}$$

| h | $\alpha$ | $t_m$ $T_p=1$ | $t_m$ $T_g=85$ | $t_m$ $T_g=90$ | $t_m$ $T_g=95$ |
|---|---|---|---|---|---|
| .9 | 1.1 | .175 | 14.85 | 15.7 | 16.6 |
| 1.0 | 1.0 | .158 | 13.5 | 14.3 | 15.1 |
| 1.05 | .98 | .156 | 13.3 | 14.0 | 14.8 |
| 1.1 | .965 | .1533 | 13.1 | 13.8 | 14.6 |
| 1.2 | .94 | .1492 | 12.75 | 13.45 | 14.2 |
| 1.3 | .912 | .145 | 12.35 | 13.05 | 13.8 |
| 1.4 | .885 | .1408 | 12.0 | 12.65 | 13.4 |
| 1.5 | .86 | .137 | 11.65 | 12.3 | 13.0 |
| 1.7 | .82 | .130 | 11.1 | 11.7 | 12.4 |
| 2.0 | .766 | .122 | 10.4 | 11.0 | 11.6 |
| 3.0 | .641 | .102 | 8.7 | 9.16 | 9.7 |

# APPENDICES

# APPENDIX A

## EXPERIMENTAL MEASUREMENT OF PHASE VELOCITY DISPERSION

In the following paragraphs a summary of the techniques available for experimental measurements of phase velocity in both the time domain and frequency domain are given along with some of the requirements and assumptions involved in each.

### I. TIME DOMAIN ANALYSIS

#### A. Recording Conditions

To obtain phase velocity dispersions from records in the time domain alone, several conditions of recording must be met.

(1) The three or more stations used must have approximately matched instruments so that crests, zeros, and troughs may be reliably correlated across the array.

(2) The dimensions of the array must be of the order of a wave length for the shortest period of interest so that phase correlation is possible.

(3) Timing must be accurate enough to give the desired precision in phase velocity.

(4) Distances and azimuths between stations must be accurately known.

#### B. Data

(1) Correlate and successively number extrema (crests, zeros, troughs) across the array such that extremum

number k at one station is also extremum number k at each of the other stations. ($k/4 = 0,1,2,3,\ldots$ when zeros, crests, and troughs are all used.)

(2) Measure the arrival time of each extremum and plot arrival time versus extremum number at each station. For a given phase* the slope of this curve gives its period. Horizontal components of Rayleigh waves may be included to give a composite curve, if the extremum numbers are changed by $\pm\frac{1}{4}$ to allow for the $\pi/2$ phase difference between the horizontal and vertical displacements. The period to be associated with the phase velocity of a particular crest, zero, or trough is the mean of the individual periods from all the stations for that phase (Savarensky, 1959, pp. 1106).

(3) Choose the $m^{th}$ station as a standard and apply a correction to the arrival time of the $k^{th}$ peak at the $i^{th}$ station given by

$$ {}_k\epsilon_{mi} = \left[ {}_kT_i\,\varphi({}_kT_i) - {}_kT_m\,\varphi({}_kT_m) \right] / 2\pi \qquad (1) $$

where ${}_kT_i$ is the period of the $k^{th}$ peak at the $i^{th}$ station and $\varphi({}_kT_i)$ is the instrument phase delay in radians for period ${}_kT_i$. It should be noted that if there is dispersion, this correction, in general, cannot be zero, even if the instruments are perfectly matched, since

$${}_kT_i \neq {}_kT_m \qquad \varphi({}_kT_i) \neq \varphi({}_kT_m) \text{ and } \varphi(T) \neq \text{CONSTANT.}$$

---

*A phase is defined as any feature on the seismogram which can be correlated from one station to another, such as a peak, zero, trough, impulse, etc. In this case a single period may be assigned to each phase.

Instrument mismatch also is taken into account by this correction.

(4) Compute the distance and azimuth of each of the stations from some arbitrarily chosen "pseudo-origin." for the tripartite method distances and azimuths between stations are required. It is useful to know the distances and azimuths from the epicenter as well, as will be seen presently.

Since the method of computing phase velocity assumes plane wave fronts, errors occur because this assumption is violated for earthquake or explosion sources. In most cases only distant events are used so that this effect is not important. However, a correction can be made to take curvature of the wave fronts into account. The center station of the array (with respect to the source) is taken as a standard and a correction to the arrival times of corresponding phases at other stations is applied.

This correction can be approximated by

$$t_j = dr_j / \bar{C} \qquad (2a)$$

$$dr_j = \frac{D_j^2}{2r}\left[1 - \frac{D_j^2}{12r} + \mathcal{O}\left(\frac{D_j^2}{r^3}\right)\right] \qquad (2b)$$

Where

$r$ = mean of the epicentral distances of the reference station and the $j^{th}$ station

$D_j$ = mean arc distance from the reference station to the $j^{th}$ station given by $r|\alpha_j - \alpha_0|$

$\alpha_j$ = azimuth from $j^{th}$ station back to source

$\bar{C}$ = mean phase velocity for the phase being measured

Another more precise way of correcting for this effect is to form a pseudo-array by modifying the station coordinates in the following way:

$\Phi_j = \varphi_j + dr_j \sin\alpha_j$ (pseudo-longitude of $j^{th}$ station)

$\Theta_j = \theta_j + dr_j \cos\alpha_j$ (pseudo-latitude of $j^{th}$ station)

where

$\varphi_j$ = true longitude of $j^{th}$ station

$\theta_j$ = true geographical latitude of $j^{th}$ station

$\alpha_j$ = azimuth from $(\varphi_j, \theta_j)$ back to the source

$dr_j$ = same as in equation 2b above

This correction modifies distances between stations so that the curved wave fronts are effectively plane. This correction is the most accurate of the two suggested, although more computation is required, since distances between stations must be recomputed for each event analyzed.

Some caution should be exercised in applying this correction when the travel path from the source to the array traverses transition zones, because lateral refraction effects may significantly alter the location of the "effective" epicenter (see Appendix B).

C. Methods

Given data in the form described above, it is then possible to compute the phase velocity by one of the

following methods.

(1) One Station Method

Using a single station, phase velocity may be computed for either (a) multiple transits of the same wave train around the earth, or (b) wave trains for which the initial phase at the source is known or assumed.

Then

$$C(\overline{T}_k) = \frac{r}{{}_k\tau} \qquad (3)$$

where

$r$ = geodesic distance around the earth for (a) above, or epicentral distance for (b) above

${}_k\tau$ = travel time of $k^{th}$ extremum around the earth for (a) above, or travel time from the epicenter for (b) above, including initial phase at the source.

$\overline{T}_k$ = average period of the $k^{th}$ extremum

This method has the advantage of simplicity and no requirement of plane wave fronts.

It has the disadvantages that it assumes the surface waves follow a geodesic on the earth's surface, that averaging the periods in case (a) may introduce significant errors (Savarensky, 1959), and that it requires knowledge or assumption of initial phase at the source.

(2) Two Station Method

Using any two stations not equidistant from the source the phase velocity of the $k^{th}$ extremum is given by

$$C(\overline{T}_k) = \frac{r_2 - r_1}{{}_k\tau_2 - {}_k\tau_1} \qquad (4)$$

where

$r_i$ = epicentral distance of $i^{th}$ station

${}_k\tau_i$ = arrival time of $k^{th}$ extremum at $i^{th}$ station

$\overline{T}_k$ = average period of $k^{th}$ extremum

Advantages of this method are that the numerical calculation is simple and that the wave fronts need not be plane.

Disadvantages are that the direction of propagation to each station is assumed to be along a geodesic, when often this is not the case, it assumes no azimuthal variation of initial phase at the source, and it assumes no azimuthal difference in velocity over the distances $r_i$ for the two azimuths involved. These disadvantages are minimized if the two stations are on the same azimuth from the source.

(3) Tripartite Method

Using any array of three non-colinear stations across which phases can be correlated, the phase velocity

and direction of propagation can be determined for that array by the technique described in Figure 33. The first to apply this technique was Press in a study of crustal structure in California (Press, 1956).

The phase velocity of the $k^{th}$ phase is given by

$$C_k = \frac{\Delta_{12} \sin A_k}{{}_k\tau_{12}} = \frac{\Delta_{13} \sin (A_k + \alpha)}{{}_k\tau_{13}} \quad (5)$$

and the direction of propagation by

$$A_k = \tan^{-1}\left[\frac{\sin\alpha}{\frac{{}_k\tau_{12}\Delta_{13}}{{}_k\tau_{13}\Delta_{12}} - \cos\alpha}\right]$$

where

$\Delta_{1j}$ = distance from station 1 to station i (i = 2, 3)

${}_k\tau_{1i}$ = measured travel time of $k^{th}$ phase from station 1 to station i, corrected by ${}_k\epsilon_{1i}$ as defined in equation 1 above

$\alpha$ = angle between stations 2 and 3 measured from station 1

Basic assumptions in this technique are (1) that the wave fronts are plane and (2) that the underlying structure is laterally homogeneous over the dimensions of the array.

Advantages of this method are (1) that one need not know the source location, (2) direction of propagation is measured rather than assumed, (3) greater precision in phase velocity results from the fact that distance

between stations can be more accurately determined than epicentral distance, and (4) the average period of each phase is determined from three measurements instead of two.

Disadvantages are that no measure of precision can be assigned to the phase velocity and direction of propagation and no check is available on the assumption of homogeneity and plane wave fronts.

(4) Least Squares Method

Given the arrival time of a particular phase and the geographical co-ordinates appropriate for each station of a multi-partite array of N stations, the best (in the least squares sense) phase velocity and direction of propagation for that phase may be determined, as well as an error estimate for each.

The idea was first used by Aki in a study of dispersion in Japan (Aki, 1961). With minor modifications the technique is summarized in Figure 34. The arrival time of the $k^{th}$ phase at the $i^{th}$ station is given by

$$\tau_{ik} = \Delta_i \cos\alpha_i \frac{\cos\theta_k}{C_k} + \Delta_i \sin\alpha_i \frac{\sin\theta_k}{C_k} + \tau_{ok} \qquad (6)$$

$$= a_i x + b_i y + c_i z$$

where

$\Delta_i$ = distance of the $i^{th}$ station from an arbitrary pseudo-origin

$\alpha_i$ = azimuth of the $i^{th}$ station from the pseudo-origin

$\tau_{ok}$ = predicted arrival time of the $k^{th}$ phase at pseudo-origin

$\theta_k$ = direction of propagation of $k^{th}$ phase across the array

$C_k$ = phase velocity of $k^{th}$ phase across the array

$$x = \frac{\cos \theta_k}{C_k}$$

$$y = \frac{\sin \theta_k}{C_k}$$

$$z = \tau_{0k}$$

Therefore,

$$\theta_k = \tan^{-1}(y/x) \qquad (7)$$

$$C_k = (x^2 + y^2)^{\frac{1}{2}}$$

$$\sigma_\gamma = \left[\sum_j \left(\sigma_{u_j} \frac{\partial \gamma}{\partial u_j}\right)^2\right]^{\frac{1}{2}}$$ standard deviation of $\gamma$

$\gamma(u_1, u_2, \cdots, u_j) \equiv \gamma(x, y, z)$

$$\overline{T}_k = \frac{\sum_{i=1}^{N} T_i}{N}$$ average period

The advantages of this method are that (1) it gives error estimates for phase velocity and direction of propagation, (2) $a_i$, $b_i$, and $c_i$ in equation 6 above, being independent of direction of propagation, are determined once for all, so that subsequent events require measurement only of arrival times of phases correlated across the array, (3) the average period $\overline{T}_k$, determined

from N measurements, is more reliable, (4) it affords an opportunity to check the assumption of lateral homogeneity and plane wave fronts by replacing a station by the "pseudo-origin" and determining the difference between the predicted and observed arrival time of each phase, and (5) all those previously mentioned for the tripartite method.

Disadvantages are that the computation requires either a high speed digital computer or much laborious hand calculations.

## II. FREQUENCY DOMAIN ANALYSIS

### A. Data Requirements

To compute phase velocity in the frequency domain the following data requirements should be satisfied.

(1) Digital samples of each analog signal at intervals $\Delta t$ such that the shortest period visible on the record is $\geq 2\Delta t$. This minimizes errors due to aliasing (Blackman and Tukey, 1958).

(2) The beginning time $t_1$ and ending time $t_2$ should be such that there is zero signal for $t \leq t_1$ and for $t \geq t_2$. This insures that at each station all of the transient signal is included for the computation of the Fourier transform.

When more than one dispersed wave train is included in $t_2-t_1$, certain digital filtering operations (described in Appendix F) can be performed to insure that only one mode is analyzed at a time. This is important,

since the Fourier transform will mix the phases from two such transients and lead to serious errors in phase velocity.

(3) Instrument phase response at each station must be known as a function of frequency.

(4) Relative time among all the stations must be known very accurately; hence, some time standard must be established which is common to all the stations.

(5) The co-ordinates (latitude and longitude) must be accurately known for each station, so that the necessary distances and azimuths can be computed.

B. Methods

All the methods in the frequency domain are identical to those in the time domain when the travel time of a particular phase of average period T between stations is replaced by

$$\delta t_{ij} = t_i - t_j + T[\varphi_j(T) - \varphi_i(T) \pm N_{ij}] \qquad (8)$$

where

$t_i$ = the time (with respect to some standard common to all the stations) of the first digital sample at the $i^{th}$ station

$t_j$ = the time (with respect to the same standard as $t_i$) of the first digital sample at the $j^{th}$ station

$\varphi_i(T)$ = observed phase (fractions of a circle) with respect to $t_i$ at the $i^{th}$ station minus the instrument phase for period T at the $i^{th}$ station

$\varphi_j(T)$ = observed phase (fractions of a circle) with respect to $t_j$ at the $j^{th}$ station minus the instrument phase for period T at the $j^{th}$ station

$N_{ij}$ = arbitrary integer, which, once determined, remains fixed for all T

To show that this transformation is valid, consider the propagating transient wave train at a distance r from the source and represent it (Sato, 1955) by

$$f(t,r) = \int_{-\infty}^{\infty} F(\omega,r)\, e^{i\left[\omega\left(t-\frac{r}{C(\omega)}\right)+\beta(\omega)\right]} \frac{d\omega}{2\pi} \qquad (9)$$

where

$F(\omega,r)$ = amplitude spectrum at distance r

$C(\omega)$ = phase velocity dispersion

$\beta(\omega)$ = initial phase at the source

$\omega$ = frequency (radians/sec)

Then the Fourier transform of f(t,r) with respect to time is given by

$$\int_{-\infty}^{\infty} f(t,r)\, e^{-i\omega t}\, dt = A(\omega,r)\, e^{i\psi(\omega)} = F(\omega,r)\, e^{i\left[-\frac{\omega r}{C(\omega)}+\beta(\omega)\pm 2n\pi\right]} \qquad (10)$$

Thus taking the ratio of the transforms at two stations, the $i^{th}$ and $j^{th}$, say, one obtains

$$\frac{F(\omega, r_j)}{F(\omega, r_i)} e^{i[\omega(r_i - r_j)/C(\omega) \pm 2\pi(n_i - n_j)]} = \frac{A(\omega, r_j)}{A(\omega, r_i)} e^{i[\psi_j(\omega) - \psi_i(\omega)]} \qquad (11)$$

Note that the initial phase at the source cancels. Equating the phases in equation 11 (assuming F(w,r) and A(w,r) are real for all r) and solving for C(T) one gets

$$C(T) = \frac{r_i - r_j}{T\left[\left(\psi_j(T) - \psi_i(T)\right)/2\pi \pm N_{ij}\right]} \qquad (12)$$

where

$N_{ij} = n_i - n_j$ = an integer

$T = \frac{2\pi}{\omega}$ = period

To get equation 12 in a more tractable form for computational use one can rewrite equation 10 as follows

$$\int_{-\infty}^{\infty} f(t,r) e^{-i\omega t} dt = \int_{t_i}^{t_i + D} f(t,r) e^{-i\omega t} dt = e^{-i\omega t_i} \int_0^D f(\tau, r) e^{-i\omega\tau} d\tau$$

$$= A(\omega, r) e^{i[2\pi\varphi(\omega, r) - \omega t_i]} \qquad (13)$$

where

$\tau = t - t_1$

D = duration of the transient f(t,r) which has the property that it is identically zero for $t \leq t_1$ and for $t \geq t_1 + T$ at distance r

Therefore, equating the phase in equation 10 with that in equation 13 and substituting $\omega = 2\pi/T$ one gets

$$\frac{\psi(T,r)}{2\pi} = \varphi(T,r) - t_1/T \qquad (14)$$

so that equation 12 becomes

$$C(T) = \frac{r_i - r_j}{t_i - t_j + T(\varphi_j(T) - \varphi_i(T) \pm N_{ij})} \qquad (15)$$

where*

$t_i = (t_1)_i$ time of first digital sample at $i^{th}$ station

$t_j = (t_1)_j$ time of first digital sample at $j^{th}$ station

Hence, it can be seen that equation 4 in the time domain and equation 15 are connected through equation 8.

---

*Note that $\varphi_k$ is the phase obtained when the Fourier transform is defined by $\int_{-\infty}^{\infty} f(t) e^{-i\omega t} dt$ . If $e^{i\omega t}$ were used, then

$\varphi_k(\omega) \rightarrow -\varphi_k(\omega)$ in equation 15.

For a multi-station array of L stations one should choose one station as a standard, say the $m^{th}$ station, and determine the $N_{mj}$ (all $j \neq m$). Then the $\delta t_{mj}(T)$ can be determined and used in any of the time domain formulas previously given in this Appendix. In the least squares formulation set the arrival time at the $m^{th}$ station to zero and use $\delta t_{mj}(T)$ for the arrival time of period $T$ at the $j^{th}$ station.

When uncontaminated wave trains are available, frequency domain analysis is preferable, since it involves no errors in determining the period and allows exact correction for instrumental phase delay. Frequency domain analysis is essential for computing dispersion for cases where the group velocity dispersion is slight, such as the mantle G waves. It is also essential when the dimensions of the array are so large that phase correlation in the time domain is not reliable, as well as when the instruments used are not matched.

In addition, frequency domain analysis provides the amplitude spectrum of the signal as a byproduct of the phase determination.

Disadvantages are the necessity of a high speed digital computer, the necessity of analog to digital conversion, and the danger of phase distortions being introduced when more than one transient (such as a higher mode) is included in the time series analyzed.

# APPENDIX B

## LATERAL REFRACTION OF SURFACE WAVES

If a surface wave is obliquely incident on a boundary S separating regions of different velocity structure, this wave is laterally refracted in a manner governed by the phase velocities in the two regions (Stonely, 1934; Evernden, 1954). The signal arriving at a station B from a source at point A across the boundary is given by

$$\int_S \int_{-\infty}^{\infty} f(\omega)\, g(\theta)\, e^{i\omega\left(t - r_1/C_1(\omega) - r_2/C_2(\omega)\right)} \, d\omega \, ds \qquad (1)$$

where

$g(\theta)$ = source function of azimuth

$f(\omega)$ = source function of frequency

$C_1(\omega)$ = phase velocity in 1st medium

$C_2(\omega)$ = phase velocity in 2nd medium

$r_1$ = epicentral distance from A to intersection with boundary S

$r_2$ = distance from intersection of $r_1$ and S to station B

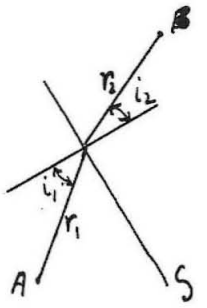


Making equation 1 stationary with respect to $\omega$ and s, assuming $f(\omega)$ and $g(\theta)$ are slowly varying functions of $\omega$ and s, gives

$$\frac{d}{d\omega}\left[\omega t - r_1 C_1^{-1}(\omega) - r_2 C_2^{-1}(\omega)\right] = t - r_1 \frac{d}{d\omega}\left(\omega C_1^{-1}(\omega)\right) - r_2 \frac{d}{d\omega}\left(\omega C_2^{-1}(\omega)\right)$$

$$= t - r_1/U_1(\omega) - \frac{r_2}{U_2(\omega)} = 0 \quad \text{(travel time)} \qquad (2)$$

$$\frac{d}{ds}\left[\omega t - r_1 C_1^{-1}(\omega) - r_2 C_2^{-1}(\omega)\right] = \frac{1}{C_1(\omega)}\frac{dr_1}{ds} + \frac{1}{C_2(\omega)}\frac{dr_2}{ds} = 0$$

(lateral refraction) (3)

If S is a linear boundary, then $\frac{dr_1}{ds} = \sin i_1$, $\frac{dr_2}{ds} = -\sin i_2$,

so that equation 3 above becomes

$$\frac{\sin i_1}{C_1(\omega)} = \frac{\sin i_2}{C_2(\omega)}$$

Since in general $C_1(\omega)/C_2(\omega) \neq$ constant, the angle of refraction $i_2$ is a function of $\omega$, so that the spectrum of $i_1(\omega)-i_2(\omega)$ is a measure of the relative phase velocity contrast between the two regions.

For more complicated geometry equation 1 may be appropriately evaluated to determine the distortion of each wave front due to crossing the boundary S. This type of analysis would be pertinent in studies of beat phenomena and other complications often observed in the surface wave portion of seismograms.

Strike of Linear Features

In the case where the boundary S is linear and $r_1$ is sufficiently great that the wave fronts may be considered plane, one can use the measured refraction of surface waves to determine the "strike" of the boundary S, as well

as to assign a lower bound on the phase velocity in the other region by a technique which is outlined in Figure 44.

The angles $\beta_i(\omega)$ are obtained from the difference between the measured direction of propagation and the geodesic direction back to the source. The intersection with the $\alpha$ axis gives the strike of the boundary for each frequency.

In this way the orientation of the velocity boundary with depth may be inferred, since the depth sampled by surface waves is frequency dependent.

Once the strike of this boundary is determined, then a bound on the phase velocity in the medium containing the source can be obtained. If the location of one point on the boundary is known, then estimates of the true phase velocity rather than a bound can be obtained.

In addition, the approximate extent of the velocity contrast with depth can be determined by using a range of frequencies and finding a frequency below which there is no appreciable refraction. The maximum depth of the discontinuity is, then, the depth to which this first unaffected frequency "sees." For example, this frequency for fundamental mode Rayleigh waves crossing from the Pacific to the continental United States in Southern California is .02 cps, corresponding to a wave length of the order of 150 km.

Effective Epicenter

For propagation from a high velocity material to a

low velocity material across a linear boundary the refraction is such that the "effective epicenter"* is moved further away from the boundary along the normal through the true epicenter. Conversely the effective epicenter is moved closer for propagation from low to high velocity material. This effect should be taken into account when the correction for curved wave fronts is made (see Appendix A). This effective epicenter changes for every frequency and for every different angle of incidence on the boundary. However, over the small range of angles of incidence spanning local arrays, the effective epicenter may be considered fixed for each frequency (but different from the actual epicenter).

Thus, lateral refraction of surface waves may provide a practical means of delineating the shape of boundaries between bodies of different velocity material. The procedure would be to use an array of dimension small compared to the radius of curvature of the boundary and measure the strike of a small segment of the interface, as outlined above. Moving this array or operating several arrays simultaneously will then permit mapping of the entire boundary.

In addition, many of the concepts of geometrical optics may be used to treat cases where the boundary separating the regions is not linear, compared to the dimensions of the

---

*This term is used to designate that geographical position from which the wave appears to come after it has been refracted across the boundary.

array(s) available. This type of approach may prove useful in explaining observed interference phenomena, different levels of background microseism noise from site to site, and the long coda often observed following the principal part of a surface wave train.

# APPENDIX C

## EXPERIMENTAL ERRORS

The experimental measurements presented in the text are subject to one or more of the sources of error to be enumerated and discussed in this Appendix.

I. Timing Errors: Absolute time could, for the most part, be determined to about .1 second at each station. Arrival time of phases (peaks and troughs) could be measured to better than .5 seconds on the long period instruments and to better than .3 on the short period instruments.

II. Distance Errors: Distances between points on the earth's surface can be computed with an accuracy of at least .1 km and azimuths to .01 degree. Thus, distances and azimuths between stations have accuracies of this order, since the station co-ordinates are known very precisely.

However, epicenter location is rarely better than ±5 km and often is an order of magnitude worse. The co-ordinates reported by the United States Coast and Geodetic Survey, the most common source of epicentral information, are given only to the nearest tenth of a degree, or about ±10 km. This means that epicentral distance may be in error by ±10 km.

III. Least Time Path Errors: Errors may result if the least time path travelled by the surface waves is not along a geodesic on the earth's surface. These errors are very difficult to estimate since the three-dimensional velocity distribution in the earth's crust and upper mantle, which controls this effect, is poorly known.

The late arrivals of surface wave energy commonly observed following many events can be attributed to such non-geodesic travel paths. Whenever possible, therefore, one should experimentally verify that the direction of propagation is nearly along a geodesic before computing average velocity using geodesic distances, or else attempt to estimate the true distance travelled.

Within geologic provinces these effects appear to be negligible for fundamental mode surface waves of period above about 10 seconds and for higher modes above about 2 seconds. However, for transmission through or near transition zones, these effects were found to be appreciable for periods of 40 seconds or more for the fundamental Rayleigh mode. Therefore, some care should be taken to test for these effects, even for the longer periods, when the wave train has traversed more than one geologic province.

IV. Phase Velocity

A. Time Domain

Errors in phase velocity measured in the time

domain may result from

(1) inaccurate distances between stations

(2) inaccurate travel time of a phase between stations

(3) inaccurate determination of the period to assign to a phase at each station

(4) interference effects

(5) instrument mismatch

(6) dispersion induced errors

(7) violations of assumptions made in the computational method

(8) microseism noise

The combined effects of these errors can cause an uncertainty of as much as 1 percent in the average phase velocity values obtained in this study using tripartite arrays. With the least squares technique standard deviations considerably under 1 percent were obtained for most events.

A maximum error of less than .2 percent can be attributed to (1) for the arrays used in this study.

The most significant error in phase velocity results from (2). At each station the arrival time of a phase can be determined to about .5 seconds which implies errors up to 2 percent in individual values of phase velocity. However, averaging the values from several events gives a resultant with a standard deviation of about .5 percent,

a value comparable with the other errors enumerated above. When the least squares technique was used, the standard deviations were, for the most part, well under 1 percent, even for individual events.

By smoothing the phase number vs. arrival time curve, errors due to (3) can be kept within about .5 percent.

Errors due to (4) may be considered insignificant, since only events which clearly could be correlated across the array were used. This is further substantiated by the smooth Fourier spectra (phase and amplitude) obtained for the events analyzed.

Errors due to (5) for individual tripartite arrays used are less than .5 percent for periods under 20 seconds and less than 1 percent for longer periods. Since the true magnitude of this error depends on the array dimensions, the direction of propagation, and the phase velocity, it may be more instructive to give the maximum differences in instrument phase delay. These differences can be obtained from Figure 41. With the exception of Riverside, all the stations used are matched to within .3 seconds in the period range studied and some combinations are matched considerably better. Below 20 seconds period all the instruments are matched to within about .15 second. When several stations are combined in the least squares technique, these errors are in effect further reduced, so that for the purposes of this investigation effects of

instrument mismatch may be neglected.

Errors due to (6) occur because the predominant period of a particular phase changes from station to station due to dispersion. Savarensky (1959) gives the following expression for this effect on phase velocity:

$$C(\tau) = \frac{\partial \Delta}{\partial t}\left[1 - \frac{1}{4}\frac{C}{U}\left(\frac{C}{U} - 1\right)\left(\frac{\delta\tau}{\tau}\right)^2\right]^{-1} \qquad (1)$$

where $\tau = (T_2 + T_1)/2$

$\delta\tau = T_2 - T_1$

$T_i$ = period at $i^{th}$ station

$\frac{\partial \Delta}{\partial t}$ = phase velocity of a particular extremum (peak, zero, trough) having period $T_i$ at the $i^{th}$ station

$C(\tau)$ = true phase velocity for period $\tau$

The second term in the bracket in equation 1 gives the error introduced by assigning to the observed velocity of a given phase the mean period $(T_2 + T_1)/2$, when that velocity is, in fact, appropriate for some other period in the interval between $T_2$ and $T_1$. The magnitude of this error depends on the group velocity dispersion of the medium and the distance between stations. For the arrays studied in Southern California, this error is never more than .5 percent, and for the most part it is considerably less. Hence this source of error can be neglected.

Another dispersion induced effect is given by the time delay $T_2\,\varphi_2(T_2) - T_1\,\varphi_1(T_1)$

where

$\varphi_i(T_i)$ = instrumental phase shift at the $i^{th}$ station

$T_i$ = period of a given phase at the $i^{th}$ station

Note that this error exists even when the two instruments are perfectly matched in phase, since $T_2 \neq T_1$ and $\varphi(T_2) \neq \varphi(T_1)$ in general. However, for the instruments used and dispersion encountered in this study this error amounts to less than .5 percent in phase velocity.

Effects of (7) are caused by either departure from plane wave fronts or strong lateral inhomogeneities under the array perpendicular to the direction of propagation. Corrections for the first can be made when necessary (see Appendix A). However, for the epicentral distances and array dimensions involved in this study departure from plane wave fronts introduces errors considerably less than .5 percent in phase velocity. A test for both these effects is provided by the least squares method. Using one of the station locations as the pseudo-origin one obtains the predicted arrival time for each phase at that station, as well as its standard deviation. If the observed and predicted arrival times agree, then the assumptions of the method are considered verified. For the events checked in this way the observed and predicted arrival times agree within the standard deviation, so the applicability of the method in Southern California is assured.

The effects of (8) are considered insignificant since

only large events with very high signal to noise ratios were used (see Figure 36, for example).

B. Frequency Domain

The sources of error discussed above for the time domain all exist for the frequency domain analysis, except (3) and (6). Of these, only (2) is different in its effect in the frequency domain. The travel time for period T between two stations is given by

$$\tau_{12} = \delta t_{12} + T(\delta\varphi_{12}(T) \pm N) \qquad (2)$$

where

$\delta t_{12}$ = difference in feducial time between the two records

$\delta\varphi_{12}(T)$ = measured phase difference (fractions of a circle) between the two stations for period T

$N$ = arbitrary integer

The error in phase velocity is given by

$$\frac{\Delta C}{C} = \frac{T\Delta[\delta\varphi_{12}(T)]}{\tau_{12}} \qquad (3)$$

It is very difficult to estimate the magnitude of $\Delta[\delta\varphi_{12}(T)]$ since it is made up of noise, both from microseisms and from digitizing and computation.

However, all of these errors may be considered random, so that the smoothness of the phase spectrum is an indication of the accuracy in phase determination.

Moreover, actually smoothing the phase spectrum can further reduce the effects of these errors. For the array dimensions and the period range considered in this study the maximum error in phase velocity due to the error in determining phase shift is estimated to be about .5 percent. Therefore the results from frequency domain analysis are also accurate to within 1 percent.

V. Group Velocity

Errors in group velocity result from

(1) inaccurate epicentral distance

(2) group delay of the instrument

(3) group delay of the source

(4) interference of modes

(5) errors in origin time

(6) timing errors on the seismogram

(7) period determination

(8) noise

Errors due to (1), given by $\frac{\partial U}{U} = \frac{\partial \Delta}{\Delta}$ result principally from inaccurate epicenter location and deviation from geodesic travel paths. The first introduces an error of less than 1 percent, since the epicenters used are located to ±10 km and the distances used are 1000 km or more. As well as could be determined, deviation from a geodesic travel path was not important, since the observed deviations from geodesic travel paths were small.

Errors due to (2) are very small since a correction

for this effect was made using the measured instrument response.

Errors due to (3) are difficult to estimate, since the effective time duration of the source is not known. It is assumed throughout that this error is small. The only check on this assumption is that several events of different magnitude from the same general area gave the same dispersion results to within about .5 percent.

Errors due to (4) result from interference of modes such that spurious group arrivals are obtained which are appropriate to no mode. Special care was taken to avoid this problem as much as possible. The fundamental mode is free of this type of error, as are the higher modes above about 7 seconds period. The increased scatter of the results at shorter periods is, in part, due to this source of error.

Errors due to (5) are less than 1 percent. In addition this error is partly compensated by the errors in epicenter location, since epicenter location and origin time are made consistent for body waves at many stations.

Errors due to (6) are much less than 1 percent, since the timing accuracy is .2 seconds or better.

Errors due to (7) are about 1 percent or less for periods above 7 seconds and roughly 2 percent at shorter periods, depending on the interference among modes and background noise.

The largest errors occur as a result of (8), since the signal to noise ratio for the short periods sometimes approaches unity, especially for the higher modes. The difficulty in distinguishing between microseism noise and higher mode signal may sometimes cause very large errors in measurements at an individual station. However, averaging the results for several events from the same source region at one station and/or the results from several different stations gives a resultant which is more trustworthy. The composite curves obtained in this study indicate an accuracy approaching 1 percent in group velocity for periods under 7 seconds. For the longer periods accuracies of 1 percent or better can easily be achieved.

# APPENDIX D

## MODEL EXPERIMENT

The peculiar phase velocity dispersion results obtained near the coast in Southern California prompted an ultrasonic model experiment to investigate the effects of sloping interfaces and changes in slope on Rayleigh wave propagation. No adequate theoretical treatment of the sloping interface problem exists. Numerous attempts have been made to solve this problem, but none have been very successful, even for the simpler Love wave problem. Therefore, analog models offer the best opportunity to investigate the effects of such structures at present.

The available refraction and gravity data were used as a basis to construct the model about to be described, so that it was a reasonable approximation of the structure at the continental margin of Southern California.

### Design of the Model

The model was designed such that a 1/4 inch layer increased with a slope of 5 degrees to a thickness of 1 inch (see Figure 45). This is the analog of an increase in crustal thickness from 10 km to 40 km. The compressional velocity was chosen to be the analog of

an average crustal velocity of 6.5 km/sec and a mantle velocity of 8.2 km/sec. The shear velocity contrast is the analog of 3.0 km/sec in the crust and 4.68 km/sec in the mantle. A density contrast of 1.6075 gm/cm$^3$ in the layer and 2.77 gm/sec$^3$ in the half space resulted.

Although this model is obviously oversimplified and the elastic parameters not an accurate representation of the true structure, it is considered adequate to allow a qualitative comparison of the model results with the real earth measurements.

It should be noted, however, that the only limitations in principle, to achieving precise analogs of earth models are in obtaining suitable materials and constructing the model with sufficiently small tolerances.

To achieve the desired compressional velocity in the layer the results of Healy and Press (1960) for controlling the velocity and density of a thin laminated plate were used. That is,

$$\overline{V}^2 = \sum_{i=1}^{N} \alpha_i \rho_i V_i^2 \Big/ \sum_{i=1}^{N} \alpha_i \rho_i \qquad (1)$$

where $\overline{V}$ = velocity of the composite laminated plate

$\alpha_i$ = thickness of $i^{th}$ layer

$\rho_i$ = density of $i^{th}$ layer

$V_i$ = shear or plate velocity in $i^{th}$ layer

N = number of layers in the composite.

In order that equation 1 hold, the total width D of the composite should be small compared to the shortest wavelength of interest. Therefore,

$D = \sum_{i=1}^{N} \alpha_i \ll \lambda_{min}$ is one condition which must always be satisfied.

The scaling was such that the period in microseconds corresponds reasonably closely to the period in seconds in the earth.

Model Construction

The model was fabricated from an aluminum sheet of dimensions 48" × 30" × .087". The contour of the desired crustal shape was uniformly milled from the aluminum to a remaining thickness of .022". The "depth" of this layer was .25" from 0-20 inches and 1" from 28-48 inches with a linear increase from 20-28 inches (see Figure 45). Epoxy resin plastic was poured onto this contour and allowed to solidify, restoring the total thickness of this laminated portion to .087". Shell Epon No. 828 plastic was used with 10 percent (by weight) diethylenetrianamene hardener.

The resulting elastic parameters of the model are given in the following table.

TABLE 7

MODEL PARAMETERS

| Material | Plate Velocity (inches/$\mu$sec) | Shear Velocity (inches/$\mu$sec) | Density ($g/cm^3$) |
|---|---|---|---|
| Laminated layer | .16 | .078 | 1.6075 |
| Aluminum half space | .2196 | .1248 | 2.77 |

Equipment

The attendant equipment for making measurements on the model was essentially that described in previous publications of Healy and Press (1960) and Oliver, Press, and Ewing (1954). Barium titanate cylinders were used as sources and barium titanate bimorph transducers were used as receivers.

Experimental Results

With the source at the thin end of the model, records were taken at 1 inch spacings from station 17 to station 34 (see Figure 45) across the regions where the layer thickened. Then, the source was placed at the thick end and records taken at these same stations, thus reversing the profile.

The range of period ($\mu$-sec) which the source adequately excited, so that reliable measurements could be made, was from 10 to 50 microseconds. This spans the period range of interest for which the analog model was constructed.

Several different methods were used to measure the dispersion. These were all simple applications of the general techniques for measuring dispersion described in Appendix A. Phase velocity was measured primarily in the frequency domain using the Fourier transform of the time records at each station. However, these results were amply checked by measurements in the time domain. These less precise time domain measurements consistently fell on or scattered close to the corresponding frequency domain measurements.

The time domain measurements were facilitated by adjusting the high and low frequency cutoffs on a Krohn-Hite filter such that only a very narrow band of frequencies about a selected frequency was passed. This serves the same purpose as a long travel path in the earth which disperses a wave train sufficiently that the period changes only slightly over several oscillations in the time domain. Samples were taken at the same stations as before. Repeating this procedure for a succession of center frequencies made

it possible to define the whole dispersion curve. This approach was particularly useful when the source was at the thin end of the model, where the Rayleigh wave traveled to the sloping region essentially non-dispersed as shown in Figure 48.

One can appreciate the necessity for simplifying the time domain measurements by examining Figure 47, which shows the set of seismograms obtained with the source at the thick end and an open pass band. Figure 48 shows the simpler narrow band pass records over this same profile.

Figure 45 gives a summary of the results obtained, along with a comparison with plane parallel layer theory. The agreement between theoretical and experimental dispersion between stations where the layer is of uniform thickness is very good. However, where the thickness is not uniform, certain departures from the theory are apparent. Among these is a difference in phase velocity on a reversed path keeping the stations fixed. The data shown for the phase velocity between stations 22 and 27 in Figure 45 illustrates this effect, which is analogous to the body wave refraction over a dipping interface. Another is the appearance of a kink in the dispersion curve near 25 $\mu$-seconds period when the receivers span a region where the slope of the interface is changing. In one case (station 29-25 curve in Figure 45) an actual minimum

was observed. Moreover, at the longer periods the phase velocities across these regions fell below those measured entirely in the thickest portion of the model beyond the sloping region.

Below 20 $\mu$-seconds period, however, the usual inference of a greater average thickness where the phase velocity is lower seems valid, because even when the average thickness was only slightly different, there was the expected systematic difference in phase velocity (compare profile 25-29 dispersion with profile 26-29 dispersion in Figure 45). That is, without exception the greater the mean layer thickness between stations, the lower the observed phase velocity at a given period below 20 $\mu$-seconds. Therefore, these shorter periods, with wave lengths less than 3 times the mean layer thickness, seem to give the most reliable indication of how the average layer thickness changes over regions where the layer thickness varies.

Conversely, the period range most strongly affected by underlying changes in slope of the interface corresponds to wave lengths 3 to 5 times the mean layer thickness.

In addition, the apparent attenuation is different for propagation in opposite directions between fixed stations. That is, the apparent attenuation for propagation downslope is less than for propagation

upslope, especially in the intermediate period range (15-30 $\mu$-sec). The apparent attenuation downslope is uniform and small (Figure 48), while that upslope is extreme at the intermediate periods ($M_{11}$ in Figures 47 and 48).

Figure 46 shows that the large amplitude portion labeled $M_{21}$ in Figure 47 is a higher mode, because it conforms to the theoretical displacement with depth predicted for the first higher mode, shown schematically at the right of Figure 46. That is, it exhibits a reversal in polarity at depth and a subsequent gradual decrease in amplitude with depth.

It can be seen from Figure 47 that this higher mode ($M_{21}$) attenuates very differently from the fundamental mode ($M_{11}$), propagating essentially unattenuated upslope over most of the sloping region.

A discussion of these results as they relate to measured phase velocity dispersion in Southern California is included in Part II of the main text.

# APPENDIX E

## INSTRUMENT RESPONSE

For many types of investigation in seismology instrument response must be taken into account. The object of this Appendix is to indicate how instrument response may be determined for the seismograph systems used in this study.

1. General Linear System

The result of passing a time function f(t) through a linear system is given by

$$R(t) = \int_{-\infty}^{\infty} f(\tau)W(t - \tau)\, d\tau \qquad (1)$$

where W(t) = transfer function (time) of the system

$$\text{then } F.T.[R(t)] = R(\omega) = F(\omega)\,W(\omega) \qquad (2)$$

where $F(\omega)$ = Fourier spectrum (amplitude and phase) of f(t)

$W(\omega)$ = Fourier spectrum (amplitude and phase) of W(t)

$$\text{or, } W(\omega) = R(\omega)/F(\omega) \qquad (2a)$$

In the special case when $f(t) = \delta(t)$ (impulse) $F(\omega) = 1$, so that $W(\omega) = R(\omega)$

Hence, to calibrate any linear seismometer system

using this technique, one should apply to the system some convenient time function for which the Fourier transform is known or can be accurately computed. Numerically compute the Fourier transform of the resultant time function R(t) by use of existing digital or analog computer programs described in Appendix H. The response of the system is obtained then by use of equation 2a above, where both $R(\omega)$ and $F(\omega)$ have been determined.

This technique is particularly useful when complicated amplifiers and other electronic circuitry constitute part of the recording system, since the theoretical response of the ensemble of all these components is often extremely difficult to calculate.

## II. Particular Systems

In certain simple seismograph recording systems it is practical to compute the theoretical response, since the procedure is straightforward. To do this, one must measure the appropriate instrument constants and use them in the expressions for the response of the system.

### A. Pendulum Galvanometer Systems

#### 1. Velocity transducer

The impulse response of this system is given by

$$W(\omega) = Q\omega^3(X^2(\omega) + Y^2(\omega))^{-\frac{1}{2}} \quad \text{(Amplitude)} \tag{3}$$

$$\varphi(\omega) = \tan^{-1}(X(\omega)/Y(\omega)) \quad \text{(Phase)}$$

where

$\omega$ = frequency (radians/sec)

$$X = \omega^4 - w^2\left[n_1^2 + n_2^2 + 4\,k_1k_2(1 - \sigma^2)\right] + n_1^2n_2^2$$

$$Y = -2w^3(k_1 + k_2) + 2\omega(n_2^2k_1 + n_1^2k_2)$$

$n_1$ = natural frequency of the pendulum

$n_2$ = natural frequency of the galvanometer

$k_1/n_1 = h_1$ damping factor for the pendulum with the galvanometer clamped ($h_1 = 1$) for critical damping)

$k_2/n_2 = h_2$ damping factor for the galvanometer with the pendulum clamped ($h_2 = 1$) for critical damping

$\sigma$ = coupling factor

Q = constant determined by parameters of the electrical and mechanical system (see Hagiwara, 1958)

The techniques used to measure these constants as well as the response for the stations calibrated will be given later in this Appendix.

Examples of this type of seismograph are numerous.

Among those commonly encountered are the Benioff long period seismograph ($T_1 = 1$, $T_2 = 90$), the Benioff short period seismograph ($T_1 = 1$, $T_2 = .2$), and Press-Ewing long period seismograph ($T_1 = 15$ or $30$, $T_2 = 90$)

2. D.C. Transducer

The impulse response of this system is given by

$$W(\omega) = \frac{D\ \omega^2}{|Z_n|}\left[X^2(\omega) + Y^2(\omega)\right]^{-\frac{1}{2}} \quad \text{(Amplitude)} \tag{4}$$

$$\varphi(\omega) = \tan^{-1}\left[-Y(\omega)/X(\omega)\right] - \tan^{-1}\left[Z_i/Z_r\right] \quad \text{(Phase)}$$

where

$X(\omega)$ = same as for velocity transducer (equation 3 above)

$Y(\omega)$ = same as for velocity transducer (equation 3 above)

$Z_n$ = circuit impedence where the subscript n denotes the type of circuit ($\pi$, T, or Box)

$Z_i$ = imaginary part of $Z_n$

$Z_r$ = real part of $Z_n$

D = constant determined by parameters of the electrical and mechanical system.

B. Damped Pendulum

The impulse response of a simple, damped pendulum is given by

$$W(\omega) = M\left\{\left[1-(n/\omega)^2\right]^2 + 4h^2n^2/\omega^2\right\}^{-\frac{1}{2}} \quad \text{(Amplitude)} \tag{5}$$

$$\varphi(\omega) = \tan^{-1}\left[2hn\omega/(\omega^2 - n^2)\right] \quad \text{(Phase)}$$

where

n = natural frequency of the pendulum

h = damping factor

M = static magnification

Common examples having this type of response are the Wood-Anderson torsion seismograph, the Benioff strain seismograph, and the Caltech digital seismograph.

III. Procedure for Measuring Instrument Constants and Response

The instruments used in this study were primarily of the pendulum-galvanometer type. Therefore, only the procedure adopted for measuring the constants of this type instrument will be given, although essentially the same procedures can be used for the damped pendulum and displacement systems.

The equations of the pendulum galvanometer system are

$$\frac{d^2X}{dt^2} + 2k_1\frac{dX}{dt} + n_1^2X = -B\frac{d^2u}{dt^2} + 2\sigma_1 k_1 \frac{d\phi}{dt} \tag{6}$$

$$\frac{d^2\phi}{dt^2} + 2k_2\frac{d\phi}{dt} + n_2^2\phi = 2\sigma_2 k_2 \frac{dX}{dt} \tag{7}$$

where

$\phi$ = deflection of the galvanometer

X = pendulum displacement

u = ground displacement

$n_1$ = natural frequency of the pendulum

$n_2$ = natural frequency of the galvanometer

$k_1/n_1 = h_1$ damping factor for the pendulum

$k_2/n_2 = h_2$ damping factor for the galvanometer

$\sigma_1 \sigma_2$ = coupling factor $(\sigma^2)$

B = constant

The basic equation to be solved for determining the constants is equation 6 or 7 with the right hand side equal to zero, i.e.

$$\frac{d^2y}{dt^2} + 2hn \frac{dy}{dt} + n^2 y = 0 \qquad (8)$$

The Laplace transform of (8) is

$$\overline{y} = \frac{(\omega + 2k)y_o + y'_o}{(\omega^2 + k)^2 + (1-h^2)n^2} \qquad (9)$$

where $y_o$ = initial displacement

$y'_o$ = initial velocity

In the following paragraphs the detailed procedures for measuring the constants, $n_1$, $n_2$, $h_1$, $h_{01}$, $h_2$, $h_{02}$, $\sigma$, and $Q$ necessary for computing the instrument response will be given.

A. Free Period and Air Damping of Galvanometer

Disconnect the leads to the galvanometer and deflect the mirror by a small applied voltage to the terminals. Record the decay curve which, for an impulse with the system initially at rest, (i.e. $y_o = 0$ in equation 9) is given by

$$y(t) = y'_o e^{-h_{02} n_2 t} \sin \sqrt{1-h_{02}^2}\, n_2 t \qquad (10)$$

The ratio R of successive maxima of $|y(t)|$ permits calculation of $h_{02}$ (air damping of the galvanometer) using the following expression

$$h_{02} = (1 + \pi^2/\ell n R)^{-\frac{1}{2}} \qquad (11)$$

Several such determinations of $h_{02}$ can be made and averaged, since equation 10 has several oscillations for which R can be measured. Then the free period of the galvanometer is given by

$$T_2 = 2 \sqrt{1-h^2_{02}}\, \frac{\tau}{p} \qquad (12)$$

$$n_2 = 2\pi/T_2$$

where

$\tau$ = measured time interval between p half cycles of equation 10.

B. Free Period and Air Damping of the Pendulum

Disconnect the transducer leads, deflect the pendulum, and record the subsequent motion using an auxiliary high impedence recorder. A Varian recorder was used for this purpose.

The air damping, $h_{01}$, is obtained as in (A) above, using equation 11. The free period, $T_1$, is obtained using equation 12 with $h_{01}$.

C. Galvanometer Damping

Clamp the pendulum (before reconnecting the leads to the galvanometer), connect the galvanometer leads, deflect the galvanometer mirror with a small applied voltage, and record the resultant motion as before. The result for $y_o = 0$ in equation 9 is given by

$$y(t) = Ce^{-h_2 n_2 t} \sin \sqrt{1-h_2^2}\, n_2 t \qquad h_2 < 1 \quad \text{(oscillatory)} \tag{13}$$

$$= Ce^{-n_2 t}\, t \qquad h_2 = 1 \text{ (non-oscillatory)}$$

$$= Ce^{-h_2 n_2 t} \sin h \sqrt{h_2^2-1}\, n_2 t \qquad h_2 > 1 \text{ (non-oscillatory)}$$

For $h_2 < 1$ use the same procedure as in (A) above to find $h_2$.

For $h_2 = 1$ the time interval from $t = 0$ to $t_m$ is $2\pi/T_2$, where

$\frac{\max}{t}\left[y(t)\right] = y(t_m)$, so the test for critical damping involves only measurement of this time

interval.

For $h_2 > 1$ one can use the interval from t = 0 to $t_m$ where $\max_t \left[y(t)\right] = y(t_m)$ and solve for $h_2$ by inverse interpolation using the expression

$$t_m = \frac{\tanh^{-1}(\sqrt{h^2-1}\,/h)}{\sqrt{h^2-1}} \frac{T}{2\pi} \tag{14}$$

Table 5 gives values of h for various values of $t_m$ with period T as a parameter.

In addition inverse interpolation using the method of regula falsi can be used to determine more estimates of $h_2$ using the ratio $y(t_2)/y(t_1)$ where $0<t_1<t_2$. This method is summarized as follows:

$$y(t_2)/y(t_1) = e^{-n_2 h_2 (t_2-t_1)} \frac{\sinh\sqrt{h_2^2-1}\; n_2 t_2}{\sinh\sqrt{h_2^2-1}\; n_2 t_1}$$

$$= f(h_2, t_2, t_1, T_2)$$

Let

$$h = h_2$$

$$F(h) = f(h, t_2, t_1, T_2) - y(t_2)/y(t_1)$$

Then the recursion relation for obtaining h is

$$h_{v+1} = h_v - \frac{h_v - h_{v-1}}{1 - F(h_{v-1})/F(h_v)} \tag{15}$$

Technically this procedure will work for any h, but for $h < 1$ the procedures outlined previously are much simpler and require little calculation.

D. Pendulum Damping

Clamp the galvanometer, apply either an impulse or an initial displacement to the pendulum, and record the resulting motion with an auxiliary recorder attached to the transducer terminals. A Varian recorder was used for this purpose.

Depending on the initial conditions, the resultant can be analyzed appropriately to give the pendulum damping.

Initial Impulse

$$y(t) = Ce^{-h_1 n_1 t}\left[\sqrt{1-h_1^2}\ \cos\sqrt{1-h_1^2}\,n_1 t - h_1 \sin\sqrt{1-h_1^2}\,n_1 t\right] \qquad h_1 < 1$$

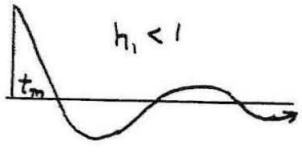


$$= Ce^{-n_1 t}(1-n_1 t) \qquad h_1 = 1$$

$$= Ce^{-h_1 n_1 t}\sqrt{h_1^2-1}\ \cosh\sqrt{h_1^2-1}\,n_1 t - h_1 \sinh\sqrt{h_1^2-1}\ n_1 t \qquad h_1 > 1$$

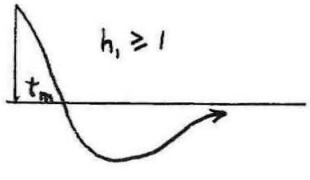

Initial Displacement

$$y(t) = Ce^{-h_1 n_1 t} \sin \sqrt{1-h_1^2}\, n_1 t \qquad h_1 < 1$$

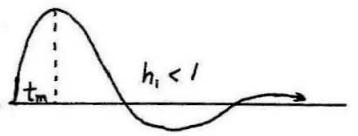


$$= Ce^{-h_1 n_1 t} \qquad h_1 = 1$$

$$= Ce^{-h_1 n_1 t} \sinh \sqrt{h_1^2-1}\, n_1 t \qquad h_1 > 1$$

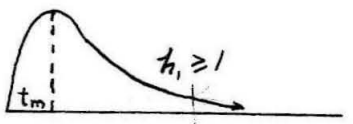


For $h_1 < 1$ the motion is oscillatory and the techniques in (A) above can be used.

When $h_1 \geq 1$ the same table 5 may also be used to determine the pendulum damping for either initial condition by using the appropriate $t_m$ shown above.

In addition, the method of regula falsi can be used, provided the appropriate F function is used in equation 15.

E. Coupling Factor

The coupling factor $\sigma$ is given by

$$\sigma^2 = \frac{(h_1 - h_{01})(h_2 - h_{02})}{h_1 h_2} \frac{Z_{22}}{Z_{11}} \mu_1^2 \qquad (18)$$

where

$$Z_{22} = Z_b + \frac{Z_c Z_a}{Z_a Z_c}$$

$$Z_{11} = Z_a + \frac{Z_b Z_c}{Z_b + Z_c}$$

$$\mu_1 = \frac{Z_c}{Z_b + Z_c}$$

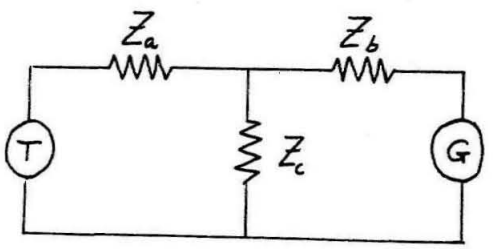

$Z_a$ includes the impedance of the transducer and $Z_b$ includes the impedance of the galvanometer.

With these measured constants ($n_1$, $n_2$, $h_1$, $h_{01}$, $h_2$, $h_{02}$, $\sigma$) one can compute the phase and relative amplitude using equation 3.

F. Magnification Factor for Absolute Amplitude Response

While one can compute the magnification factor Q for absolute amplitude response, knowing the mechanical and electrical constants of the system (moment of inertia of pendulum, distance of recording drum from the galvanometer, field strength of the magnet, etc.), it is simpler to drive the pendulum with a sinusoidal wave of some known amplitude $A_o$ and frequency $\omega_o$ and record the resulting amplitude to get the absolute magnification M at $\omega_o$. One such value with the relative response curve computed from equation 3 gives the complete absolute amplitude response.

Hence, one can determine the complete amplitude and phase response of the system. Since only phase calibration was of concern in this study, however, the absolute magnification was not measured. The response curves determined for the stations used are shown in Figure 41.

# APPENDIX F

## MODE DELINEATION METHOD

The details of the method developed to separate the various modes will be given in this Appendix.

### I. Basis of the Method

The definition of group velocity provides the foundation of the method developed to separate the modes. That is, for a given epicentral distance, mode, and frequency ($\omega_o$) the group arrival occurs at a time when the spectral components in a narrow band of frequency about $\omega_o$ add up in phase. Except for a discrete set of frequencies where two or more modes cross, each mode has a distinct dispersion curve, so that the group arrivals of each mode are separated in time for any given frequency.

This makes it possible in principle to delineate the dispersion appropriate to each mode present by either or both of the following procedures.

(A) Perform a very narrow band pass about a selected frequency, and plot all the group arrivals observed for that frequency. Each such arrival presumably belongs to a particular mode. Repeating this procedure for a succession of frequencies then defines dispersion curves for all the modes present.

(B) Using the proper combination of velocity windows and band pass filtering, a time record representing any

specified region of the group velocity-frequency plane can be obtained. Then a region can be chosen such that it contains only one branch of any single mode, and the resulting time record can be analyzed using conventional methods to obtain the dispersion. Using this technique one pass is made on the data for each branch of each mode. This procedure requires some general knowledge of where the dispersion curve for each mode is located.

II. Narrow Band Pass (Method A)

Construct a set of filter coefficients (see Appendix G) which allows a very narrow pass band of frequencies. Then peaks in the envelope of the filtered seismogram represent group arrivals for a frequency in the band-pass interval. This is seen as follows:

The operation of filtering a time series gives a new time series $y(t) = \int_{-\infty}^{\infty} g(\tau)\, h\,(t-\tau)\,d\tau$, and its frequency spectrum from the Fourier transform of $y(t)$ is $Y(\omega)=G(\omega)H(\omega)$. The filtering function $h(t)$ can be constructed such that $H(\omega) \approx 1 \quad \omega_1 \leq \omega \leq \omega_2$ and zero elsewhere with no phase shift (see Appendix G).

Then

$$y(t) = Re \int_{-\infty}^{\infty} G(\omega)\, H(\omega)\, e^{i\omega t}\, d\omega = Re \int_{\omega_1}^{\omega_2} G(\omega)\, e^{i\omega t}\, d\omega \qquad (1)$$

$$G(\omega) = \left| S(\omega) W(\omega)\, e^{-\alpha(\omega) x} \right| e^{-i[\varphi_0(\omega) + \varphi(\omega) + k(\omega) x]}$$

where

$S(\omega)$ = source spectrum

$W(\omega)$ = instrumental amplitude distortion

$\varphi(\omega)$ = instrumental phase delay

$\alpha(\omega)$ = attenuation factor during propagation

$\varphi_0(\omega)$ = initial phase at the source

$k(\omega)X$ = phase delay due to propagation over distance X

Defining

$$\Delta\omega = (\omega_2 - \omega_1)/2 \qquad \bar{\omega} = (\omega_1 + \omega_2)/2$$

$$A(\omega,x) = S(\omega)\,W(\omega)\,e^{-\alpha(\omega)X}$$

$$\Theta(\omega,x) = k(\omega)X + \varphi(\omega) + \varphi_0(\omega)$$

Expanding $A(\omega,x)$ and $\Theta(\omega,X)$ in Taylor series about $\bar{\omega}$ and suppressing the $X$ dependence,

$$A(\omega) = A(\bar{\omega}) + \left(\frac{\partial A(\omega)}{\partial \omega}\right)_{\bar{\omega}}(\omega-\bar{\omega}) + \mathcal{O}[(\omega-\bar{\omega})^2] \tag{2}$$

$$\Theta(\omega) = \Theta(\bar{\omega}) + \left(\frac{\partial \Theta}{\partial \omega}\right)_{\bar{\omega}}(\omega-\bar{\omega}) + \left(\frac{\partial^2 \Theta}{\partial \omega^2}\right)_{\bar{\omega}}\frac{(\omega-\bar{\omega})^2}{2} + \mathcal{O}[(\omega-\bar{\omega})^3]$$

Inserting these expansions into equation 1, making the change of variable $\omega' = \omega - \bar{\omega}$ and rearranging gives

$$y(x,t) = Re\left[e^{i\eta(t)}\int_{-\Delta\omega}^{\Delta\omega}\left\{A(\bar{\omega}) + \left(\frac{\partial A}{\partial \omega}\right)_{\bar{\omega}}\omega' + \mathcal{O}[(\omega')^2]\right\}e^{i[\omega' t - P(\omega')]}\,d\omega'\right] \tag{3}$$

where

$$\eta(t) = \bar{\omega} t - \Theta(\bar{\omega})$$

$$P(\omega') = \left(\frac{\partial \Theta}{\partial \omega}\right)_{\bar{\omega}} \omega' + \left(\frac{\partial^2 \Theta}{\partial \omega^2}\right)_{\bar{\omega}} \frac{\omega'^2}{2} + \mathcal{O}[(\omega')^3]$$

Then retaining only 1st order terms in the expansion of $A(\omega)$ gives

$$y(x,t) = Re\left\{ e^{i\eta(t)} \left[ A(\bar{\omega})\, I(t) + \left(\frac{\partial A}{\partial \omega}\right)_{\bar{\omega}} \frac{d(-iI(t))}{dt} \right] \right\} \qquad (4)^*$$

where $$I(t) = \int_{-\Delta\omega}^{\Delta\omega} e^{i[\omega' t - P(\omega')]}\, d\omega'$$

Evaluation of $I(t)$

$$I(t) = \int_{-\Delta\omega}^{\Delta\omega} \cos(\omega' t - P(\omega'))\, d\omega' + i \int_{-\Delta\omega}^{\Delta\omega} \sin(\omega' t - P(\omega'))\, d\omega' \qquad (5)$$

$$P(\omega') = \left[ x \left(\frac{\partial k}{\partial \omega}\right)_{\bar{\omega}} + \varphi'(\bar{\omega}) + \varphi_0'(\bar{\omega}) \right] \omega' + \left[ x \left(\frac{\partial^2 k}{\partial \omega^2}\right)_{\bar{\omega}} + \varphi''(\bar{\omega}) + \varphi_0''(\bar{\omega}) \right] \frac{(\omega')^2}{2} + \mathcal{O}[(\omega')^3] \qquad (6)$$

---

*This expression can readily be generalized to include higher order terms, i.e.

$$y(x,t) = Re\left[ e^{i\eta(t)} \sum_{n=0}^{\infty} \frac{(-i)^n}{n!} \left(\frac{\partial^n A(\omega)}{\partial \omega^n}\right)_{\bar{\omega}} \frac{d^n I(t)}{dt^n} \right]$$

Noting that

$$k = \omega / C(\omega)$$

$$\frac{\partial k}{\partial \omega} = 1/U(\omega)$$

$$\frac{\partial^2 k}{\partial \omega^2} = -\frac{dU(\omega)}{d\omega} \Big/ U^2(\omega) = -U'(\omega)/U^2(\omega)$$

Equation 6 becomes

$$P(\omega') = \left[\frac{X}{U(\bar{\omega})} + \varphi'(\bar{\omega}) + \varphi_0'(\bar{\omega})\right]\omega' + \left[\frac{-X\,U'(\bar{\omega})}{U^2(\bar{\omega})} + \varphi''(\bar{\omega}) + \varphi_0''(\bar{\omega})\right]\frac{\omega'^2}{2} + \mathcal{O}(\omega'^3) \tag{7}$$

If $\Delta\omega$ is chosen such that

$$\left|\left[-\frac{X\,U'(\bar{\omega})}{U^2(\bar{\omega})} + \varphi''(\bar{\omega}) + \varphi_0''(\bar{\omega})\right]\frac{\Delta\omega^2}{2}\right| = \alpha\,\Delta\omega^2 << 1 \tag{8}$$

even order terms of order $(\omega')^4$ and above can be neglected. Then $P(\omega') - \alpha(\omega')^2$ is an odd function. Therefore, $\omega' t - P(\omega') + \alpha(\omega')^2 = Q(\omega')$ is also an odd function of $\omega'$. Hence,

$$-\int_{-\Delta\omega}^{\Delta\omega} \sin\left[\omega' t - P(\omega')\right] d\omega' = -\int_{-\Delta\omega}^{\Delta\omega} \sin\left[Q(\omega') - \alpha\omega'^2\right] d\omega'$$

$$= -\int_{-\Delta\omega}^{\Delta\omega} \sin Q(\omega') \cos(\alpha\omega'^2)\, d\omega' + \int_{-\Delta\omega}^{\Delta\omega} \cos Q(\omega') \sin(\alpha\omega'^2)\, d\omega'$$

$$= \int_{-\Delta\omega}^{\Delta\omega} \cos Q(\omega') \sin(\alpha\omega'^2)\, d\omega' = 2\int_{0}^{\Delta\omega} \cos Q(\omega) \sin(\alpha\omega'^2)\, d\omega' \tag{9}$$

$$\leq 2\,\Delta\omega \sin(\alpha\,\Delta\omega^2) = \mathcal{O}(\Delta\omega^3)$$

and

$$\int_{-\Delta\omega}^{\Delta\omega} \cos[\omega' t - P(\omega')]\, d\omega' = \int_{-\Delta\omega}^{\Delta\omega} \cos Q(\omega') \cos(\alpha\omega'^2)\, d\omega' - \int_{-\Delta\omega}^{\Delta\omega} \sin Q(\omega') \sin(\alpha\omega'^2)\, d\omega' \tag{10}$$

$$= 2\int_{0}^{\Delta\omega} \cos \omega'\xi \cos(\alpha\omega'^3)\, d\omega' = 2\frac{\sin \Delta\omega\xi}{\xi} + \mathcal{O}(\omega'^5)$$

where

$$\xi = t - \frac{x}{U(\bar{\omega})} - \varphi'(\bar{\omega}) - \varphi_0'(\bar{\omega})$$

Thus, neglecting terms of order $(\Delta\omega)^3$ and above, equation 5 becomes

$$I(t) = 2\frac{\sin \Delta\omega\xi}{\xi} \tag{11}$$

Therefore, equation 4 may be approximated by

$$y(x,t) \cong 2\,\mathrm{Re}\left[e^{i\eta(t)} \sum_{n=0}^{\infty}{}' \frac{1}{n!}\left(\frac{\partial^n A}{\partial\omega^n}\right)_{\bar{\omega}} \frac{d^n}{dt^n}\left((-i)^n \frac{\sin \Delta\omega\xi}{\xi}\right)\right] \tag{12a}$$

$$= 2\, A(\bar{\omega}, x) \cos\eta(x,t) \frac{\sin \Delta\omega\xi(x,t)}{\xi(x,t)}$$

$$+ \left(\frac{\partial A}{\partial\omega}\right)_{\bar{\omega}} \frac{\sin\eta(x,t)}{\xi(x,t)}\left[\Delta\omega \cos\Delta\omega\xi(x,t) - \frac{\sin \Delta\omega\xi(x,t)}{\xi(x,t)}\right] \tag{12b}$$

where only the first two terms of equation 12a are retained.

The dominant term in this expression is amplitude modulated by $\frac{\sin \Delta\omega \xi}{\xi}$ which attains its maximum as

$$\xi \to 0 \quad \text{i.e. as} \quad t \to \tau = \frac{X}{U(\bar{\omega})} + \varphi'(\bar{\omega}) + \varphi_o'(\bar{\omega})$$

Thus

$$U(\bar{\omega}) = \frac{X}{\tau - \varphi'(\bar{\omega}) - \varphi_o'(\bar{\omega})} \tag{13}$$

$$y(x,\tau) = \Delta\omega\, S(\bar{\omega})\, W(\bar{\omega})\, e^{-\alpha(\bar{\omega})X}$$

Narrow band pass filtering about $\bar{\omega}$ permits determination of $\tau$ ; $\varphi'(\bar{\omega})$ is determined from the instrument response; and $\varphi_o'(\bar{\omega})$ may be assumed small when X is several wave lengths from the source, so $U(\bar{\omega})$ can be readily measured.

Generalization to Multi-mode Case

Equation 11 applies to any particular mode. Then the resultant for more than one mode is obtained by superposition of time functions of the form of equation 11. That is,

$$y(x,t) = 2\sum_{n=1}^{N} \left\{ A_n(\bar{\omega}) \cos \eta_n(t) \frac{\sin \Delta\omega \xi_n(t)}{\xi_n(t)} \right. \tag{14}$$

$$\left. + \left(\frac{\partial A_n}{\partial \omega}\right)_{\bar{\omega}} \frac{\sin \eta_n(t)}{\xi_n(t)} \left[ \Delta\omega \cos \Delta\omega \xi_n(t) - \frac{\sin \Delta\omega \xi_n(t)}{\xi_n(t)} \right] \right\}$$

where

$$A_n(\bar{\omega}) = S_n(\bar{\omega})\, W(\bar{\omega})\, e^{-\alpha_n(\bar{\omega})X}$$

$$\eta_n(t) = \bar{\omega}\left(t - X/C_n(\bar{\omega})\right) - \varphi(\bar{\omega}) - \varphi_o(\bar{\omega})$$

$$\xi_n(t) = t - X/U_n(\bar{\omega}) - \varphi'(\bar{\omega}) - \varphi_o'(\bar{\omega})$$

$y(x,t)$ then has N relative maxima in its envelope given by the zeros of $\xi_n'(t)$ (i.e. the succession of group arrivals for the various modes).

In addition, spurious maxima can occur due to constructive interference among the modulating factors $\frac{\sin \Delta\omega \xi_n(t)}{\xi_n(t)}$ of the various modes, as well as among the carriers $\cos \eta_n(t)$ of the various modes. The latter is most troublesome where the group velocity dispersion curves of two or more modes coalesce.

Keeping only those group arrivals common to an array of stations and consistent for a number of adjacent frequencies minimizes these difficulties. In addition it is sometimes useful to use slightly different $\Delta\omega$ intervals about $\bar{\omega}$ and retain those envelope maxima which are invariant under small changes in $\Delta\omega$.

The bottom seismogram of Figure 8 shows the results of narrow band pass filtering a seismogram. Each peak in the envelope of the curve corresponds to a group arrival for frequency $\bar{\omega} \approx .146$ cps. The location of maxima in the envelope can be determined from a plot of the integral of the absolute value of the filtered seismogram over a half cycle of oscillation.

Note that using equation 14, it is possible to obtain a rough estimate of the relative excitation of the modes by comparison of amplitudes of the group arrivals of the various modes at each frequency sampled.

II. Mode Isolation (Method B)

The raw seismogram to be analyzed can be represented by

$$y(x,t) = 2\sum_{n}\sum_{i}\left\{A_n(\omega_i)\cos\eta_n(\omega_i,t)\ \frac{\sin\Delta\omega_i\,\xi_n(\omega_i,t)}{\xi_n(\omega_i,t)}\right. \qquad (15)$$

$$\left. +\left(\frac{\partial A_n}{\partial\omega}\right)_{\omega_i}\frac{\sin\eta_n(\omega_i,t)}{\xi_n(\omega_i,t)}\left[\Delta\omega_i\cos\Delta\omega_i\,\xi_n(\omega_i,t) - \frac{\sin\Delta\omega_i\,\xi_n(\omega_i,t)}{\xi_n(\omega_i,t)}\right]\right\}$$

The inner sum gives the seismogram for each mode and the outer sum superposes all the modes*. The idea of this method is to isolate each branch of each mode by a combination of band pass filtering and velocity windows. That is, the inner sum for the frequency interval between successive Airy phases must be found for each mode. The selection of a region enclosing only one such branch requires a determination of the general location of the dispersion curves in the group velocity-frequency plane. This can be accomplished by one or a combination of the following:

(a) use of the previous method at a few selected frequencies

---

*The inner sum is a generalization of the Aki synthesis method (Aki, 1960), including amplitude as well as phase, which may be used numerically to construct theoretical seismograms for each mode. The entire expression (15) can also be used to construct a complete seismogram including the relative excitation of the modes for different types of sources.

(b) computing theoretical curves for an approximate structure derived from refraction results, gravity results, and/or fundamental mode dispersion.

(c) linear interpolation between Airy phases

(d) using peaks in the spectrum of short velocity windows*

(e) trial and error

Figure 3 shows typical dispersion curves for the first three modes. If the spectrum of the velocity window shown in Figure 3 were computed, a peak due to the 1st higher mode should appear in the vicinity of 12 seconds period, another at about 7 seconds due to the 2nd higher mode, and one due to the fundamental mode above 30 seconds. Figure 2 (unshaded portions) shows three band passes in frequency about these periods. The time record corresponding to each of these band passes has only one mode arriving at any given instant. Figure 8 shows three such passes made on the same seismogram. Each pass allows determination of a portion of the dispersion curve of one or more modes using conventional time domain analysis.

---

*This procedure is termed the "transform" of Method A, since it is applied in the same way as Method A with the roles of group velocity and frequency interchanged. Further discussion of this point may be found under Methods of Analysis in Part I of this thesis.

# APPENDIX G

Contained in this Appendix are several results, each of which supplements the text and one or more of the appendices and yet is sufficiently distinct to be included separately here.

1. Numerical Band Pass Filter

Find a time function, $h(t) = h(-t)$ (real) such that F.T. $[h(t)] = \int_{-\infty}^{\infty} h(t) e^{-i\omega t}\, dt = H(\omega) e^{i\varphi(\omega)}$ has the following properties

$$
\begin{aligned}
H(\omega) &= 1 && |\omega| \leq \omega_c \\
&= \frac{(\omega + \omega_r)^p}{(\omega_r - \omega_c)} && -\omega_r \leq \omega \leq -\omega_c \\
&= \frac{(\omega_r - \omega)^p}{(\omega_r - \omega_c)} && \omega_c < \omega \leq \omega_r \\
&= 0 && |\omega| > \omega_r \\
\varphi(\omega) &= 0 \text{ everywhere}
\end{aligned}
\qquad (1)
$$

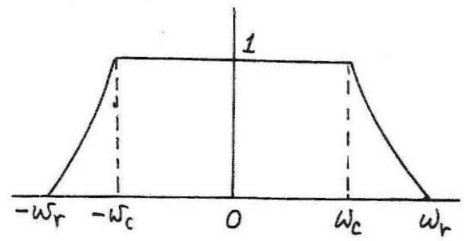


Now,

$H(\omega) = H^*(-\omega)$ since $h(t)$ is real

and

$H(\omega) = H(-\omega)$ since $h(t)$ is symmetric

hence

$H(\omega) = H^*(\omega)$ which implies $\varphi(\omega) \equiv 0$

Taking the inverse transform of equation 1 and simplifying, one obtains its corresponding time function given by

$$h(t) = \frac{1}{2\pi(\omega_r-\omega_c)^p}\left[\frac{e^{-i\omega_c t} - e^{-i\omega_r t}}{(i)^{p+1}} + \frac{e^{i\omega_c t} - e^{i\omega_r t}}{(-i)^{p+1}}\right] \frac{d^p}{dt^p}\left(\frac{1}{t}\right) \tag{2a}$$

or

$$h(t) = \frac{(-1)^p p!}{2\pi(\omega_r-\omega_c)^p}\left[\frac{\cos\omega_c t - \cos\omega_r t - i(\sin\omega_c t-\sin\omega_r t)}{(i)^{p+1}} + \frac{\cos\omega_c t - \cos\omega_r t + i(\sin\omega_c t-\sin\omega_r t)}{(-i)^{p+1}}\right] t^{-p+1} \tag{2b}$$

If one shifts the center frequency away from zero then the results above must be modified by multiplying h(t) in equations 2a and 2b by $2\cos\omega_o t$.

Discretizing and normalizing frequency to the sampling frequency $f_s = \frac{1}{\Delta t}$ as follows:

$$h_n = h(t_n)\Delta t = \frac{h(t_n)}{f_s}$$

$$t_n = n\Delta t$$

$$\lambda_c = \frac{f_c}{f_s}$$

$$\lambda_D = \frac{f_r - f_c}{f_s}$$

$$\lambda_o = \frac{f_o}{f_s}$$

Then equation 2b becomes

$$h(t_n) = \frac{p!}{\pi}\left(\frac{-1}{2\pi\lambda_D}\right)^p \Big[(\cos 2\pi n\lambda_c - \cos 2\pi n\lambda_r)(1 + (-1)^{p+1}) - i(\sin 2\pi n\lambda_c - \sin 2\pi n\lambda_r)(1 + (-1)^p)\Big] (in)^{-(p+1)} \cos(2\pi n\lambda_0) f_s \tag{3}$$

$$= h_n f_s \tag{4}$$

where

$$h_n = \frac{p!}{\pi}\left(\frac{-1}{2\pi\lambda_D}\right)^p \Big[(\cos 2\pi n\lambda_c - \cos 2\pi n\lambda_r)(1 + (-1)^{p+1}) - i(\sin 2\pi n\lambda_c - \sin 2\pi n\lambda_r)(1 + (-1)^p)\Big] (in)^{-(p+1)} \cos 2\pi n\lambda_0 \tag{5}$$

Case p = 1

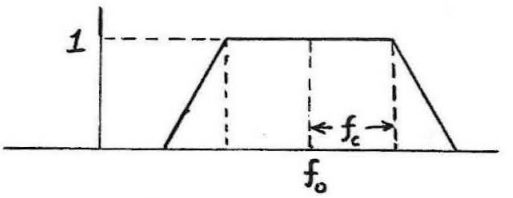


$$h_n = (\pi n)^{-2}(\cos 2\pi n\lambda_c - \cos 2\pi n\lambda_r)\cos 2\pi n\lambda_0/(2\lambda_D) \tag{6}$$

note that $h_o = 1/(2\pi)$

Multiplication in the frequency domain is accomplished by convolution in the time domain, so in order to band pass filter a signal S(t), one convolves h(t) with S(t) to get the filtered record

$$f(t) = \int_{-T}^{T} h(\tau)S(t-\tau)d\tau = \int_{-T}^{T} h(\tau)S(t+\tau)d\tau \tag{7}$$

discretizing such that

$$S(t_k) = S(k\Delta t) = S_k$$

equation 7 becomes

$$f(t_k) = f_k = \sum_{n=-N}^{N} h_n S_{n+k} \qquad (8)$$

Note that $\Delta t$ for the integration was included previously in $h_n$.

General Filter

A more general numerical filter can be constructed simply by computing the Fourier transform of the desired frequency function either analytically or numerically.

Let $H(\omega)$ be the desired spectrum (amplitude and phase) to be passed. Then the time function to convolve with the signal to achieve the desired filtering is

$$h(t) = \int_{-\infty}^{\infty} H(\omega) e^{i\omega t} d\omega/2\pi \qquad (9)$$

The only restriction on $H(\omega)$ is that it is $\mathcal{L}_1$ integrable.

In practice $h(t)$ is discretized and truncated for use in equation 8 above. In principle this approximate $h(t)$ can be made arbitrarily close to the desired $h(t)$, so any particular frequency shaping of the signal can be accomplished.

## 2. Group Velocity Inversion

From an energy method published by Jeffreys (1961) it is possible to determine the effect of each portion of a given structure on both the phase and group velocity dispersion for any mode of surface waves.

Existing Love wave dispersion programs have been modified by Anderson (1963) to use Jeffrey's method, and similar modification of Rayleigh wave programs is now in progress. Therefore, only the expression for the group velocity of Rayleigh waves will be discussed here in order to indicate how the structure controls group velocity dispersion and how one can use existing dispersion programs to find the structure which best fits the observed data.

After rearranging Jeffrey's expression, using the definitions of shear and compressional velocity in terms of the elastic parameters, the following result is obtained for the group velocity:

$$U = \gamma^{-1}\left\{ k\int_0^\infty \rho(\alpha^2 u^2 + \beta^2 w^2)\,dz + \int_0^\infty \rho\left[-(\alpha^2 - 2\beta^2)\,w'u + \beta^2 u'w\right]dz\right\}\left\{\int_0^\infty \rho(u^2+w^2)\,dz\right\}^{-1} \qquad (1)$$

where

$\gamma$ = frequency

k = wave number

$\rho$ = density

$\alpha$ = compressional velocity

$\beta$ = shear velocity

u = horizontal particle displacement

$u' = \frac{du}{dz}$

w = vertical particle displacement

$w' = \frac{dw}{dz}$

U = group velocity

For the N layered case equation 1 becomes

$$U = \gamma^{-1} \left\{ \sum_{i=1}^{N} \rho_i \left[ \alpha_i^2 \int_{z_{i-}}^{z_{i+}} (ku^2 - w'u)\, dz + \beta_i^2 \int_{z_{i-}}^{z_{i+}} (kw^2 + 2w'u + u'w)\, dz \right] \right\} \left\{ \sum_{i=1}^{N} \rho_i \int_{z_{i-}}^{z_{i+}} (u^2 + w^2)\, dz \right\}^{-1} \quad (2)$$

where

$z_{i+} - z_{i-} = h_i$ thickness of the $i^{th}$ layer.

For a given layered structure, $(h_i, \alpha_i, \beta_i, \rho_i)$, existing dispersion programs give u, w, k, and $\gamma$, so that all the elements necessary to compute U are available. If, for a particular dispersion point, one plots the integrands of the numerator in equation 2 as a function of z, it is apparent what portion of the structure is controlling the dispersion at that frequency. Scrutiny of several frequencies in this way will suggest what changes must be made in the assumed model to bring it into closer agreement with the observed data. That is, this provides a means of inverting group velocity dispersion.

Actually the partial derivatives of U with respect to each elastic parameter in each layer can be computed to make the inversion even more straightforward. However, as mentioned above, a computer program to do this is not yet operational.

Reformulating equation 2 with the simplifying assumption that $\lambda_i = \mu_i$, so that $\alpha_i^2 = 3\beta_i^2$ gives

$$U = \gamma^{-1} \left\{ \sum_{i=1}^{N} \rho_i \beta_i^2 \left[ k \int_{z_{i-}}^{z_{i+}} (3u^2 + w^2)\, dz + \int_{z_{i-}}^{z_{i+}} (u'w - w'u)\, dz \right] \right\} \left\{ \sum_{i=1}^{N} \rho_i \int_{z_{i-}}^{z_{i+}} (u^2 + w^2)\, dz \right\}^{-1} \qquad (3)$$

This expression enables one to use only the output from existing dispersion programs* to determine approximately what part of the assumed structure controls any given group velocity value. That is, maxima (with depth) of the integrands of the numerator correspond approximately to portions of the structure controlling the dispersion, and these integrands can be formed easily from the values of u and w provided by existing programs. In most instances zones of maximum contribution were found to correspond rather closely to zones where the absolute value of vertical displacement with depth was maximum. Therefore, merely examining the distribution of vertical displacement with depth for a given dispersion value is sufficient to indicate what part of the structure is important for that particular mode and frequency.

As an illustrative example Figure 11 shows the integrands of equation 3 (shaded regions) plotted with depth for the first higher mode ($M_{21}$) at a particular period (7.249 seconds), for the structure indicated (Case 5EEBM3). In addition the individual elements appearing in the integrands are shown. It is clear that the portion of the structure contributing most to the group velocity at this period is centered at about 25 km depth. Note the close correspondence of this zone with the maximum absolute value of vertical displacement w, as mentioned earlier.

---

*See Harkrider and Anderson, 1962; Press, Harkrider and Seafeldt, 1961.

The dispersion curve for this mode ($M_{21}$) for Case 5EEBM3 is shown in Figure 14 compared with the observed data. Figure 11 (the shaded part or just the vertical displacement with depth) immediately indicates which portion of the structure is responsible for the large discrepancy between this assumed model and the observed data at about 7 seconds period.

Therefore, using this approach, one can adjust an assumed model in a systematic fashion to find that structure which best fits the observed dispersion.

## 3. Surface Distance from Rudoe's Formula

In many investigations in geophysics it is desirable to know the surface distance between points on the earth's surface very precisely.

With the aid of modern computers it is practical to use Rudoe's formula, which gives surface distances more accurately than the standard methods of converting distance in degrees of central angle in the earth to surface distance. Since Rudoe's formula is not well known it seems worthwhile to give the formula here with a brief explanation of how it works.

The basis of the method is to approximate the geodesic distance between any two points on the ellipsoid of revolution representing the earth by normal section distances between the two points. That is, one computes the distance from one point to another along the intersection of a plane passing through the two points and the center of the earth, with the surface of the earth (ellipsoid of revolution). This intersection is an ellipse which very closely approximates the geodesic passing through the two points.*

The surface distance between the points $(\phi_1, \lambda_1)$ and $(\phi_2, \lambda_2)$ where $\phi$ is the geographic latitude and $\lambda$ is the

---

*For example the length of the normal section differs from that of the geodesic by under 1 in 150,000,000 for a distance of 2000 miles. The difference between the normal section and geodesic distances can always be ignored for the earth.

longitude is given by

$$L = b_0 \left[ C_0 (u_2' - u_1') + C_2 (\sin 2u_2' - \sin 2u_1') + C_4 (\sin 4u_2' - \sin 4u_1') + \cdots \right] \quad (1)^*$$

where

$$b_0 = \left[ \nu_1 / (1+\epsilon_0) \right] \sqrt{1 + \epsilon \cos^2 A_{12} \cos^2 \varphi_1}$$

$$\epsilon_0 = \epsilon (\cos^2 \varphi_1 \cos A_{12} + \sin^2 \varphi_1)$$

$$C_0 = 1 + \epsilon_0/4 - 3/64\, \epsilon_0^2 + 5/256\, \epsilon_0^3$$

$$C_2 = -\epsilon_0/8 + \epsilon_0^2/32 - 15/1024\, \epsilon_0^3$$

$$C_4 = -1/256\, \epsilon_0^2 + 3/1024\, \epsilon_0^3$$

$$u_2' = \tan^{-1} \left[ \frac{\nu_1 \sin \varphi_1 + (1+\epsilon_0)(z_2 - z_1)}{\sqrt{1+\epsilon_0}\,(x_2 \cos A_{12} - y_2 \sin \varphi_1 \sin A_{12})} \right]$$

$$u_1' = \tan^{-1} \left[ \tan \varphi_1 / (\sqrt{1+\epsilon_0} \cos A_{12}) \right]$$

$$x_2 = \nu_2 \cos \varphi_2 \cos \Delta\lambda$$

$$y_2 = \nu_2 \cos \varphi_2 \sin \Delta\lambda$$

$$z_2 = \nu_2 (1+\epsilon^2) \sin \varphi_2$$

$$z_1 = \nu_1 (1-\epsilon^2) \sin \varphi_1$$

---

* See Bomford, Geodesy, pages 88-89.

$$A_{12} = \tan^{-1}\left[\frac{\sin\Delta\lambda}{(\Lambda_{12} - \cos\Delta\lambda)\sin\varphi_1}\right]$$

azimuth at $(\varphi_1, \lambda_1)$ of normal section containing $(\varphi_2, \lambda_2)$

$$\Lambda_{12} = \frac{\tan\varphi_2}{1 + \epsilon\tan\varphi_1} + e^2\sqrt{\frac{(1+\epsilon) + \tan^2\varphi_2}{(1+\epsilon) + \tan^2\varphi_1}}$$

$$\Delta\lambda = \lambda_2 - \lambda_1$$

$$\epsilon = e^2/(1 - e^2)$$

$$e = \sqrt{(a^2+b^2)/a^2}$$

eccentricity of the ellipsoid with semiaxes a and b

$\nu_i$ = radius of curvature in the prime vertical at $(\varphi_i, \lambda_i)$

Using the International Ellipsoid as the earth model the quantities necessary to use Rudoe's formula are given by

$$e^2 = 6.72267002 \cdot 10^{-3}$$

$$\nu_i = \exp\left[3.8054426856 - 7.323684 \cdot 10^{-4} \cos 2\varphi_i + 6.175 \cdot 10^{-7} \cos 4\varphi_i - 7.0 \cdot 10^{-10} \cos 6\varphi_i + \ldots.\right]$$

Equation 1 gives normal section distances correct to 1 in $10^7$ for any distance.

Rudoe's formula was incorporated in a computer subroutine for calculating distances and azimuths on the earth. (see Appendix H).

# APPENDIX H

## COMPUTER PROGRAMS

A number of computer programs and subroutines have been written to facilitate the computations described in the text of this thesis.

Some of these programs have broad enough application to be of use in future research, so that inclusion of them here seems warranted.

The source programs have some explanation of the methods used whereas, the subroutines merely state what the subroutine does and how to use it.

1. Source Programs

A. Fourier Analysis Package

This program for the IBM-7090 computer calculates the Fourier Transform of a series of points $X_i$ after any, all, or none of the following operations are performed before taking the transform:

(1) Remove a mean or linear trend from the data.

(2) Filter with up to 1000 filter coefficients and decimate by any number up to 100.

(3) Remove a mean or linear trend from the resulting series.

*(4) Print out and plot the resultant series after some, all, or none of the above.

The output format is:

| Frequency (cycles/ time unit) | Period (time units) | Cosine Trans. | Sine Trans. | Modulus (A) |
|---|---|---|---|---|

| Modulus Normed ($A/A_{max}$) | $\text{Log}_e$ A | Phase (Fractions of a circle) | Index |
|---|---|---|---|

Plot of Modulus Normed, $\left| \text{Log}_e(A/A_{max}) \right|$, and Phase as a function of frequency.

Limitations:

(1) Total number of data points $\leq$ 15,000

(2) Total number of frequencies $\leq$ 1,000

(3) Total number of filter coefficients $\leq$ 999

(4) Decimation number $\leq$ 99

(5) Any number of different sets of data may be Fourier transformed as one job by putting them one after another behind the program binary deck.

To use the program, prepare a data deck, for each series to be analyzed, consisting of the following:

---

*After step (4) one can bypass the Fourier Transform if just processing of the data with any of (1), (2), or (3) is desired.

(1) Two cards containing any identifying information; these two cards must be inserted even if one or both is left blank.

(2) One card specifying the format of the data somewhere in the first half of the card (Col. 1-36), and the format of the filter coefficients, if any, somewhere in the second half (Col. 37-72).

(3) One card of input parameters located as follows:

| | | | |
|---|---|---|---|
| Col 1-5 | NN | Number of data points | (format I5) |
| Col 6-10 | K | Number of frequencies desired | (format I5) |
| Col 11-25 | FI | Initial frequency | (format E 15.9) |
| Col 26-40 | DF | Frequency increment | (format E 15.9) |
| Col 41-55 | DT | Digital interval of data | (format E 15.9) |
| Col 56-57 | INT | Type of integration desired | (format I2) |

$$= \begin{cases} 0 & \text{Trapezoid rule} \\ 1 & \text{Modified trapezoid rule} \\ 2 & \text{Simpson's rule} \\ 3 & \text{Filon's method} \end{cases}$$

| | | | |
|---|---|---|---|
| Col 58-59 | L | Degree of trend to be removed | (format I2) |

$$= \begin{cases} 1 & \text{Linear trend} \\ 0 & \text{Mean} \\ -1 & \text{Bypass detrend} \end{cases}$$

Col 60-61 LL Degree of trend removed just before going into F.T. (format I2)
= 1, 0, or -1 as above

Col 62-64 MN Number of filter coefficients (format I3)
= 0 Bypass
= 1 Compute coefficients
> 1 Read coefficients

Col 65-66 ML Decimation number (format I2)

Col 67-68 MI Print and plot option (format I2)

$$= \begin{cases} -1 \text{ Print and plot preprocessed data and bypass F.T.} \\ 0 \text{ Bypass and go to F.T.} \\ 1 \text{ Print and plot preprocessed data and go to F.T.} \end{cases}$$

(4) Data in the format specified on the format card.

(5) Filter coefficients, if any, in the format specified on the format card. (See (2) above). Or if MN = 1 specify N and Band. (See Note 6).

(6) Additional cards of Modification A, if any.

Each data deck must be arranged in the exact sequence given above.

The complete program ready to be run then should consist of:

(1) Peripheral cards, as required by computing center

(2) an XEQ card

(3) the binary program deck, including subroutines.

(4) a DATA card

(5) Data decks as described above

(6) an END OF FILE card

Notes:

(1) To communicate between the printed values of the Fourier transform and the plotted values match index numbers at the extreme right of the printed values with those along the abscissa of the plotted values.

(2) The plotted values and their symbols are:

$*(A/A_{max})\cdot(10/9)$
$+\left|\mathrm{Log}_e(A/A_{max})\right|$ } (use scale 0 to 1.1)

$\cdot$ Phase (use scale -0.5 to 0.5)

(3) When a filtering operation is done a non-zero decimation number, ML, must be used.

(4) Methods of Integration and Formulae:

Assumption:

$$F.T. = \int_{-\infty}^{\infty} f(t)dt = \int_{-\infty}^{0} f(t)dt + \int_{0}^{T} f(t)dt + \int_{T}^{\infty} f(t)dt =$$

$$\int_{0}^{T} f(t)dt$$

Where $f(t) = X(t)e^{i\omega t}$

(i) Trapezoid

$$F.T. = \Delta t\left[f(0)/2 + f(\Delta t) + \ldots M\ f(T-\Delta t) + f(T)/2\right]$$

$$\underbrace{-T(\Delta t)^2 f''(\bar{t})/12}_{\text{Error}} \qquad 0 < \bar{t} < T$$

(ii) Modified Trapezoid

$$F.T. = \Delta t\left[f(0)/2 + f(\Delta t) + \ldots + f(T-\Delta t) + f(T)/2\right]$$

$$+ (\Delta t)^2\left[f(0) - f(T)\right]/12$$

$$\underbrace{+ T(\Delta t)^4\ f^{IV}(\bar{t})/720}_{\text{Error}} \qquad 0 < \bar{t} < T$$

(iii) Simpson's rule

$$F.T. = \frac{\Delta t}{3}\left[f(0) + 4f(\Delta t) + 2\ f(2\Delta t) + \ldots + 4\ f(T-\Delta t) + f(T)\right]$$

$$\underbrace{-\ T(\Delta t)^4\ f^{IV}(\bar{t})/180}_{\text{Error}} \qquad 0 < \bar{t} < T$$

(iv) Filon's method:

$$F.T. = \Delta t\left[\alpha(f(T) - f(0)) + \beta\left(f(0)/2 + f(2\Delta t) + \ldots + f(T)/2\right) + \gamma\left(f(\Delta t) + f(3\Delta t) \ldots + f(T-\Delta t)\right)\right]$$

$$\underbrace{\frac{-T(\Delta t)^4}{180}\left[4\omega e^{i\pi T/2} X'''(\bar{t}) + X^{IV}(\bar{t})\right] e^{i\omega\bar{t}}}_{\text{Error}} \qquad 0 < \bar{t} < T$$

Where,

$$\alpha = \frac{2\theta^3}{45} - \frac{2\theta^5}{315} + \frac{2\theta^7}{4725} - \cdots$$

$$\beta = \frac{2}{3} + \frac{2\theta^2}{15} - \frac{4\theta^4}{105} + \frac{2\theta^6}{567} - \frac{\theta^8}{5568.75} + \cdots$$

$$\gamma = \frac{4}{3} - \frac{2\theta^2}{15} + \frac{\theta^4}{210} - \frac{\theta^6}{11340} + \frac{\theta^8}{997920} - \cdots$$

(See Tranter, C.J.; Integral Transforms in Mathematical Physics, pp.67-72)

$\theta = \omega\Delta t \leq \pi/4$ ($\theta \geq \pi/4$ see Note 7)

Selection of the integration routine which should be used depends on the series to be transformed and the transform frequencies of interest.

The properties of the first three rules are well known and only a couple of points need be made in their regard. Computationally the trapezoid and modified trapezoid are the fastest, but for a very large number of points machine roundoff error can be up to twice that in Simpson's and Filon's methods. Modified trapezoid depends more on the first derivative at the end points than does Simpson's rule, but if these derivatives are reliably determined, the error in the modified trapezoid rule is 4 times smaller than that in Simpson's rule. The main disadvantage to all three is that for a given accuracy, closer and closer spacing of data points is required as the frequency of interest increases, due to the rapid oscillation of

the $e^{i\omega t}$ factor.

Filon's method eliminates this disadvantage and requires a data spacing no finer than that necessary to integrate the series without the $e^{i\omega t}$ factor. Computationally it is slightly longer since the weighting coefficients are a function of frequency and must be calculated for each new frequency; however, this is more than compensated for by the fewer data points required. In the limit as $\omega \to 0$ this method reduces to Simpson's rule.

With Simpson's rule and Filon's method an odd number of data points is required.

(5) Computation time per 1000 data points per frequency is about $\frac{1}{2}$ sec.

(6) To compute filter coefficients insert card containing:

Col 1-5 N Determines number* (2N+1), if filter coefficients to be computed and used.(I5)

Col 6-20 Band(1) Specifies center frequency (cps of desired band times DT i.e. $f_o * DT$ (E15.7)

---

*An approximate formula to determine the number, (2N+1), of filter coefficients required is

$$N = \frac{.012}{[\text{Band}(3)]\,[\epsilon]}$$

where $\epsilon$ is the maximum error (percent) between the desired filter and the one achieved. (See Ormsby, 1961, pp. 440-466.)

Col 21-35 Band(2) Specifies half band width in cps times DT = $f_c * DT$ (E 15.7)

Col 36-50 Band(3) Specifies frequency interval between cutoff ($f_c$) and total reject, ($f_r$), times DT = $(f_r - f_c) * DT$ (E 15.7)

(7) A revision has been made so that for $\theta > \pi/4$ the following formulas are used for $\alpha$, $\beta$, $\gamma$ :

$$\alpha = ( \theta^2 + \theta . \sin\theta . \cos\theta - 2 \sin^2\theta ) / \theta^3$$

$$\beta = 2( \theta ( 1 + \cos^2\theta ) - 2 \sin\theta \cos\theta ) / \theta^3$$

$$\gamma = 4( \sin\theta - \theta \cos\theta ) / \theta^3$$

B. Fourier Analysis Package - Modification A

This program does the same things as the previous package with the following added optional features:

(1) Permits any number of velocity windows on a set of data.

(2) Band-pass filters and decimates each window and plots result.

(3) Picks zeros, peaks, and troughs of windowed, filtered series.

(4) Computes and plots group velocity dispersion U(T) for each zero, peak, and trough and any number of intermediate values.

(5) Computes the envelope of the windowed, filtered series with corresponding group velocity.

(6) Transforms windowed, filtered series and plots result.

(7) Transforms filter coefficients giving transfer function and plots result.

Input:

(1) 2 cards Identification (unchanged)

(2) 1 card Format specification (unchanged)

(3) 1 Parameter card (unchanged through Col. 68 but including Col. 69-70 M2(Velocity Window option)(format I2)

= 0 Use program exactly as before modification

≠ 0 Permits new options of Modification A

(4) Data in prescribed format

(5) Filter coefficients, if any, as before.

(6) 1 card containing:

| | | | |
|---|---|---|---|
| Col 1-15 | DELTA | Epicentral distance | (format E 15.7) |
| Col 16-30 | TINIT | Arrival time of first point of series (or travel time if TORIG is made zero.) | (format E 15.7) |
| Col 31-45 | TORIG | Origin time of event | (format E 15.7) |

(7) Any number of cards each containing:

| | | | |
|---|---|---|---|
| Col 1-4 | NU | Number of intermediate group velocities | (format I4) |
| Col 1-12 | UMX | Maximum velocity for window | (format E 10.4) |

| | | | |
|---|---|---|---|
| Col 13-24 | UMN | Minimum velocity for window | (format E 10.4) |
| Col 25-36 | BAND(1) | Center of pass band times DT | (format E 12.6) |
| Col 37-48 | BAND(2) | Half band width times DT | (format E 12.6) |
| Col 49-60 | BAND(3) | Cut off to total reject times DT | (format E 12.6) |
| Col 61-63 | N | Determination number of coefficients (2N+1) | (format I3) |
| Col 64-66 | ML | Decimation number | (format I3) |
| Col 67-69 | KW > 0 | Permits "read in" of a new initial frequency and frequency increment and changes number of frequencies to be calculated to KW. | |
| | = 0 | Computes for frequencies last specified previously. | |
| Col 70-71 | NT= 0 | Finds transform of filter coefficients | (format I2) |
| | > 0 | Does not find transform of coefficients | |
| Col 72 | ND= 0 | Another pass to follow on same data | (format I1) |
| | > 0 | Last pass on current set of data | |

(7a) Follow every parameter card above on which KW = 0 with a card containing:

Col 1-15 FI New initial frequency (format E 15.7)

Col 16-30 DF New frequency increment (format E 15.7)

C. Least Squares Phase Velocity*

This program for the Bendix G-15D computer takes phases correlated across an array of N stations ($N \geq 3$) and by means of a least squares fit to the data finds estimates of the phase velocity, C, the direction of propagation across the array, $\delta$, and the arrival time of each phase at the "origin" chosen, $\tau_o$. When $N \geq 4$ the standard deviations of C, $\delta$, and $\tau_o$ are given.

Theory:

$$\tau_{ij} = \Delta_i \cos \alpha_i \frac{\cos \delta}{C_j}_j + \Delta_i \sin \alpha_i \frac{\sin \delta}{C_j}_j + \tau_{oj}$$

$$= a_i X + b_i Y + C_i z$$

where $\tau_{ij}$ = arrival time of the $j^{th}$ phase at the $i^{th}$ station

$\Delta_i$ = great circle distance from "origin" to the $i^{th}$ station.

$\alpha_i$ = azimuth of $i^{th}$ station from "origin"

---

*An IBM 7090 subroutine was also written for this calculation (see Part II this Appendix).

$$X = \frac{\cos \delta}{C}_j$$

$$Y = \frac{\sin \delta}{C}_j$$

$$z = \tau_{oj}$$

Hence $\delta = \tan^{-1}(Y/X)$

$$C = (X^2 + Y^2)^{-1/2}$$

$$\sigma_\gamma = \left( \sum_k \left( \sigma_{x_k} \frac{\partial \gamma}{\partial x_k} \right)^2 \right)^{1/2}$$ standard deviation of $\gamma(x,y,z)$

Output Format:

| | | | | |
|---|---|---|---|---|
| X | $\sigma_X$ | Y | $\sigma_Y$ | |
| Z | $\sigma_Z$ | | | |
| C | $\sigma_C$ | $\delta$ | $\sigma_\delta$ | N |

Procedure:

1. Load IC 1000 DP

2. Read program (551700 then 691700; wait for photo reader light to remain off)

*3. Enter: a) $\Delta_i$ in consecutive locations in CH 13 starting at 1300

b) $\alpha_i$ in consecutive locations in CH 15 starting at 1500

4. a) Manually set index register 47200(2(N-1))

---

*If the $a_i$, $b_i$ are already computed, enter the $a_i$ in CH 13 and $b_i$ in CH 14, set index register 47200(2(N-1)), and go to step 5.

b) Compute automatically beginning at 1179 (691179). The coefficients $b_i$ and $a_i$ will be computed and typed out in pairs, $b_i$ then $a_i$. When the computer halts, the $a_i$ will be stored in CH 13 and the $b_i$ in CH 14.

5. Enter: a) $\tau_{ij}$, (i=1,N) in CH 12 starting at 1200

b) N in 0990 ($N \leq 47$)

6. Compute automatically beginning at 1710. N-2 calculations will be made, successively eliminating stations starting with first station. Manually stop program if less than N-2 calculations are desired. Data is not destroyed.

7. a) Reload N in 0990

b) Set index register 27000 (2(K-1)) where the $K^{th}$ station is the first to be eliminated.

c) Compute automatically beginning at 1706 (691706) N-2 (or K if $N-2 > K$) calculations will be made successively removing stations beginning with the $K^{th}$ station, then the $(K-1)^{st}$ etc.

8. Go to step 5 for next phase, $\tau_{i(j+1)}$.

Remarks:

1. The average period to be associated with each phase is not computed by this program and must be obtained elsewhere.

2. The use of this program is not restricted to dispersed surface waves. It can be used for body waves or any propagating event to find the apparent velocity and direction of propagation.

D. Group Velocity from Phase Velocity Dispersion

This program for the IBM 7090 computer takes N phase velocity (C) versus period (T) or frequency (f) points, fits a best least squares polynomial (P(x)) to the points and uses this polynomial and its derivative to obtain the group velocity as a function of period or frequency. The formula used is

$$U(x) = \frac{P(x)}{\left[1.0 + (-1)^k \times P'(x)/P(x)\right]}$$

where $x = T$ period; $P(x) = C(T)$ phase velocity; $P'(x) = \frac{dC(f)}{dT}$ } if k is even

$x = f$ frequency; $P(x) = C(f)$ phase velocity; $P'(x) = \frac{dC(f)}{df}$ } if k is odd

Any order polynomial up to 19 may be used for the fit.

Any number of values of U for arbitrary T or f may be computed, as well as values at the input values of T or f, if desired.

Input: Each set of data should consist of

(1) 2 cards of identifying information

(2) 1 card containing:

Col 1-36 Format of phase velocities to be read. e.g. (18F4.1)

Col 37-72 Format of periods or frequencies to be read.

(3) 1 card containing:

| | | |
|---|---|---|
| Col 1-6 | N | Number of input dispersion points. |
| Col 7-12 | NZ | Number of output dispersion points desired. |
| Col 13-14 | KK | Degree + 1 of desired polynomial. |
| Col 15-29 | DT | Period (frequency) increment between output points. |
| Col 30-44 | TB | Beginning period (frequency) for output points. (Computes NZ dispersion points at intervals of DT beginning at TB). |
| Col 45-46 | L | = 0 Does not compute values at the input points.<br>= 1 Computes for input periods (frequency) using fitted phase velocities.<br>= 2 Computes for input periods (frequency) using both fitted and input phase velocities. |
| Col 47-48 | LF | = 0 indicates input periods will be read. |

= 1 indicates input frequencies will be read.

= 2 indicates input periods to be computed at equal increments beginning at T1.

= 3 indicates input frequencies to be computed at equal increments beginning at T1.

= -1 indicates input C(f) to be computed at equal increments beginning at T1.

= -2 indicates input C(T) to be computed at equal increments beginning at T1.

Col 49-60 T1 Beginning input

T if LF = 2

f if LF = 3

C(f) if LF = -1

C(T) if LF = -2

Col 61-72 TINC Increment for input

T if LF = 2

f if LF = 3

C(f) if LF = -1

C(T) if LF = -2

(4) Input phase velocities if not computed internally, in the format specified above.

(5) Input periods (frequencies), if not computed

internally, in the format specified above.

Output:

(1) Coefficients of fitted polynomial

(2) Period (frequency), Phase Vel, Group Vel.

a) from TB to TB + (NZ-1)DT

b) optionally for input T, computed C

c) optionally for input T, input C

Notes:

1. $C(I) = C(T(I)) \qquad I = 1,N$

2. If T or f is computed C must be read and vice versa.

3. For experimental data a rather low order fit should be used because it smooths the data and better approximates the true group velocity curve.

4. T(1) or f(1) is used to normalize the input values of T or f before the fitting is done. Other normalizations may be used by changing a command in the Fortran source deck and recompiling. Output values are not normalized.

Limitations:

1. $N \leq 5000$

2. $KK \leq 20$

2. Subroutines

A. Subroutine DISTAZ (TH, PHI, N, K, XDEG, AZ, AZINV, DIST, STA)

Distance-Azimuth Computations

Computes distances and azimuths from the Kth point on the earth's surface to each of a set of N-1 other points, given the longitude and geographic latitude of each point.

Distance in degrees of central angle and azimuths are computed using direction cosines with geocentric latitude. Distance in kilometers is determined using Rudoe's formula. The International Ellipsoid taken as the earth model.

Input:

STA(I) = Alphanumeric designation of I'th station (16) (I = 1,N)

TH(I) = Geographical latitude of Ith station in degrees (I = 1,N)

PHI(I) = Longitude of Ith station in degrees (I = 1,N)

N = Number of stations including origin

K = Station to be used as origin

Quantities Computed:

XDEG(I)= Distance in degrees of central angle from STA(K) to STA(I)

DIST(I)= Distance in kilometers from STA(K) to STA(I)

AZ(I) = Azimuth from STA(K) to STA(I) (measured from North)

AZINV(I)= Azimuth from STA(I) to STA(K)

| PRINT | FORMAT: |
|---|---|
| Origin | STA(K) |
| Lat. | TH(K) |
| Long. | PHI(K) |

| Station | Latitude | Longitude | DIST(deg) |
|---|---|---|---|
| STA(I) | TH(I) | PHI(I) | XDEG(I) |

| DIST(km) | Azimuth | Back Azimuth |
|---|---|---|
| DIST(I) | AZ(I) | AZINV(I) |

Restriction:

Each of the subscripted variables above must be in a DIMENSION statement in the source program.

B. Subroutine PHVEL (Y, DIST, AZ,L,M,K,PV, SDPV, TH, SDTH, PAT, SDPAT)

Input:

Y(I,J) = Arrival time of the $j^{th}$ event at the $I^{th}$ station I = 1,N J = 1,K

DIST(I) =Distance of $I^{th}$ station from some point (pseudo-origin) within or near the array.

AZ(I) = Azimuth of $I^{th}$ station from the pseudo-origin.

L(JJ) = Specifies the array of stations to be used for phase velocity calculation. This enables one to use any subset of a large number of stations for a particular phase velocity calculation. M $\leq$ total number of stations. (e.g., L(1) = 2, L(2) = 4, L(3) = 8, L(4) = 3 would compute phase velocity for array of stations 2, 4, 8, and 3)

M = Number of stations in the array L

K = Number of events or phases.

Computes:

PV(J) = Phase velocity of $j^{th}$ event across the array L of M stations

SDPV(J)= Standard Deviation of PV(J)

TH(J) = Direction of propagation of $j^{th}$ event across the array L of M stations

SDTH(J)= Standard deviation of TH(J)

PAT(J) = Predicted arrival time of the $j^{th}$ event at the pseudo-origin.

SDPAT(J)=Standard deviation of PAT(J)

Restrictions:

M $\leq$ 100 can be increased by changing DIMENSION

of X(100), A1(100), and AZ(100) and recompiling.

Requires Subroutine LSQFIT and DET3

C. Subroutine PICK (X,NN,DT,YS,Y,N)

This subroutine takes an oscillatory function, X(t), having NN values sampled at an interval DT beginning at YS and picks the location $y_i$ of each zero, peak, and trough and stores them as the array Y. Y(1), Y(3), Y(5) . . . . are the zeros of X(t), and Y(2), Y(4), Y(6) . . . . are the peaks and troughs. N is the total number of values in the Y array, i.e. total number of zeros, peaks and troughs picked.

Restriction:

Arrays X and Y require DIMENSION statements in the source program.

D. Subroutine IMPRSP (M, KK, W, DW, A, TG, TP, Y)

Given:

M = number of synthesis points desired

KK = number of input frequencies to be used

W(I) = array of frequencies I = 1, KK

DW(I) = array of frequency increments DW(I) = $W(I+\frac{1}{2})-W(I-\frac{1}{2})$ I = 1, KK

A(I) = array of amplitudes I = 1, KK

TG(I) = Group delay I = 1, KK

TP(I) = Phase delay I = 1, KK

T = starting time

Computes:

$$Y(t) = 2\sum_{I=1}^{KK} \frac{A(W_i) \quad \sin\left(\frac{\Delta W_i}{2} \cdot (t-tg_i)\right) \cdot \cos\left(W_i(t-tp_i)\right)}{t-tg_i}$$

Output:

Prints and stores Y(t) as the array Y(I) I = 1, KK

Required statements in source program:

Dimension W( ), A( ), DW( ), TG( ), TP( ), Y( )

E. Subroutine LSQFIT (Y,A1,A2,N,D2,SD2,D3,SD3, D4,SD4,SD )

For a set of N equations of the form

$$Y_i = A1_i X_i + A2_i X_2 + X_3 \qquad (1)$$

Finds least square fit giving best $X_1$, $X_2$, $X_3$ and the standard deviation of each.

Restriction:

(1) $N \leq 20$ (This can be changed by changing DIMENSION statement for Y, A1, and A2)

(2) Requires SUBROUTINE DET3

(3) Coefficient of $X_3$ is always 1; this can always be achieved by dividing both sides of (1) by the coefficient of $X_3$.

Input:

Arrays Y(I,1), A1(I), A2(I) } I = 1,N

N = number of values in each of the above arrays; also number of equations of form (1)

Output:

D2 = $X_1$ where $X_i$ is quadratic mean error in determining $X_i$

SD2 = $\sigma_{X_1}^2$

D3 = $X_2$

SD3 = $\sigma_{X_2}^2$

D4 = $X_3$

SD4 = $\sigma_{X_3}^2$

SD = $\sigma^2$ where $\sigma$ is quadratic mean error in the whole set of observations

F. Subroutine NDTRND (K,KK,X,N,Z)

This subroutine takes an X, of N points, fits a least squares straight line to the first K points and a different least squares straight line to the last KK points, and removes a linear trend from all N points of X using a weighted slope

$$\left(\overline{\frac{dX}{dt}}\right) = \left[K\left(\frac{dX}{dt}\right)_K + KK\left(\frac{dX}{dt}\right)_{KK}\right] \Big/ (K + KK)$$

to give a new array, Z, of N points.

(1) Input K, KK, N, X defined above. (K, KK, N are integers)

(2) Output array Z of N "NDTRND"ed points (Z can be X in the calling statement causing original series to be replaced by new "NDTRND"ed series; i.e., calling sequence can be (K, KK, X, N, X)

(3) Limits: $K \leq 1000$

$KK \leq 1000$

This can be increased or decreased by changing DIMENSION of Y(1000)

(4) Required subroutine DETRND

G. **Function NFACT (N,K)**

Factorial Function

Computes NFACT = N · (N-1) · (N-2) · (N-3) --- (N-K) for any integer N with $K \leq (N-1)$

H. **Subroutine DET3 (A,D )**

Compute value, D, of a 3 X 3 determinant

$$A = \begin{vmatrix} A(1) & A(2) & A(3) \\ A(4) & A(5) & A(6) \\ A(7) & A(8) & A(9) \end{vmatrix}$$

I. **Subroutine POLVAL (X,B,KK,S)**

Evaluate a polynomial:

Takes an independent variable X and a set of KK

coefficients B(I,1),I = 1,KK and computes the value, S, of a polynomial of degree KK-1 having coefficients B.

i.e. $S = B(1,1) + B(2,1)X + B(3,1)X^2 + \ldots B(KK,1)X^{KK-1}$

Restrictions:

KK $\leq$ 20. This can be increased by recompiling and changing first dimension of B in DIMENSION statement.

J. Subroutine DERIV (X,B, KK, S)

Derivative of a polynomial:

For a given X computes $S = \left(\frac{dY}{dX}\right)_X$ where $Y = B(KK,1)X^{KK-1}$

$+ \ldots + B(2,1)X + B(1,1)$

Restrictions:

KK $\leq$ 20 This can be increased by changing just dimension of B in the DIMENSION statement.

K. Subroutine DPOLYC (K,N, B,A,M)

Given a set N + 1 coefficients, B, of an $N^{th}$ degree polynomial this subroutine computes the M coefficients, A, of the $K^{th}$ derivative polynomial.

Input:

B(I) I = 1,N + 1 = Array of coefficients of an $N^{th}$ degree polynomial

N = Degree of polynomial

K = Derivative desired

Output:

A(I) I = 1,M = Array of coefficients of $K^{th}$ derivative polynomial

M = Number of coefficients of $K^{th}$ derivative polynomial

Requires DIMENSION statement for B and A in source program; FUNCTION NFACT.

L. Subroutine CXPROD ( Z,S,L,K )

Complex Product:

Given a set of complex numbers Z(I,1) + iZ(I,2) I = 1,N and L(J) a set of K integers between 1 and N, this subroutine computes the complex product

$$S = \prod_{J=1}^{K} \left[ Z(L(J),1) + iZ(L(J),2) \right] = S(1,1) + iS(1,2)$$

# APPENDIX I

## MODIFIED USE OF THEORETICAL DISPERSION CURVES

Transition zones appear to be able to distort the phase velocity dispersion curves enough so that absolute thickness values derived from the ordinary theoretical dispersion for plane horizontal structures are not reliable.

Examination of typical continental phase velocity dispersion curves indicates that in the period range above about 16 seconds $\left(\frac{\partial C(T,H)}{\partial H}\right)_T$ is a slowly varying function of H for $25 \leq H \leq 45$ km. This means that it may be possible to interpret the observed dispersion using the standard theoretical dispersion calculations in a slightly different way.

Let

$C(T,H)$ = phase velocity

$T$ = period

$H$ = crustal thickness

then

$$dC(T,H) = \left(\frac{\partial C}{\partial T}\right)_H dT + \left(\frac{\partial C}{\partial H}\right)_T dH \qquad (1)$$

For a fixed T,

$$dC(T,H) = \left(\frac{\partial C}{\partial H}\right)_T dH$$

or

$$dH = dC / \left(\frac{\partial C}{\partial H}\right)_T \qquad (2)$$

Once existing body velocities and densities are determined for a region, then the usual multi-layered dispersion calculation permits a determination of $\left(\frac{\partial C}{\partial H}\right)_T$ for any interval $H_1 \lesssim H \lesssim H_2$ defining the bounds on the absolute thickness thought to exist in that region. Inherent is the assumption that only layer thicknesses change so that no lateral gradients exist in body velocity within each layer.

However, it should be pointed out that with the relative ease of computing theoretical dispersion curves, one can readily investigate cases where only some of the crustal layers vary laterally in thickness without violating this assumption.

Values of dC(T) are obtained from the experimental measurements of phase velocity over two or more adjacent local tripartite arrays.

For numerical computations, let

$$\begin{aligned} T &\rightarrow T_i \\ d\,C(T,H) &\longrightarrow \Delta C(T_i, H) = \Delta C_i \\ d\,H &\rightarrow \Delta H \\ \left(\frac{\partial C(T,H)}{\partial H}\right)_{T_i} &\longrightarrow \alpha(T_i, H) = \alpha_i \end{aligned} \tag{3}$$

Then an independent estimate of the change in thickness is obtained for every period $T_i$ $(i = 1, 2, \cdots, N)$ so that the mean change in crustal thickness is given by

$$\Delta H = \frac{1}{N} \sum_{i=1}^{N} \frac{\Delta C_i}{\alpha_i} \tag{4}$$

with a standard deviation of

$$\sigma = \left[ \frac{1}{N-1} \sum_{i=1}^{N} \left( \frac{\Delta C_i}{\alpha_i} - \Delta H \right)^2 \right]^{\frac{1}{2}} \qquad (5)$$

The following table serves as an example for values of $\left(\frac{\partial C}{\partial H}\right)_T$ . These values come from Press's standard curves.

TABLE 6

Change in phase velocity (C) with change in total crustal thickness (H) vs. period (T) using Press's standard curves.

| Period T(sec) | $\left(\frac{\partial C}{\partial H}\right)_T$ $25 \leq H \leq 35$ km | $\left(\frac{\partial C}{\partial H}\right)_T$ $35 \leq H \leq 45$ km |
|---|---|---|
| 12 | .015 | .006 |
| 14 | .020 | .0075 |
| 16 | .025 | .011 |
| 18 | .023 | .014 |
| 20 | .022 | .017 |
| 22 | .018 | .018 |
| 24 | .015 | .017 |
| 26 | .012 | .0165 |
| 28 | .010 | .015 |
| 30 | .008 | .011 |
| 36 | .005 | .008 |
| 40 | .0045 | .0055 |
| 48 | .004 | .0035 |

Note that in this example $\left(\frac{\partial C}{\partial H}\right)_T$ is a very slowly varying function of H for periods beyond 20 seconds for the depth range $25 \lesssim H \lesssim 45$ km.

To assign absolute thicknesses using this modified method requires that the crustal thickness be known at one point in the region to be studied. This is the only requirement in addition to usual ones of specifying velocity-density structure for computing the theoretical dispersion curves. It is felt that in transition zones this modified approach is the most reliable means of determining absolute crustal thickness from phase velocity dispersion.

FIGURE CAPTIONS

Figure 1. Map showing the paths from Pasadena to the continental sources used. Paths from other stations in Southern California to the source areas are not shown.

Figure 2. Typical group velocity dispersion curves showing suitable band passes (alternate shaded and unshaded portions above 6 seconds period) for separating the modes in the time domain.

Figure 3. Typical group velocity dispersion curves, velocity windowed (unshaded portion) to separate the modes in the frequency domain.

Figure 4. Sample seismograms showing continental events used. The records shown are playouts of the digitized seismograms from the various stations indicated.

Figure 5. Seismogram of a Montana aftershock recorded at Riverside. This is a good example of the complicated appearance of the seismogram when more than one mode is present with sizeable amplitude.

Figure 6. Seismograms from a Montana aftershock recorded at three stations in Southern California on matched Benioff 1-90 vertical component seismographs.

Figure 7. Result of applying the mode isolation technique to the seismograms shown in Figure 6 to recover

the fundamental mode Rayleigh Waves.

Figure 8. Result of three band passes on the Riverside seismogram in Figure 6 to delineate the modes present in each frequency band.

Figure 9. Spectra at three stations of a velocity window from about 4.5 km/sec to 3.0 km/sec for a Montana aftershock. The period in seconds is indicated for each peak. These spectra were not corrected for instrument response.

Figure 10. Normalized vertical displacement with depth at two periods for the first three Rayleigh modes ($M_{11}$, $M_{21}$, $M_{12}$) for the structure shown. This illustrates that for a given frequency each successive higher mode samples deeper into the structure. The compression velocity ($\alpha$) and shear velocity ($\beta$) are in km/sec. The density ($\rho$) is in cgs units.

Figure 11. Example of how the first higher mode ($M_{21}$) at 7.249 seconds is sampling the structure indicated. The true sampling is given by scaling the shaded zone B plus $k$ times the shaded zone A by the $\rho_i \beta_i^2$ appropriate for each layer.

Figure 12. Comparison of cases to test the sensitivity of modes to changes in thickness, velocity gradients, and thin high velocity layers. The structure for Case 5EEBM3A differs from that of 5EEBM4 only in

a thin, high velocity layer at depth as shown in Figure 18. Case 5EEBM6 has a more gradual increase in velocity with depth.

Figure 13. Test of the effect of density on fundamental mode dispersion. The crosses represent the result of changing the density from 2.9 to 2.78 in the depth interval from 26.5 to 44.5 km.

Figure 14. Composite experimental group velocity dispersion for the aftershock sequence of the Montana earthquake of August 17, 1959. The solid and dashed lines are two theoretical models derived to fit the observed data.

Figure 15. Observed Love wave dispersion from two events in Utah to Pasadena. The structure for Case 35CM2 is shown in Figure 17. The solid line shows the effect of sphericity on $L_{21}$. The narrow minimum in the dispersion at about 7 seconds period (dotted line) was obtained by computing the exact group velocity by an energy method.

Figure 16. Observed Rayleigh wave dispersion from two events in Utah to Pasadena. The structure corresponding to theoretical curves for Case 35CM2 is shown in Figure 17.

Figure 17. Structure which provides the best fit to all the Basin and Range dispersion data.

Figure 18. Structure for two models having a thin high velocity layer at depth and a mantle low velocity layer.

Figure 19. Comparison of theoretical and experimental dispersion for the Basin and Range, including several cases which do not fit the data well.

Figure 20. Theoretical phase and group velocity dispersion for the structures shown in Figure 21. The thick solid line indicates the observed group velocity dispersion for the Basin and Range.

Figure 21. Crustal models based on the compressional wave refraction results of Berg et al in the Eastern Basin and Range. Only the shear velocity is allowed to vary from one case to another.

Figure 22. Theoretical phase and group velocity dispersion for the structures shown in Figure 23. The thick solid line indicates the observed group velocity dispersion for the Basin and Range.

Figure 23. Crustal models based on the compressional wave refraction results of Berg et al in the Eastern Basin and Range. Only the shear velocity is allowed to vary from one case to another.

Figure 24. Observed phase velocity dispersion for the array Pasadena - Ruth, Nev. - Albuquerque, N.M. compared to the theoretical dispersion for Case 35CM2 shown in Figure 17. Data from the Soviet

nuclear tests at Novaya Zemlya were used to obtain the experimental points.

Figure 25. Comparison of experimental Rayleigh and Love wave dispersion for the Basin and Range with that for a path further south from Oklahoma to Pasadena.

Figure 26. Observed Rayleigh wave dispersion for a path from Southern Mexico to Southern California. The dispersion for the structure model 35CM2 is shown, as well as long period higher mode curves for a Gutenberg-Birch model. Note that between 15 and 30 seconds the observed data scatters below the theoretical values.

Figure 27. Comparison of observed dispersion for the Basin and Range, Sierra Nevada, and California coastal regions.

Figure 28. Comparison of observed and theoretical dispersion for the Sierra Nevada region. Table 4 gives the structure for the theoretical curves.

Figure 29. Observed Rayleigh wave group velocity dispersion along the California coast (solid dots) compared with theoretical curves for various assumed models consistent with refraction data. Figure 30 shows the structure for each of these cases.

Figure 30. Crustal models consistent with refraction results in the coastal region of California.

Figure 31. Graph showing the relationship of compressional and shear velocity for various Poisson ratios.

Figure 32. Map showing the location (solid dots) of stations used for phase velocity measurements.

Figure 33. Summary of Press' tripartite method for determining phase velocity and direction of propagation.

Figure 34. Least squares method for determining phase velocity and direction of propagation. The arrival time of the $k^{th}$ phase at the $i^{th}$ station is $\tau_{ik}$. The standard deviations of $C_k$ and $\theta_k$ are included in expressions (i) and (ii) respectively.

Figure 35. Modifications in Press' tripartite method (Fig. 33) for use in the frequency domain. The phase difference between the $i^{th}$ and $j^{th}$ stations is $\Delta\varphi_{ij}$; $\tau_{ij}$ is the difference in feducial times used at the $i^{th}$ and $j^{th}$ stations; m and n are integers; $\Delta r_{ij}$ is the difference in epicentral distance between the $i^{th}$ and $j^{th}$ stations; $\epsilon$ is arbitrary and small; and T is the period.

Figure 36. Typical seismograms from an earthquake in the South Pacific recorded on matched Benioff 1-90 vertical seismographs in Southern California.

Figure 37. Composite of the experimental phase velocity dispersion at the continental margin of Southern California, using tripartite arrays and Fourier analysis. Press' "standard" theoretical phase velocity curves are shown for reference.

Figure 38. Experimental phase velocity dispersion comparing propagation in opposite directions over a fixed array in Southern California.

Figure 39. Comparison of refraction and phase velocity methods for determining the depth and slope of the crust-mantle interface. The structure section is from Shor and Raitt (1958).

Figure 40. Two Bouguer gravity profiles across the continental margin of Southern California.

Figure 41. Measured phase response for the Benioff 1-90 vertical instruments at the stations shown in Figure 32. The relative amplitude response normalized to unity at 5 seconds period is also shown.

Figure 42. Sample Fourier spectra for an event in the South Pacific recorded in Southern California.

Figure 43. Experimental group velocity dispersion for an event in the Solomon Islands. The dashed curves are limits of observed group velocity in the United States from this source region.

Figure 44. Summary of a method for determining the strike of linear features from lateral refraction of surface waves.

Figure 45. Summary of results from an ultra-sonic model experiment. The solid lines represent theoretical curves for a layer of thickness H over a half space. The geometry of the model is shown below the legend.

Figure 46. Amplitude dependence with depth for the fundamental and first higher mode of Rayleigh waves at station 27 in the ultrasonic model shown schematically in Figure 45. Note the reversal of polarity in the higher mode at about $H/2$.

Figure 47. Records for a profile on the ultrasonic model (Fig. 45) with the source at the thick end and no filtering. The fundamental ($M_{11}$) and first higher mode ($M_{21}$) are labeled.

Figure 48. Records for two profiles on the ultrasonic model (Fig. 45). The profile on the left was made with the source at the thin layer end and no filtering. The profile on the right was made with the source at the thick end and a narrow band pass (compare with open band records on the same profile in Figure 47).

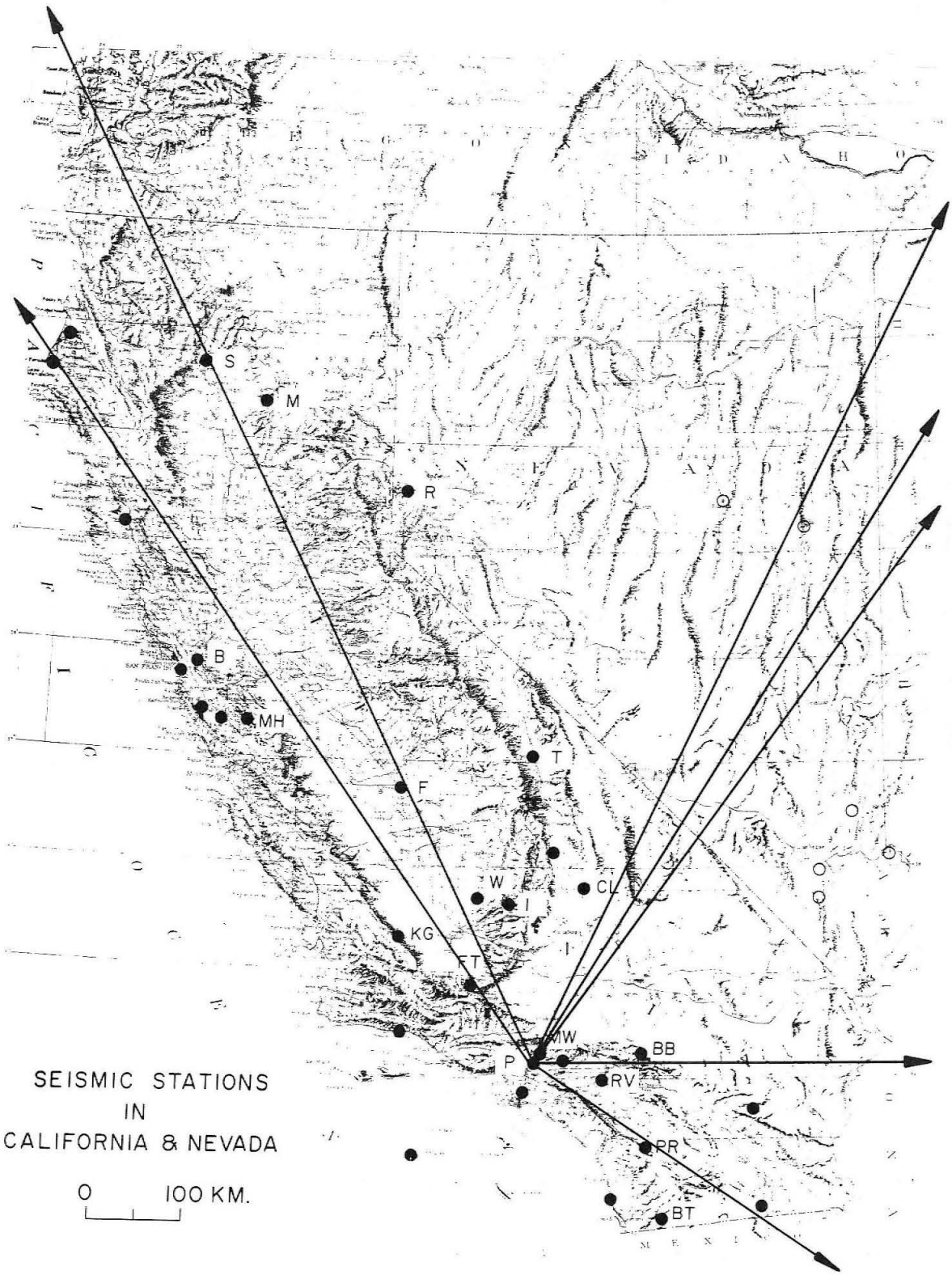
S
M
R
B
MH
T
F
W
I
CL
KG
FT
MW
BB
P
RV
PR
BT
SEISMIC STATIONS
IN
CALIFORNIA & NEVADA
0
100 KM.

Fig. 1

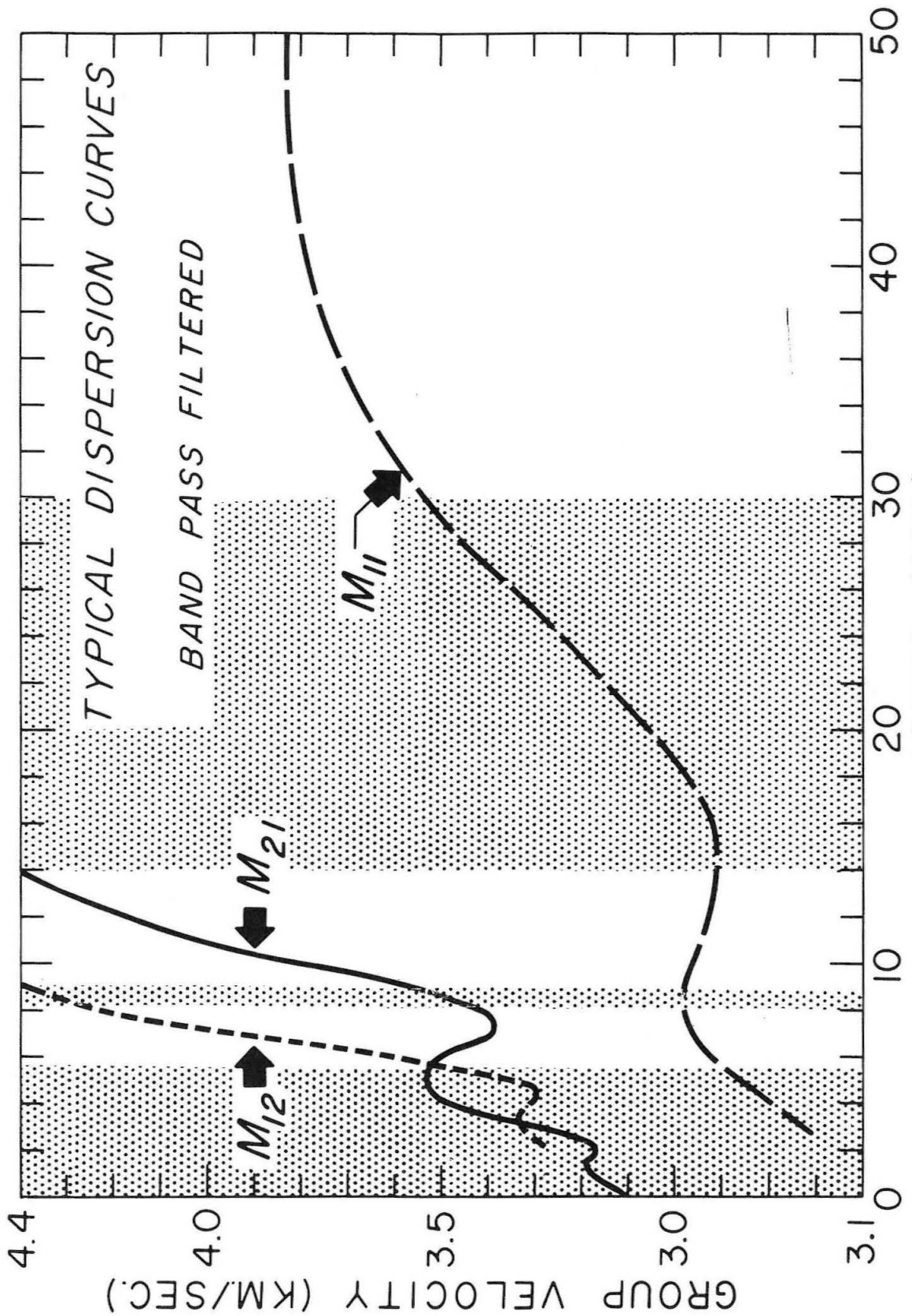
TYPICAL DISPERSION CURVES
BAND PASS FILTERED
$M_{12}$
$M_{21}$
$M_{11}$
GROUP VELOCITY (KM/SEC.)
PERIOD (SEC.)
4.4
4.0
3.5
3.0
3.1
0
10
20
30
40
50

Fig. 2

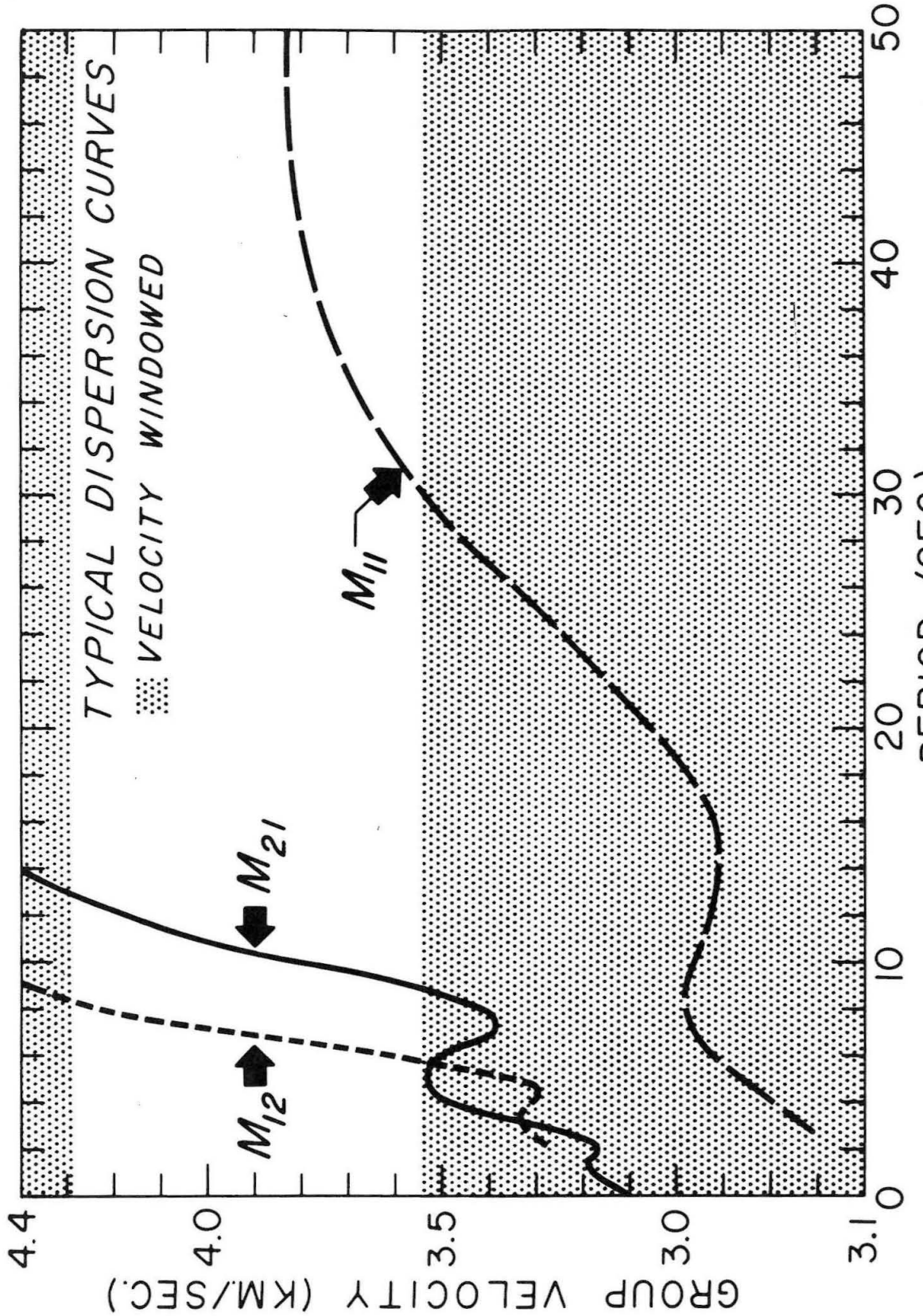
TYPICAL DISPERSION CURVES
VELOCITY WINDOWED
$M_{11}$
$M_{21}$
$M_{12}$
GROUP VELOCITY (KM/SEC.)
4.4
4.0
3.5
3.0
3.1
0
10
20
30
40
50
PERIOD (SEC.)

Fig. 3

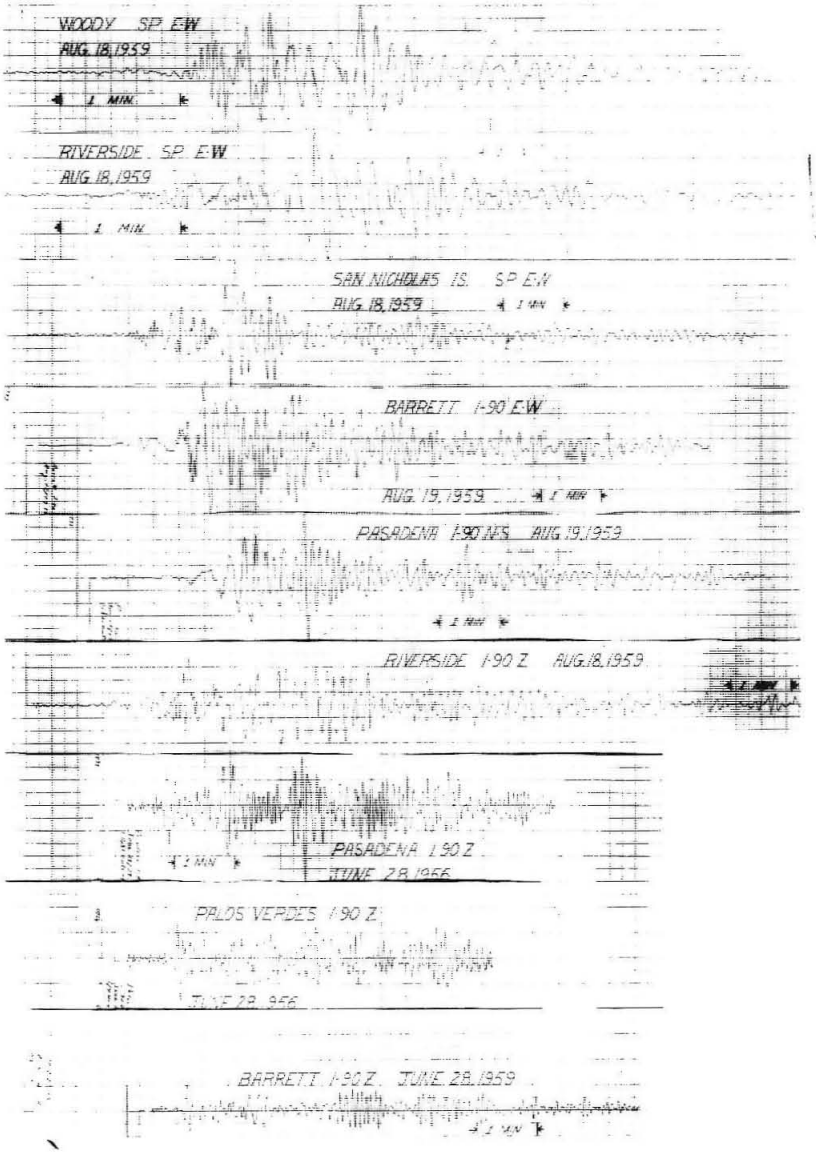
WOODY SP E-W
AUG. 18, 1959
1 MIN.
RIVERSIDE SP E-W
AUG. 18, 1959
1 MIN.
SAN NICHOLAS IS. SP E-W
AUG. 18, 1959
1 MIN.
BARRETT 1-90 E-W
AUG. 19, 1959
1 MIN.
PASADENA 1-90 N-S AUG. 19, 1959
1 MIN.
RIVERSIDE 1-90 Z AUG. 18, 1959
1 MIN.
PASADENA 1-90 Z
JUNE 28, 1956
1 MIN.
PALOS VERDES 1-90 Z
JUNE 28, 1956
BARRETT 1-90 Z JUNE 28, 1959
1 MIN.

Fig. 4

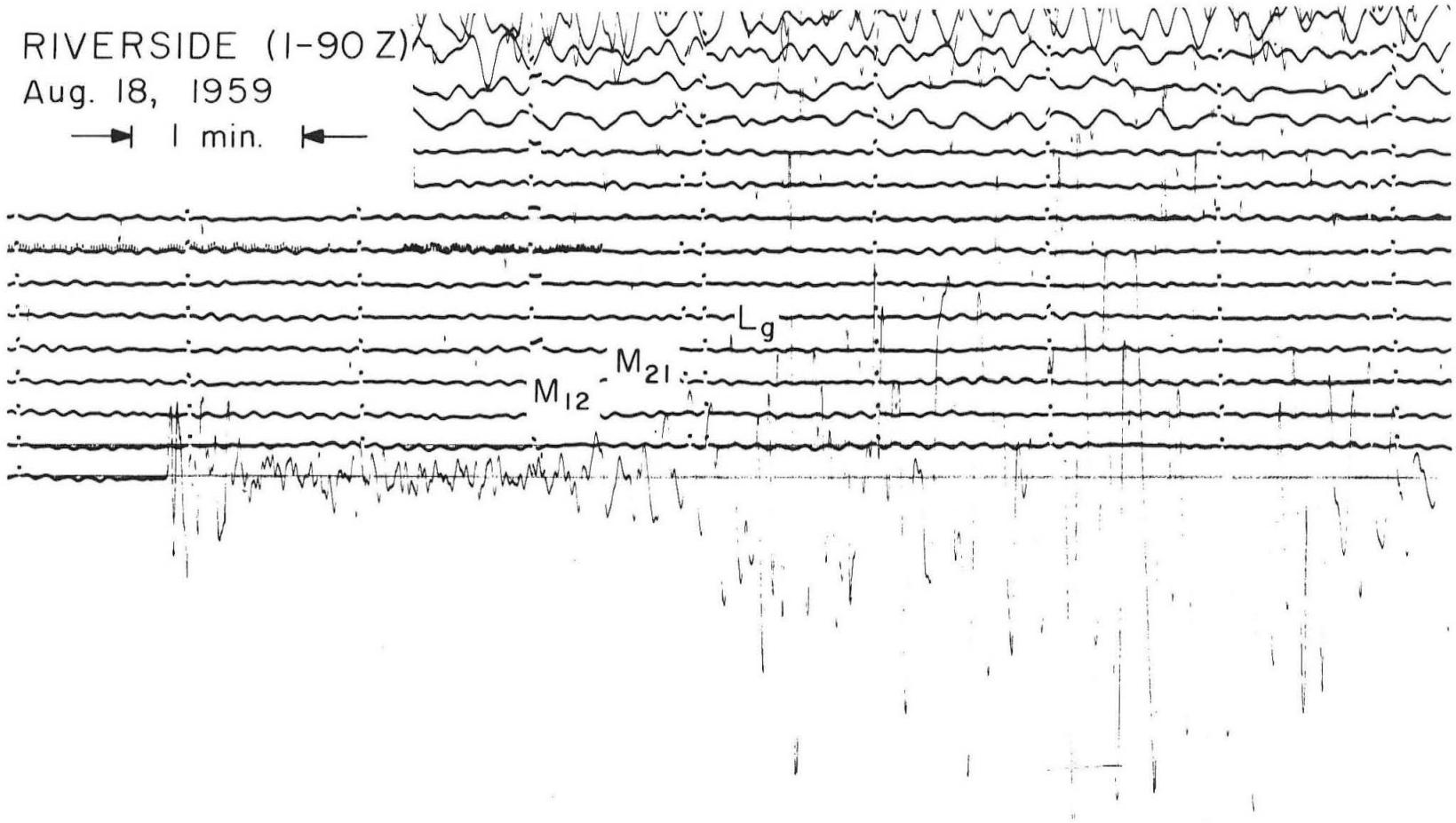


Fig. 5

MONTANA AFTERSHOCK Aug. 19, 1959


Fig. 6

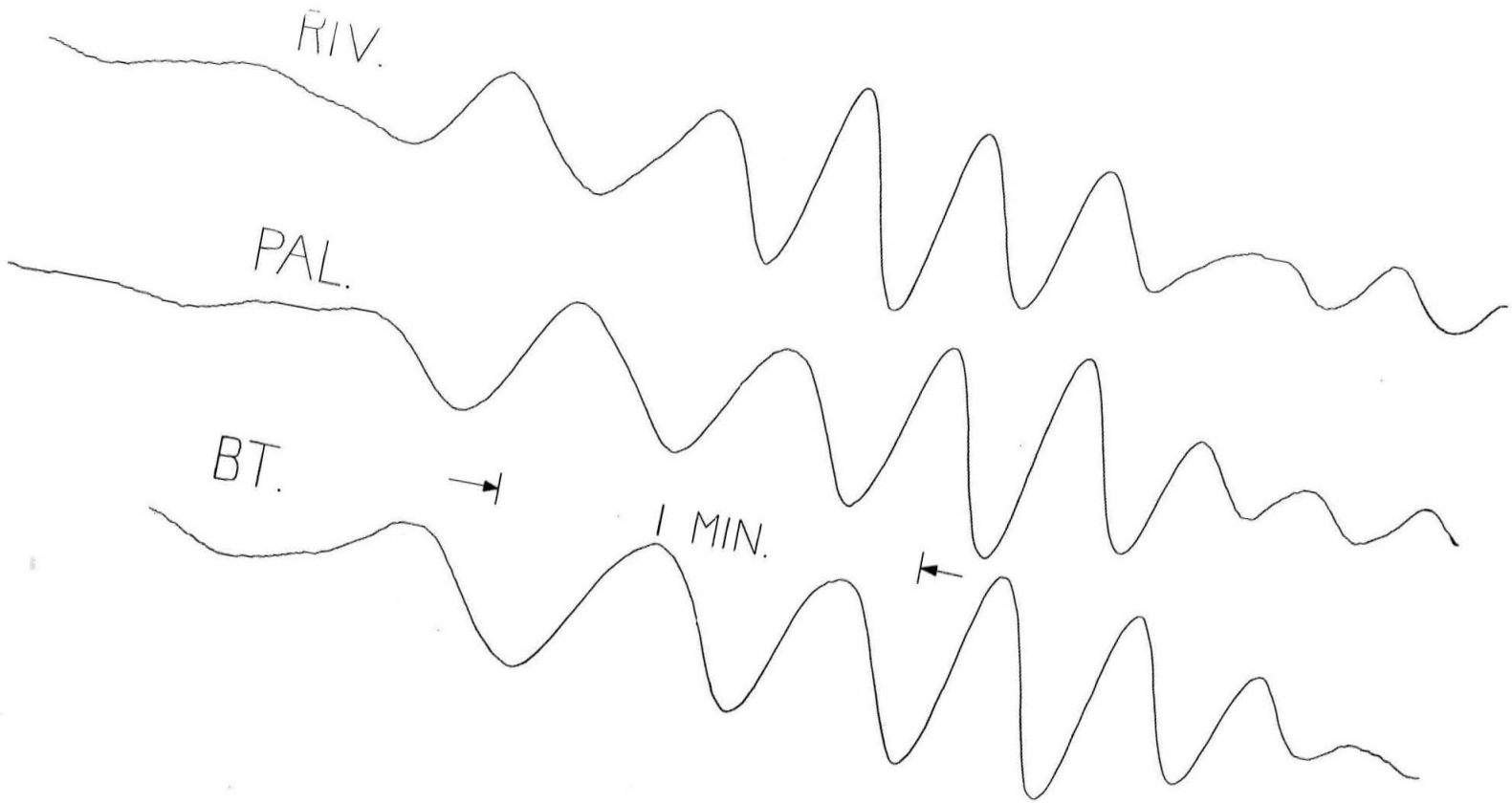


Fig. 7

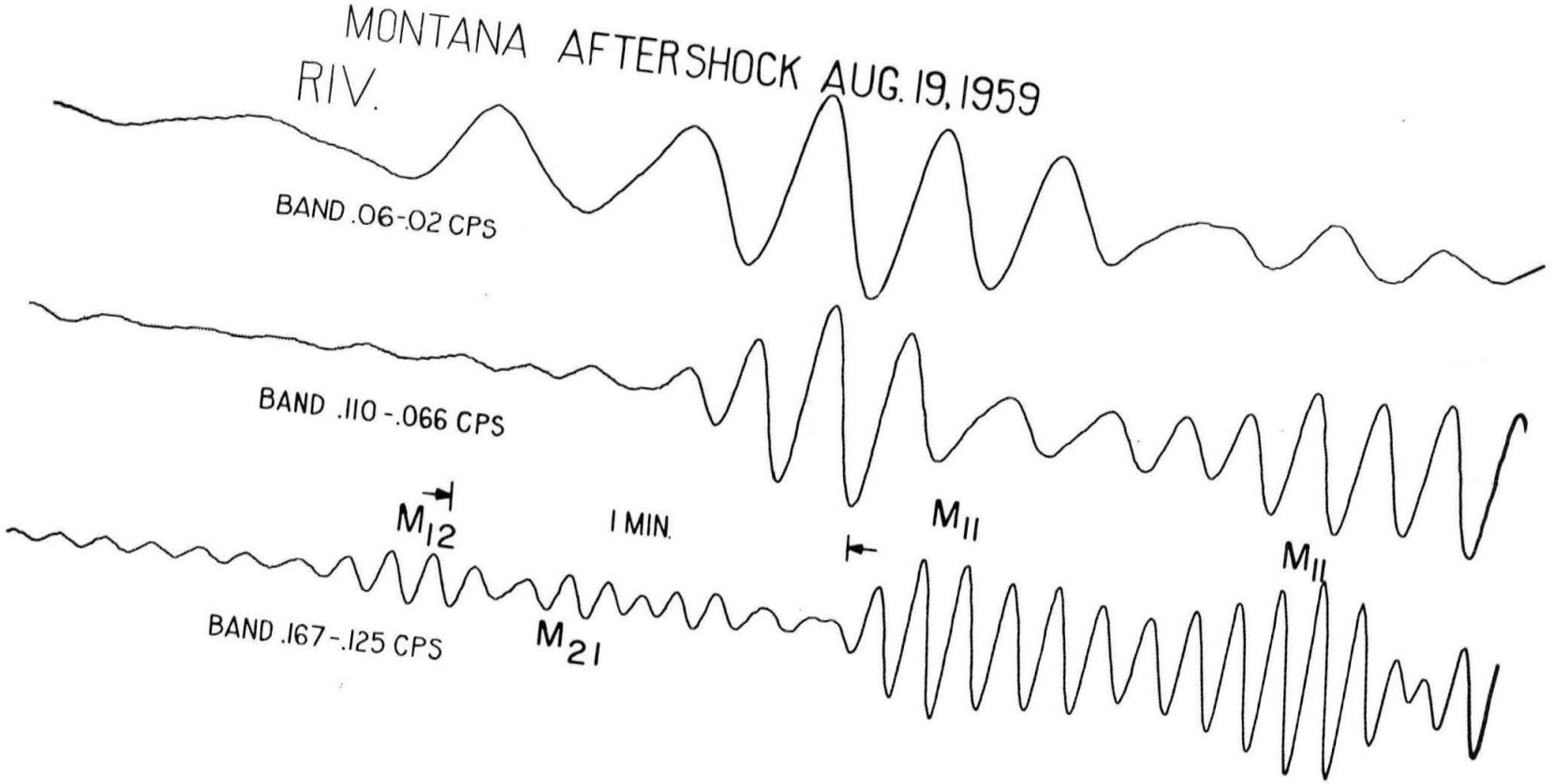
MONTANA AFTERSHOCK AUG. 19, 1959
RIV.
BAND .06-.02 CPS
BAND .110-.066 CPS
BAND .167-.125 CPS
M12
1 MIN.
M21
M11
M11

Fig. 8

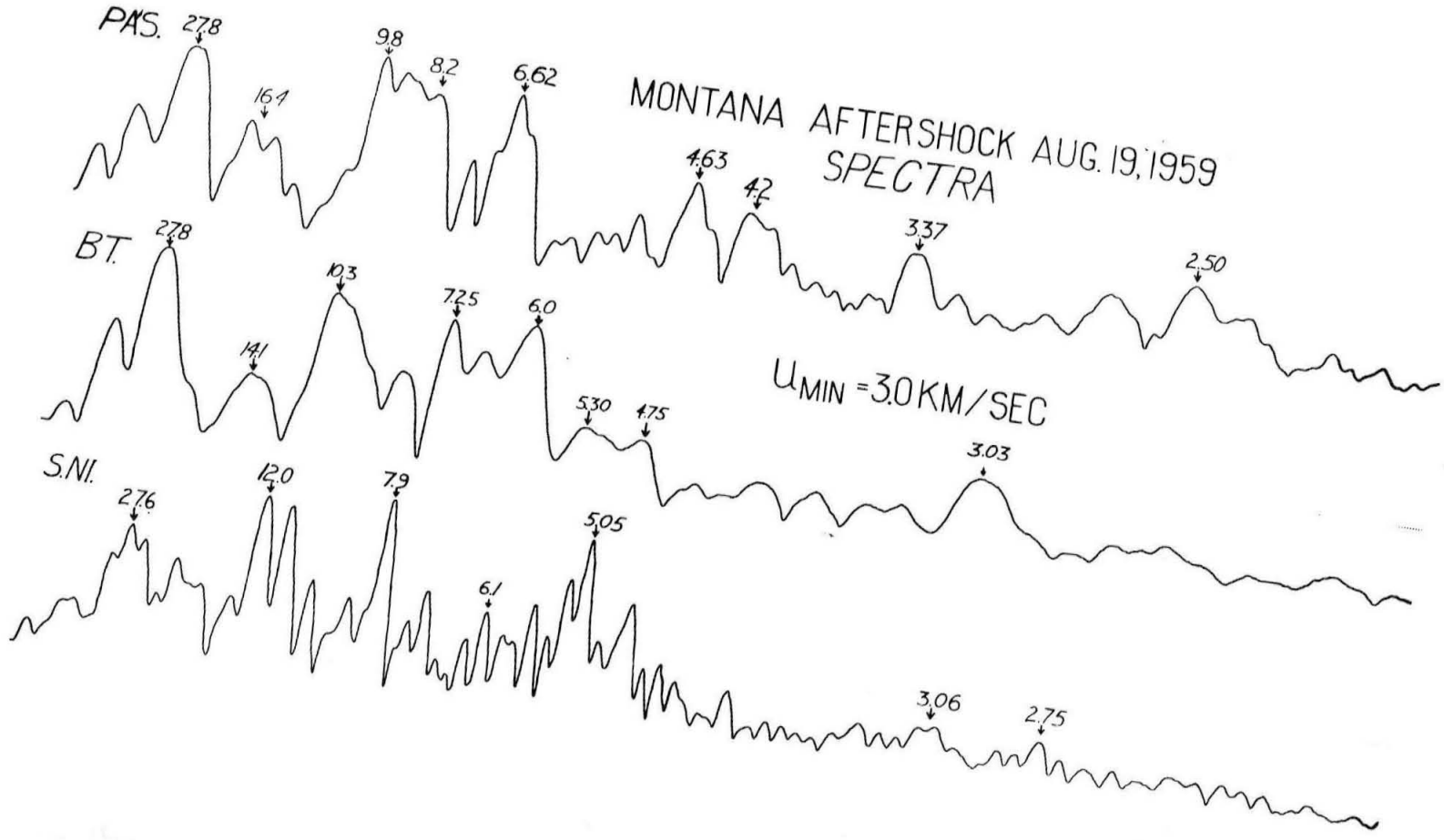
PAS.
27.8
16.1
9.8
8.2
6.62
4.63
4.2
3.37
2.50
BT.
27.8
14.1
10.3
7.25
6.0
5.30
4.75
3.03
S.NI.
27.6
12.0
7.9
6.1
5.05
3.06
2.75
MONTANA AFTERSHOCK AUG. 19, 1959
SPECTRA
UMIN = 3.0 KM/SEC

Fig. 9

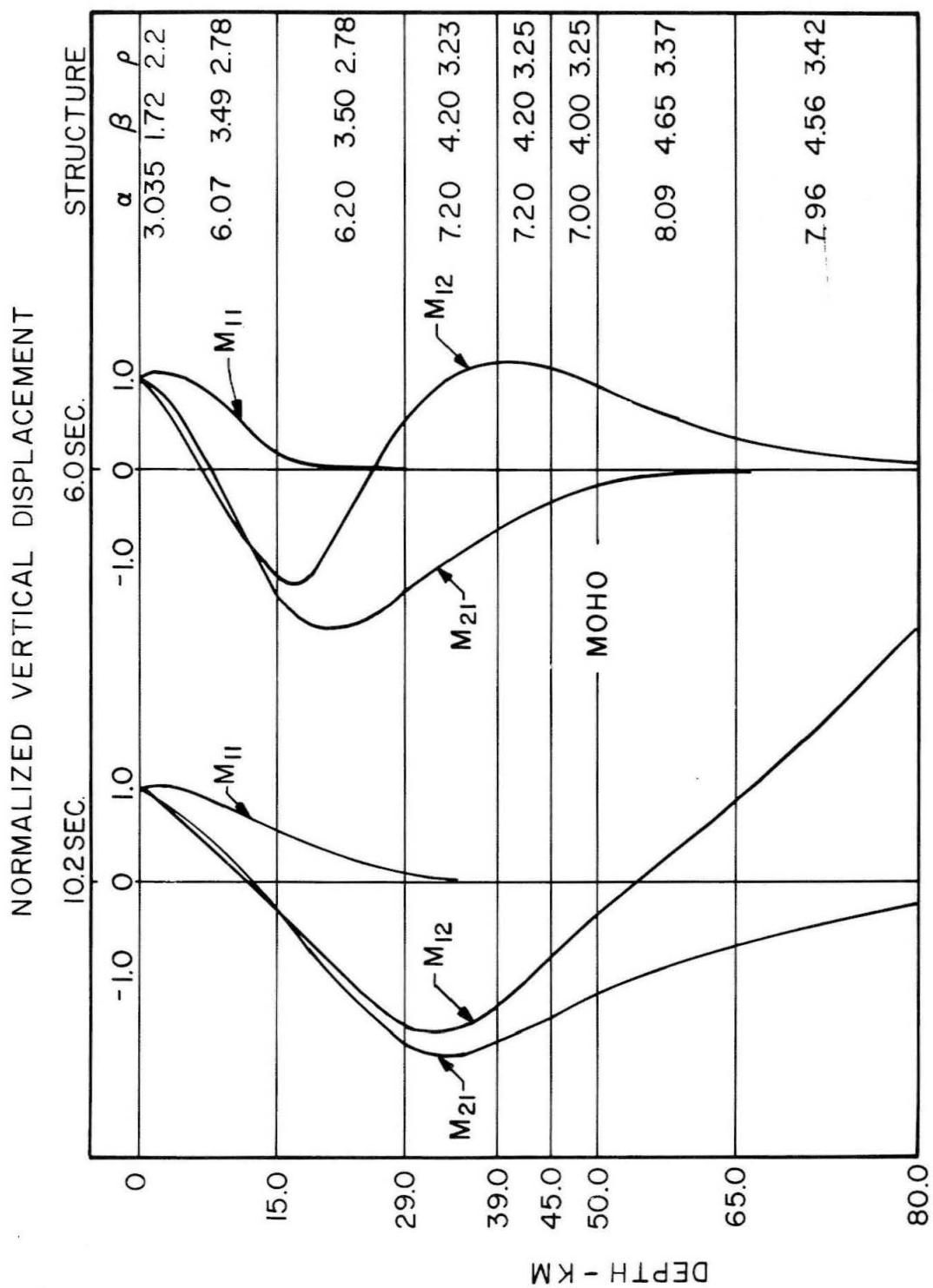
NORMALIZED VERTICAL DISPLACEMENT
10.2 SEC.
6.0 SEC.
STRUCTURE
α β ρ
3.035 1.72 2.2
6.07 3.49 2.78
6.20 3.50 2.78
7.20 4.20 3.23
7.20 4.20 3.25
7.00 4.00 3.25
8.09 4.65 3.37
7.96 4.56 3.42
M11
M12
M21
MOHO
-1.0
0
1.0
0
15.0
29.0
39.0
45.0
50.0
65.0
80.0
DEPTH - KM

Fig. 10

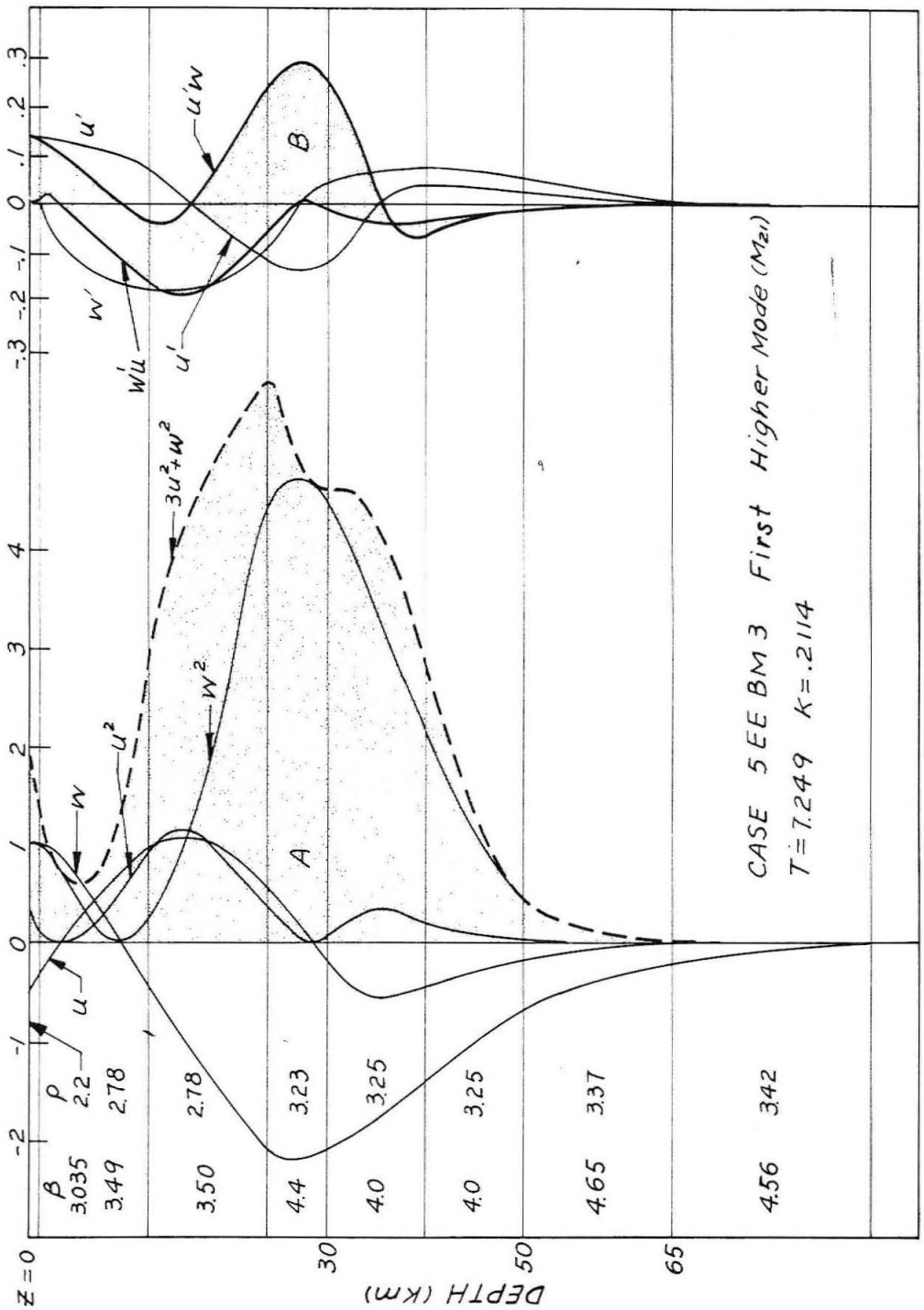
CASE 5EE BM3 First Higher Mode ($M_{21}$)
T=7.249 K=.2114
DEPTH (km)
z=0
30
50
65
A
B
w
u
u²
w²
3u²+w²
w'u'
w'
u'
u'w'
ρ
β
2.2
2.78
3.035
3.49
3.50
2.78
4.4
3.23
4.0
3.25
4.0
3.25
4.65
3.37
4.56
3.42

Fig. 11

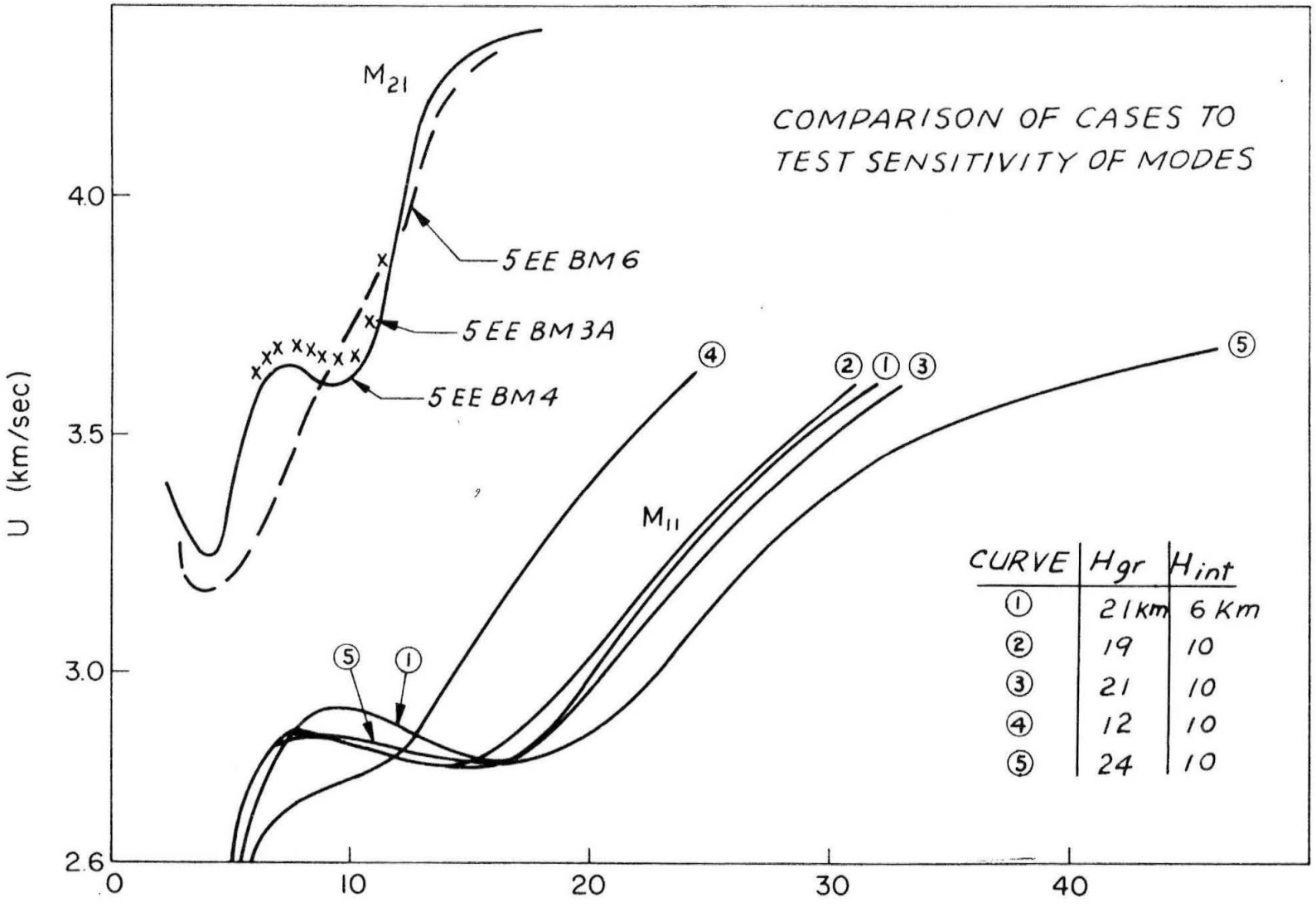
COMPARISON OF CASES TO
TEST SENSITIVITY OF MODES
M21
M11
5 EE BM 6
5 EE BM 3A
5 EE BM 4
U (km/sec)
PERIOD (sec)
4.0
3.5
3.0
2.6
0
10
20
30
40
CURVE | Hgr | Hint
① | 21 km | 6 Km
② | 19 | 10
③ | 21 | 10
④ | 12 | 10
⑤ | 24 | 10

Fig. 12

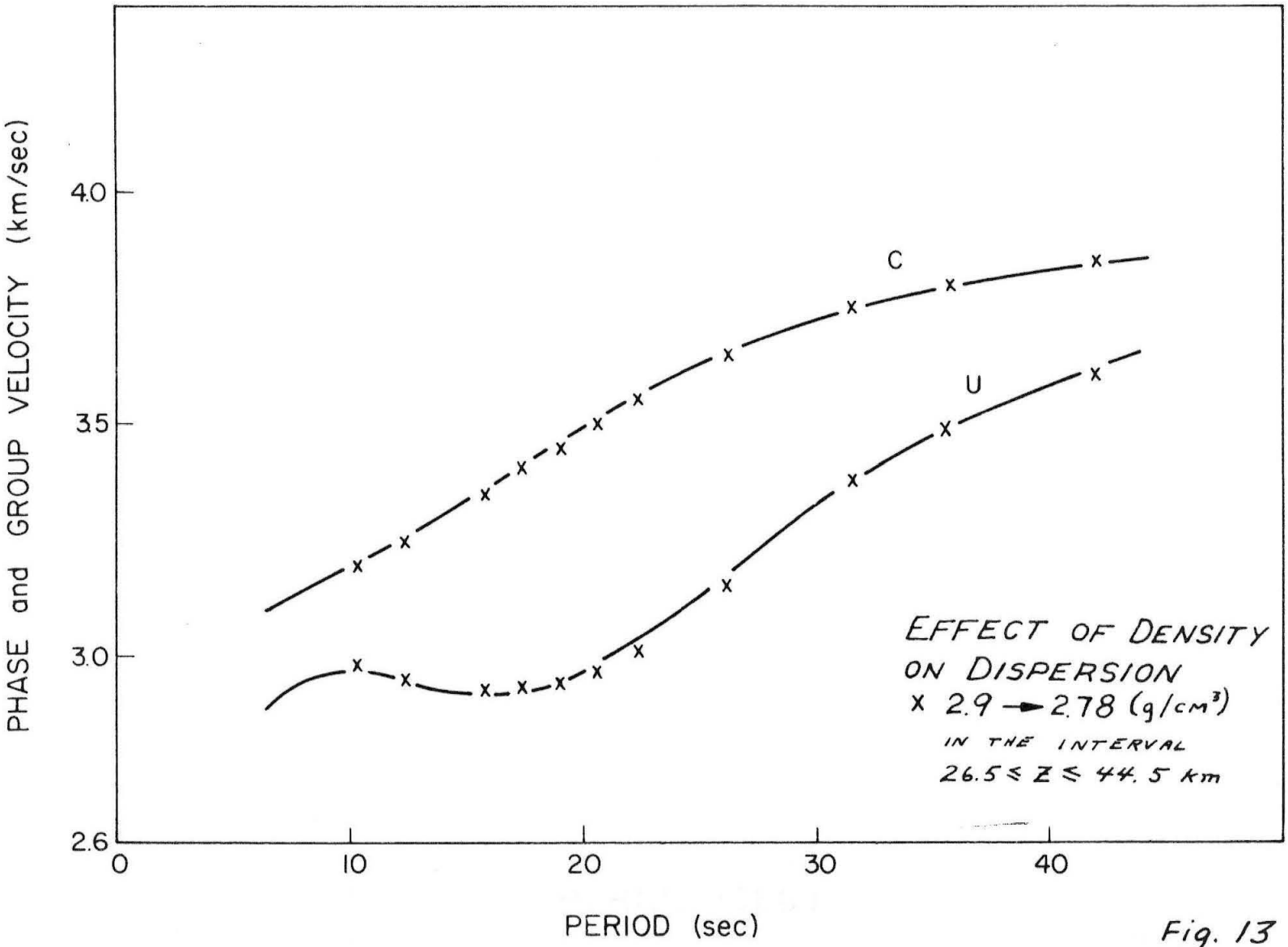
PHASE and GROUP VELOCITY (km/sec)
4.0
3.5
3.0
2.6
0
10
20
30
40
PERIOD (sec)
C
U
EFFECT OF DENSITY
ON DISPERSION
x 2.9 → 2.78 (g/cm³)
IN THE INTERVAL
26.5 ≤ Z ≤ 44.5 km

Fig. 13

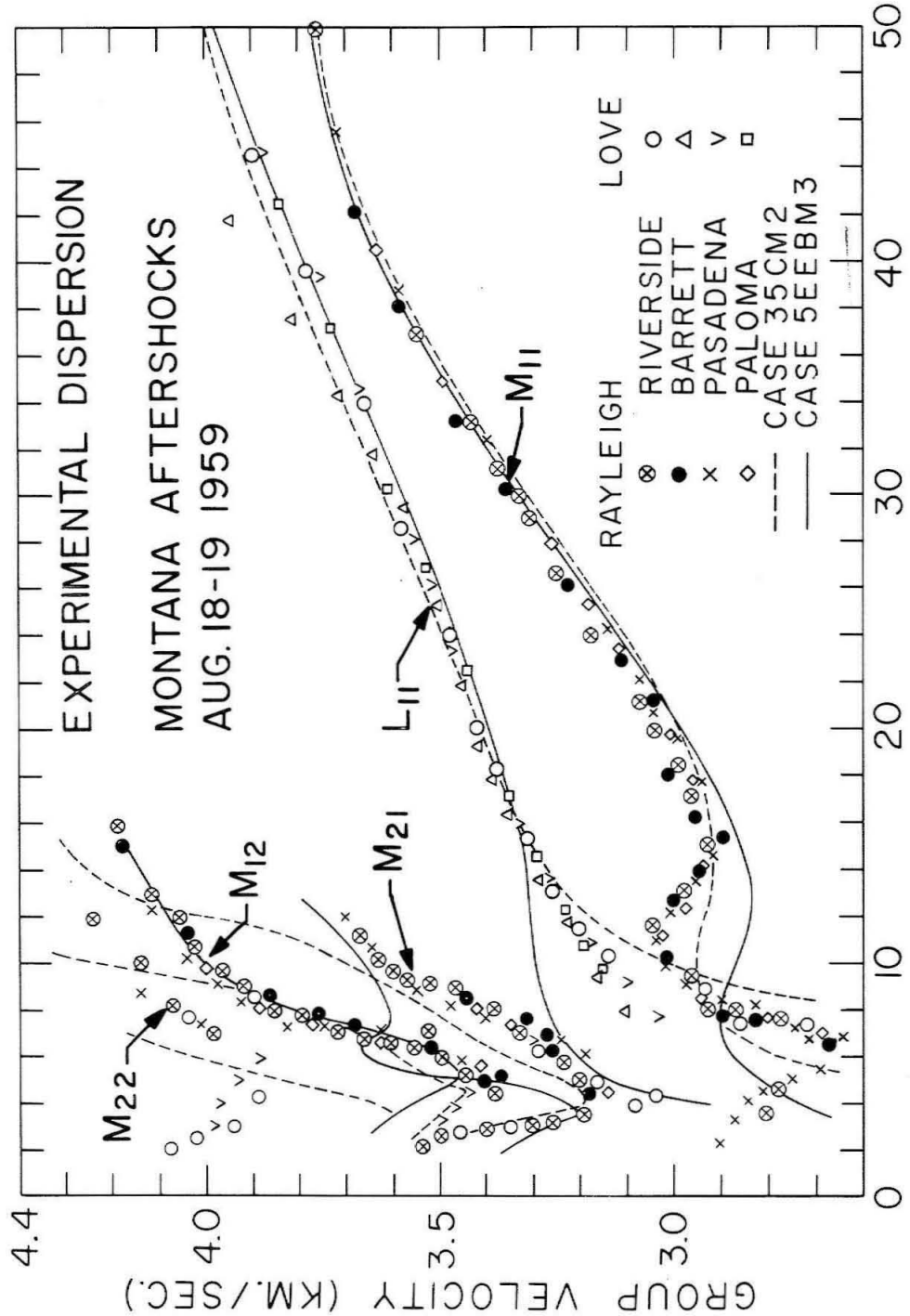
EXPERIMENTAL DISPERSION
MONTANA AFTERSHOCKS
AUG. 18-19 1959
RAYLEIGH
LOVE
RIVERSIDE
BARRETT
PASADENA
PALOMA
CASE 35CM2
CASE 5EEBM3
M22
M12
M21
L11
M11
GROUP VELOCITY (KM./SEC.)
PERIOD (SEC.)
4.4
4.0
3.5
3.0
0
10
20
30
40
50

Fig. 14

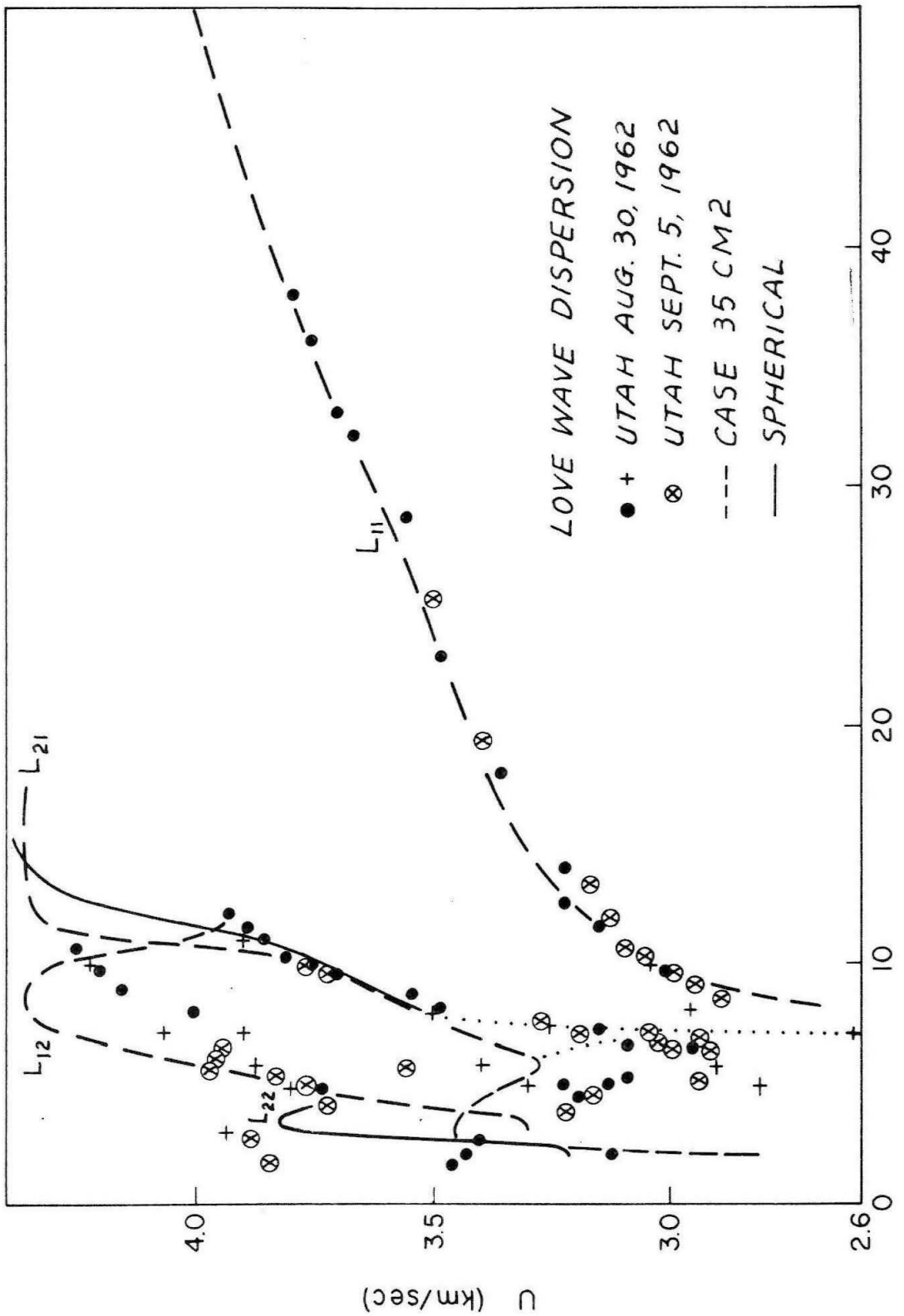
LOVE WAVE DISPERSION
+ UTAH AUG. 30, 1962
⊗ UTAH SEPT. 5, 1962
--- CASE 35 CM2
— SPHERICAL
$L_{11}$
$L_{12}$
$L_{21}$
$L_{22}$
C (km/sec)
4.0
3.5
3.0
2.6
0
10
20
30
40
PERIOD (sec)

Fig. 15

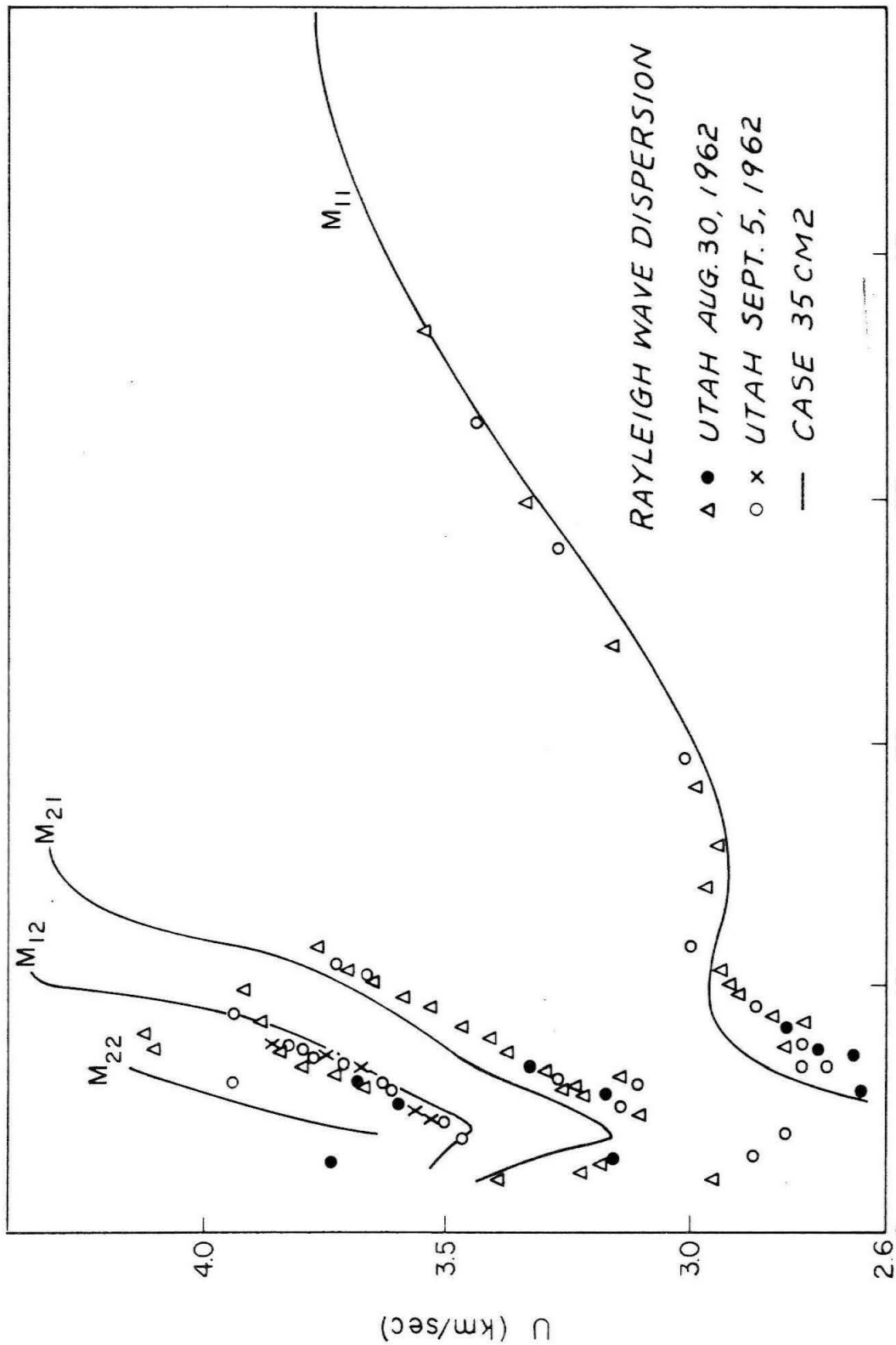
RAYLEIGH WAVE DISPERSION
▲ ● UTAH AUG. 30, 1962
○ × UTAH SEPT. 5, 1962
— CASE 35 CM2
M11
M21
M12
M22
U (km/sec)
4.0
3.5
3.0
2.6
0
10
20
30
40
PERIOD (sec)

Fig. 16

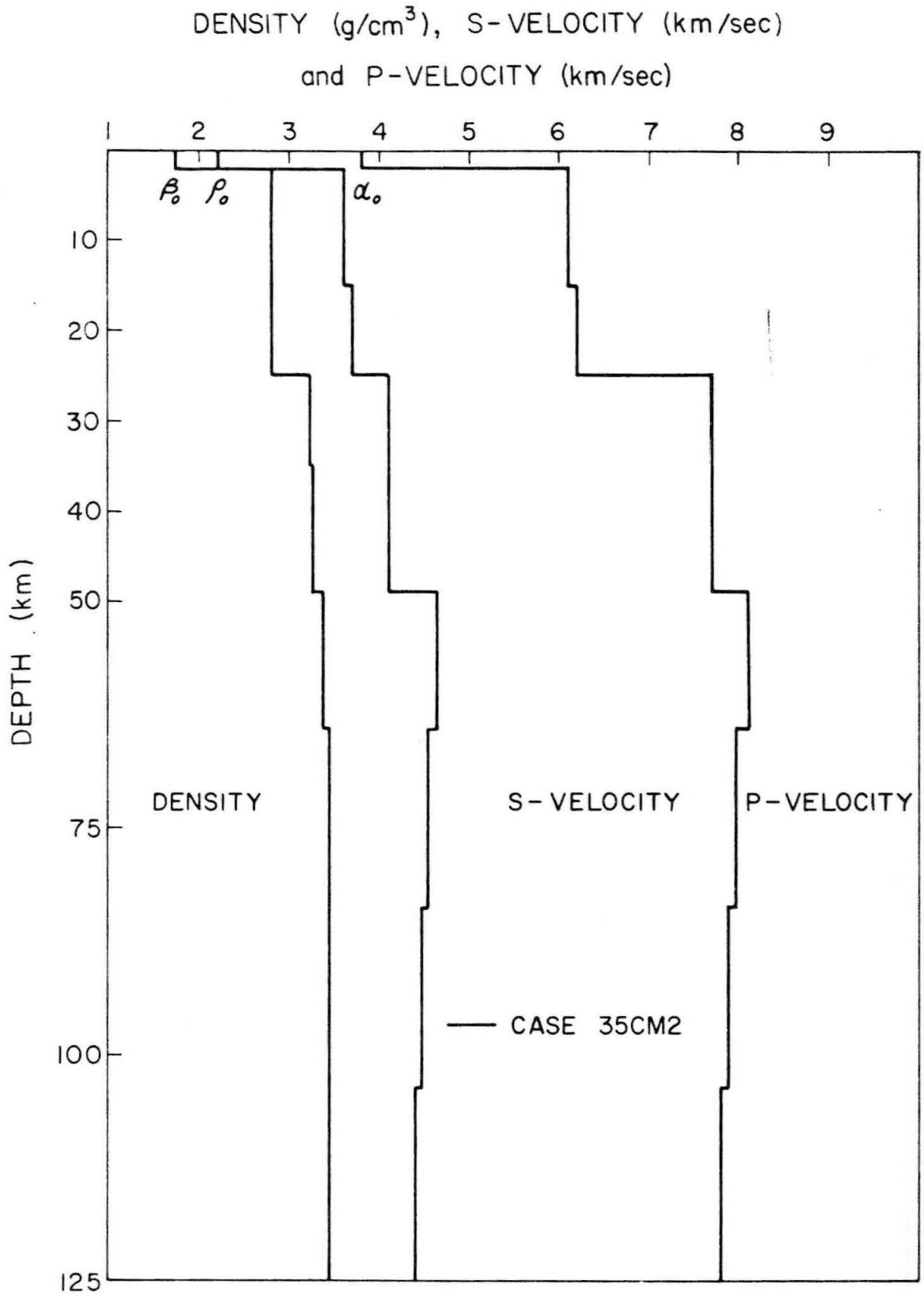
DENSITY (g/cm³), S-VELOCITY (km/sec)
and P-VELOCITY (km/sec)
1
2
3
4
5
6
7
8
9
β₀
ρ₀
α₀
10
20
30
40
50
75
100
125
DEPTH (km)
DENSITY
S-VELOCITY
P-VELOCITY
CASE 35CM2

Fig. 17

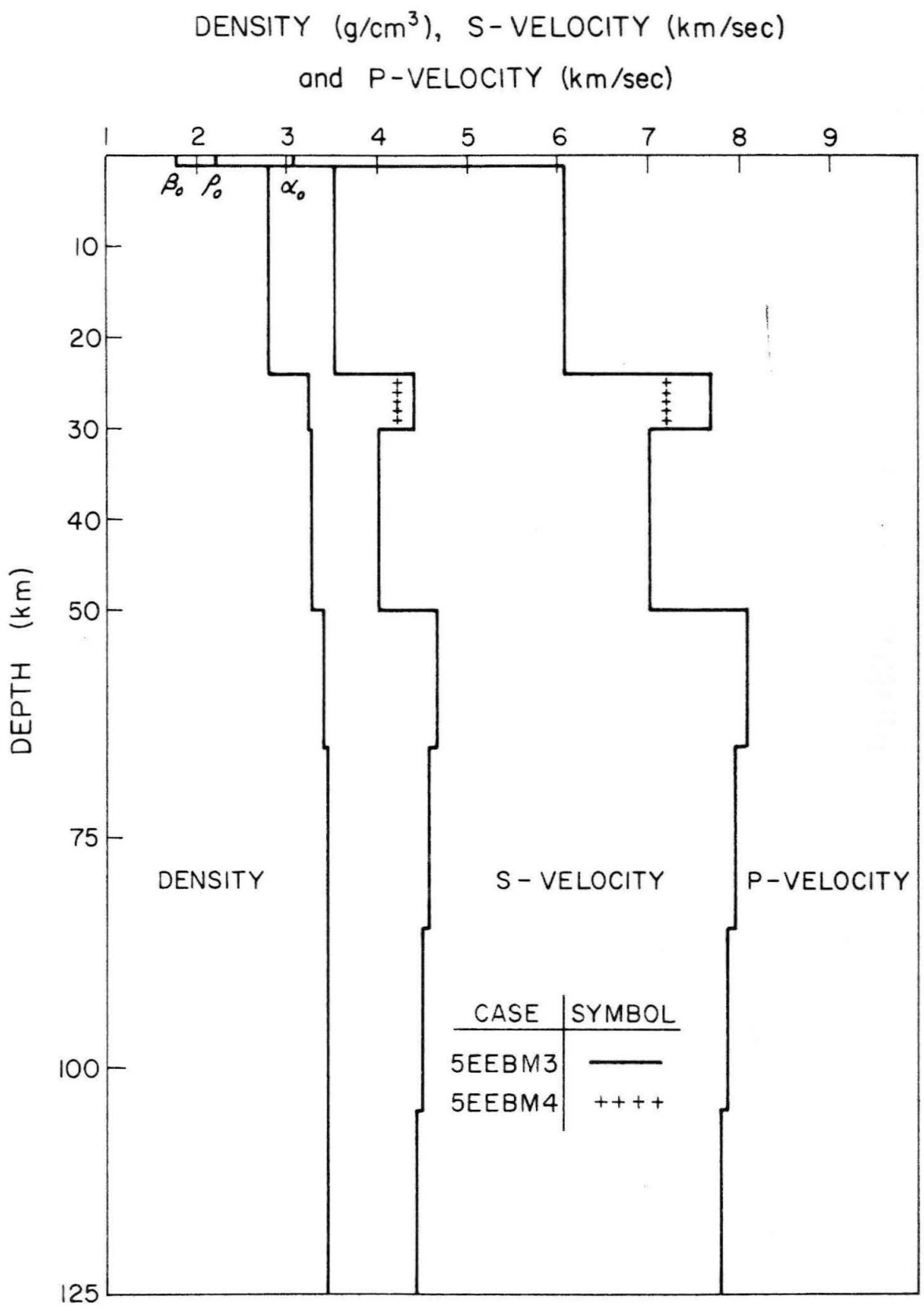
DENSITY (g/cm³), S-VELOCITY (km/sec)
and P-VELOCITY (km/sec)
1
2
3
4
5
6
7
8
9
β₀
ρ₀
α₀
10
20
30
40
50
75
100
125
DEPTH (km)
DENSITY
S-VELOCITY
P-VELOCITY
CASE
SYMBOL
5EEBM3
5EEBM4

Fig. 18

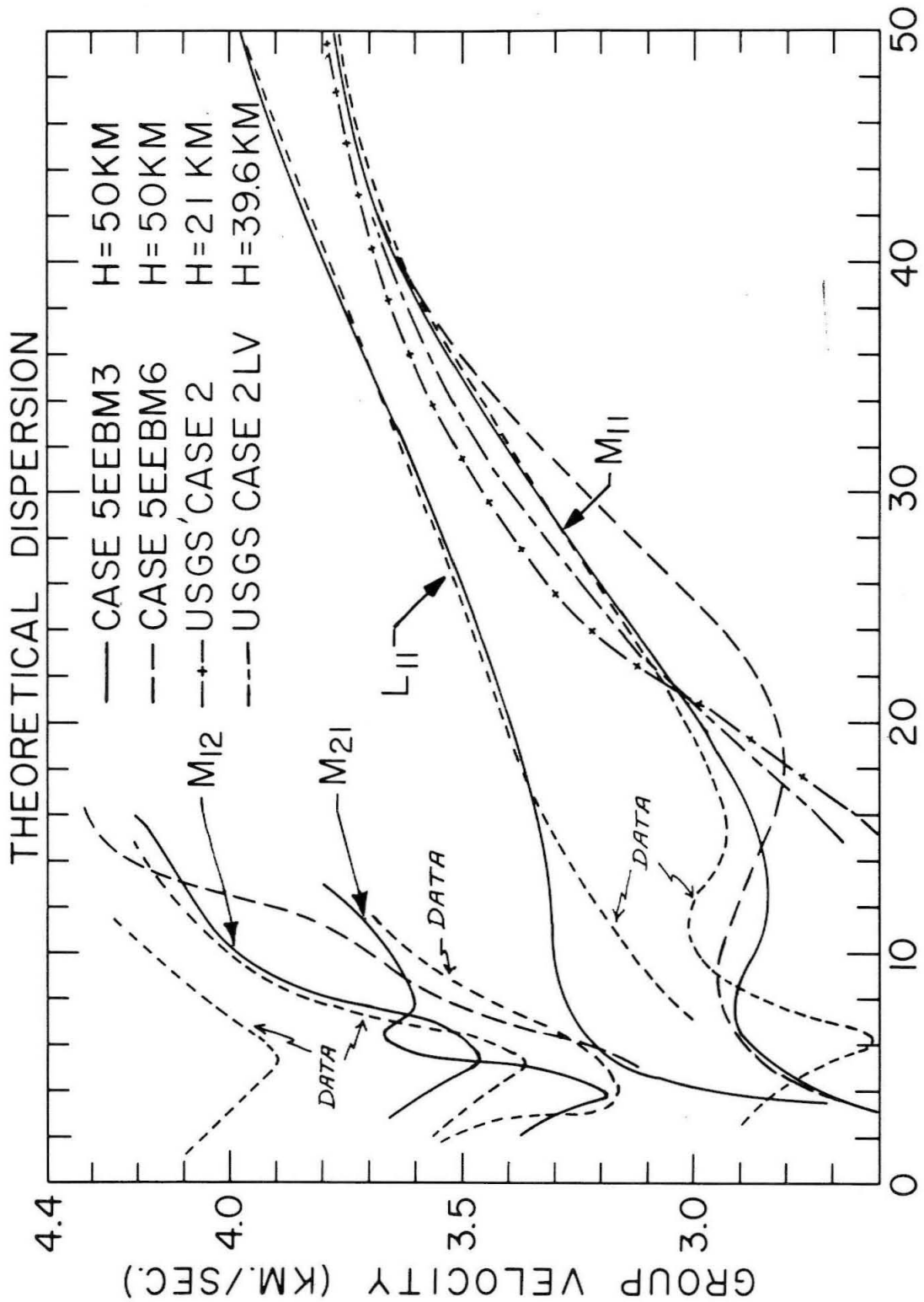
THEORETICAL DISPERSION
CASE 5EEBM3 H=50KM
CASE 5EEBM6 H=50KM
USGS'CASE 2 H=21 KM
USGS CASE 2LV H=39.6KM
$M_{12}$
$M_{21}$
$L_{11}$
$M_{11}$
DATA
DATA
DATA
GROUP VELOCITY (KM./SEC.)
4.4
4.0
3.5
3.0
0
10
20
30
40
50
PERIOD (SEC.)

Fig. 19

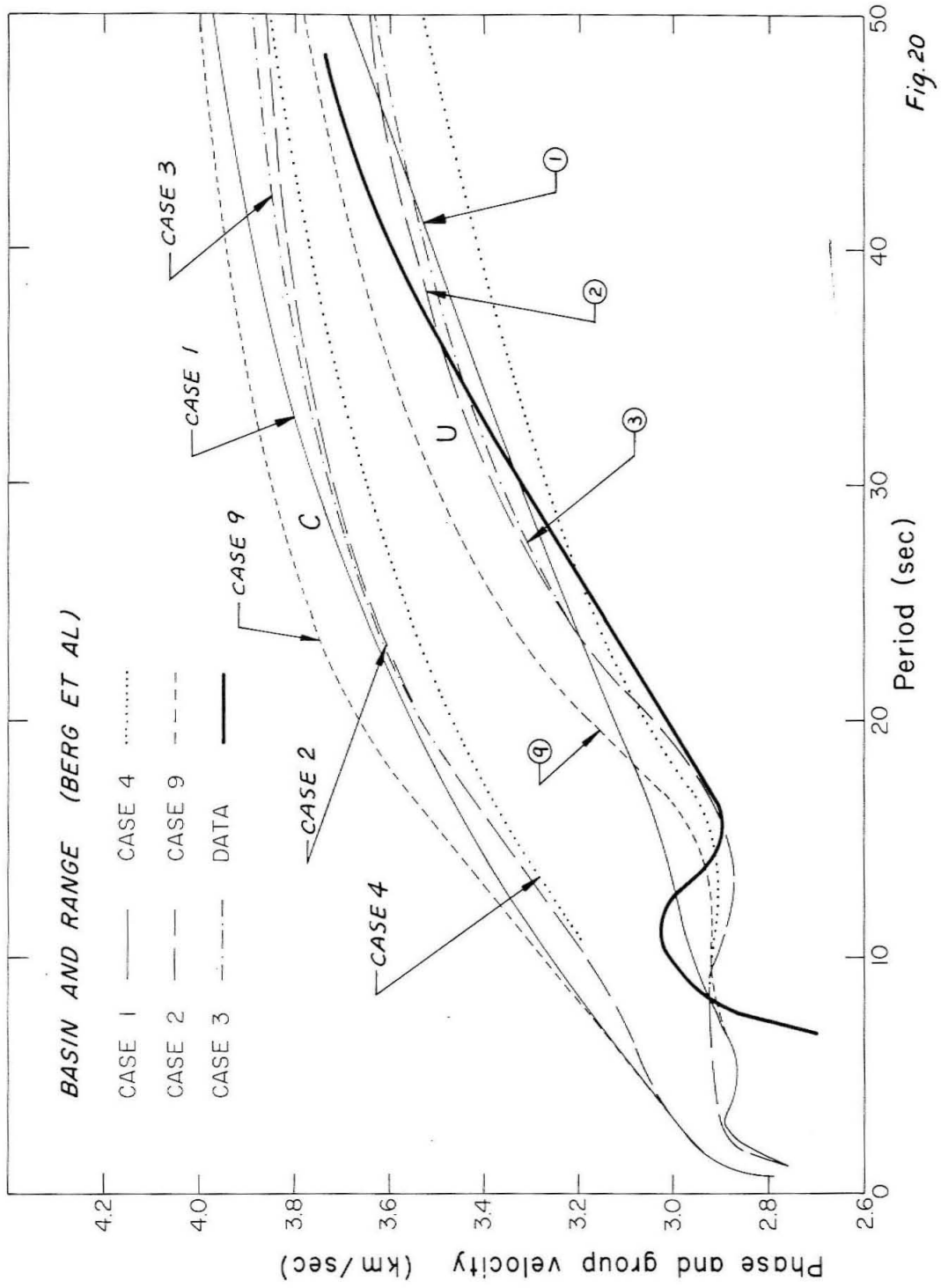
BASIN AND RANGE (BERG ET AL)
CASE 1 —— CASE 4 .....
CASE 2 — — CASE 9 - - - -
CASE 3 —·—·— DATA
CASE 1
CASE 2
CASE 3
CASE 4
CASE 9
C
U
①
②
③
④
Phase and group velocity (km/sec)
Period (sec)
4.2
4.0
3.8
3.6
3.4
3.2
3.0
2.8
2.6
0
10
20
30
40
50

Fig. 20

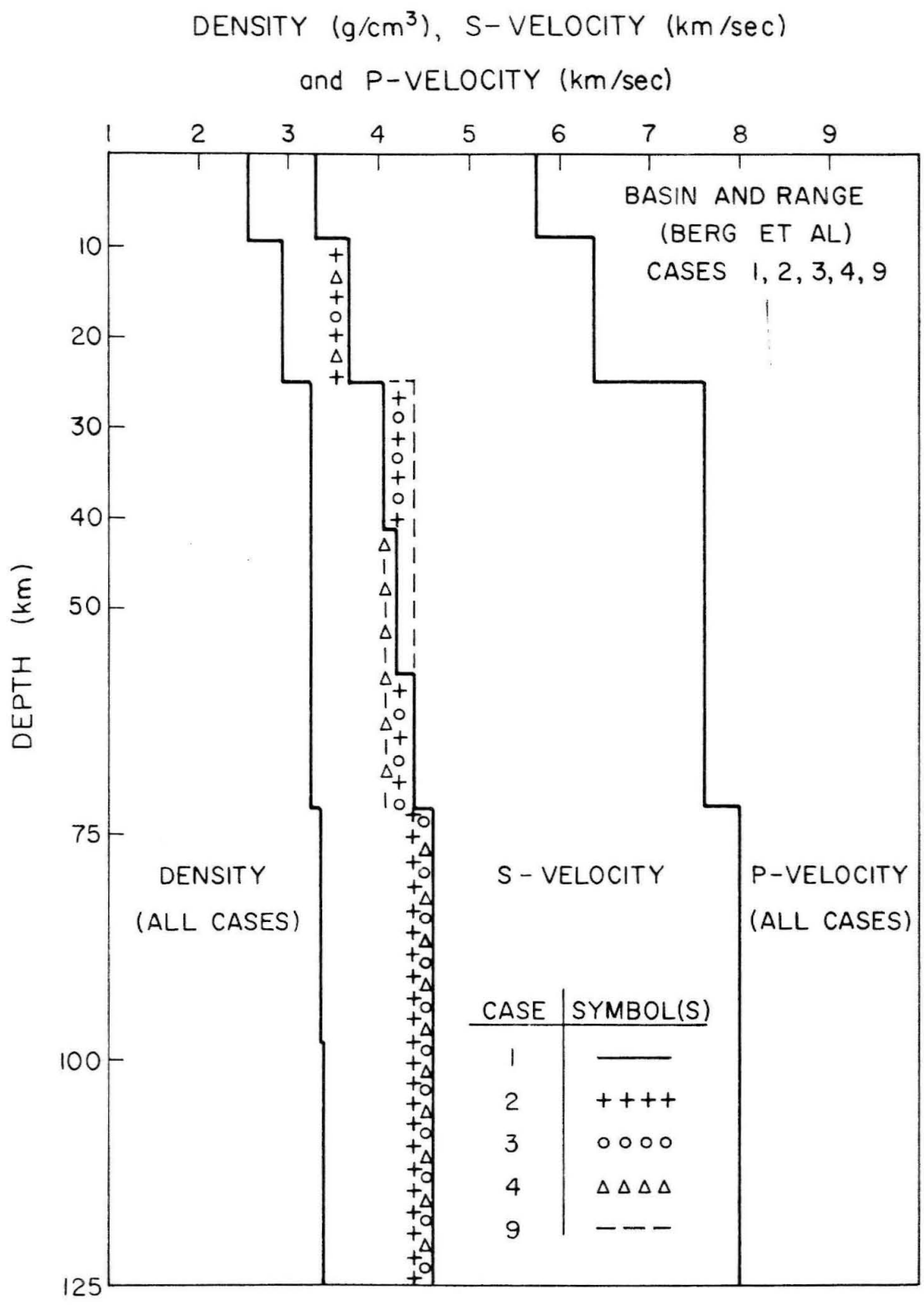
DENSITY (g/cm³), S-VELOCITY (km/sec)
and P-VELOCITY (km/sec)
1
2
3
4
5
6
7
8
9
BASIN AND RANGE
(BERG ET AL)
CASES 1, 2, 3, 4, 9
DEPTH (km)
10
20
30
40
50
75
100
125
DENSITY
(ALL CASES)
S - VELOCITY
P-VELOCITY
(ALL CASES)
CASE
SYMBOL(S)
1
2
3
4
9

Fig. 21

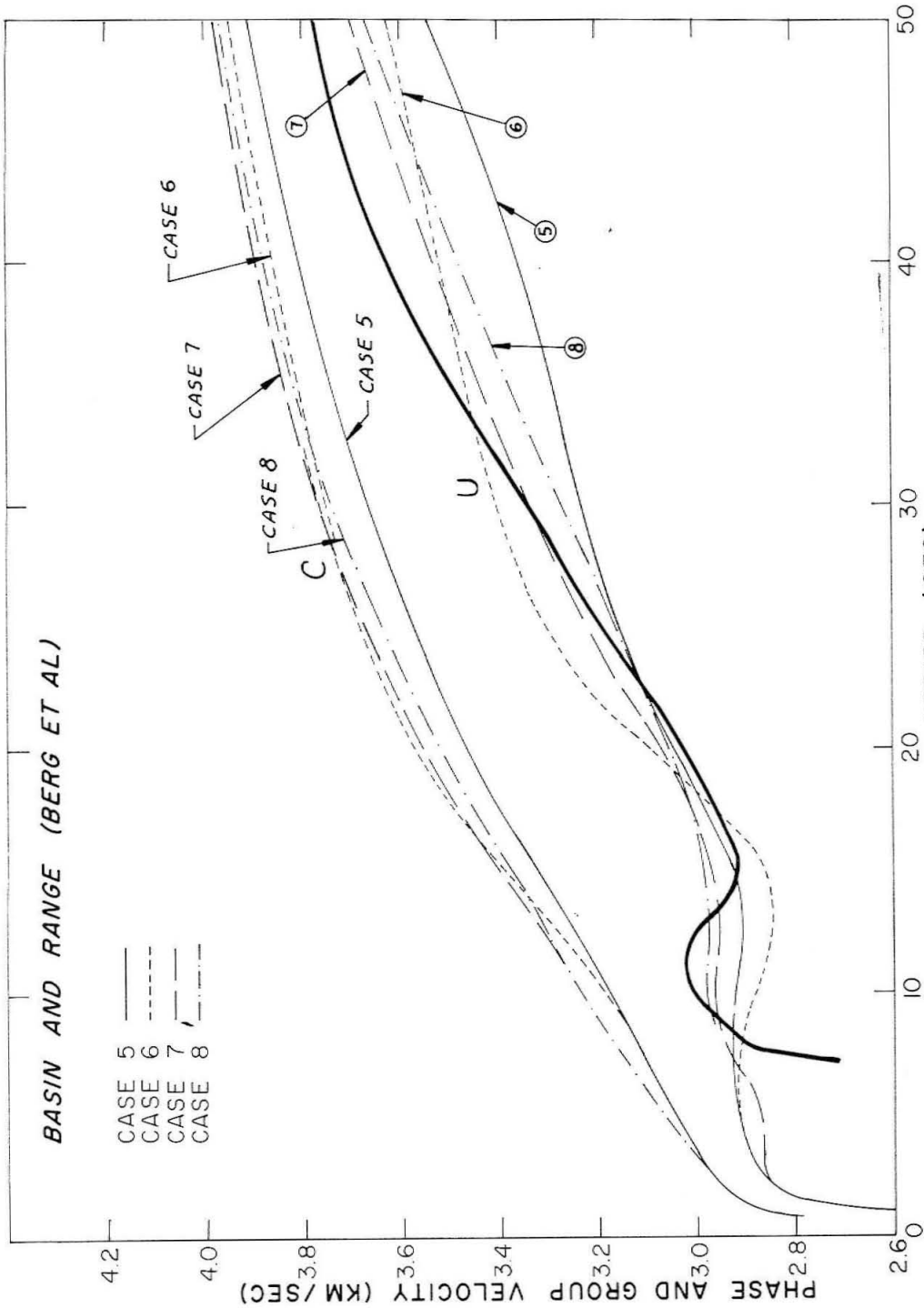
BASIN AND RANGE (BERG ET AL)
CASE 5
CASE 6
CASE 7
CASE 8
CASE 6
CASE 7
CASE 8
CASE 5
C
U
PHASE AND GROUP VELOCITY (KM/SEC)
PERIOD (SEC)
4.2
4.0
3.8
3.6
3.4
3.2
3.0
2.8
2.6
0
10
20
30
40
50

Fig. 22

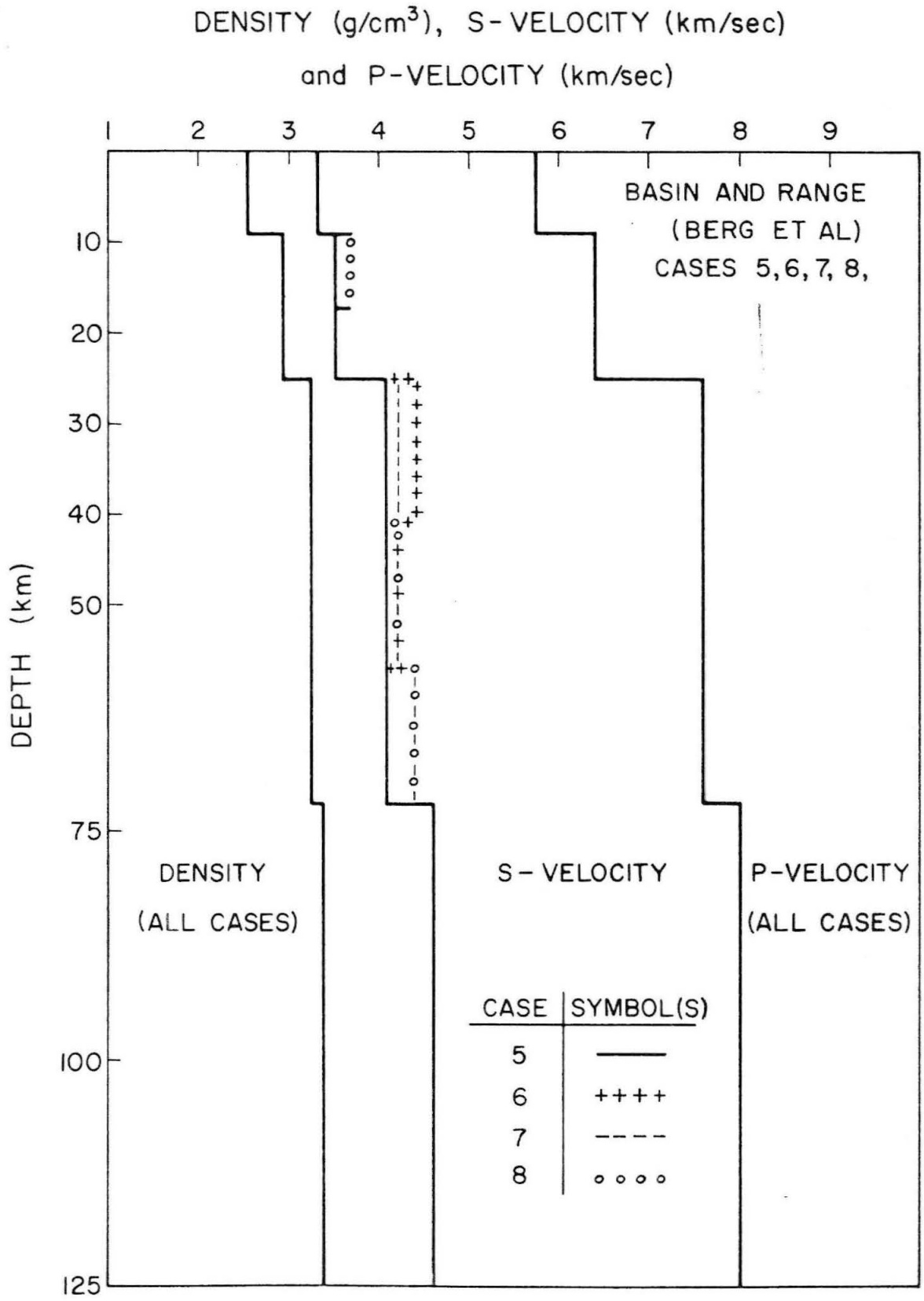
DENSITY (g/cm³), S-VELOCITY (km/sec)
and P-VELOCITY (km/sec)
1
2
3
4
5
6
7
8
9
BASIN AND RANGE
(BERG ET AL)
CASES 5,6,7, 8,
10
20
30
40
50
75
100
125
DEPTH (km)
DENSITY
(ALL CASES)
S-VELOCITY
P-VELOCITY
(ALL CASES)
CASE
SYMBOL(S)
5
6
7
8

Fig. 23

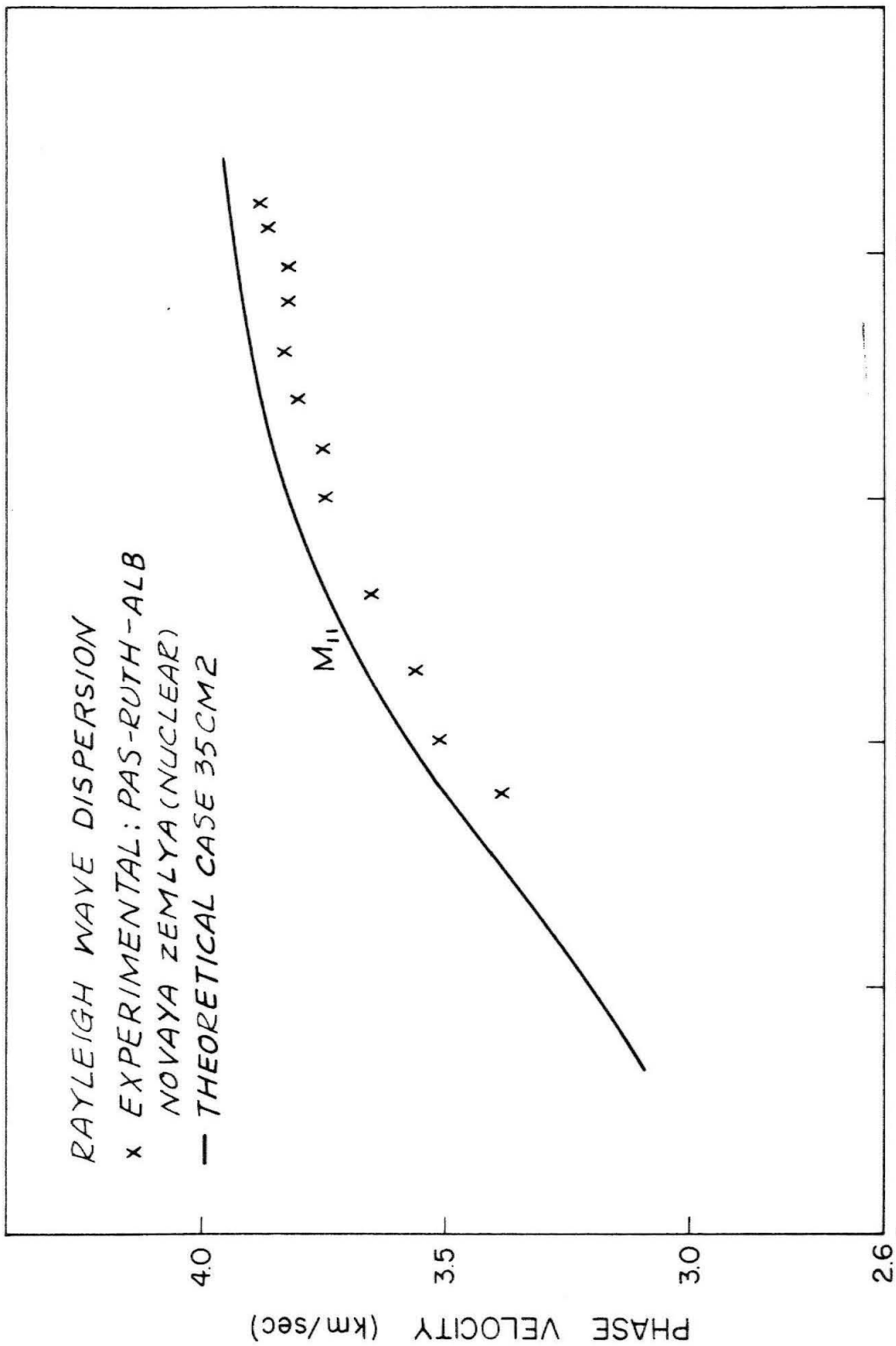
RAYLEIGH WAVE DISPERSION
x EXPERIMENTAL: PAS-RUTH-ALB
NOVAYA ZEMLYA (NUCLEAR)
— THEORETICAL CASE 35CM2
$M_{11}$
PHASE VELOCITY (km/sec)
4.0
3.5
3.0
2.6
0
10
20
30
40
PERIOD (sec)

Fig. 24

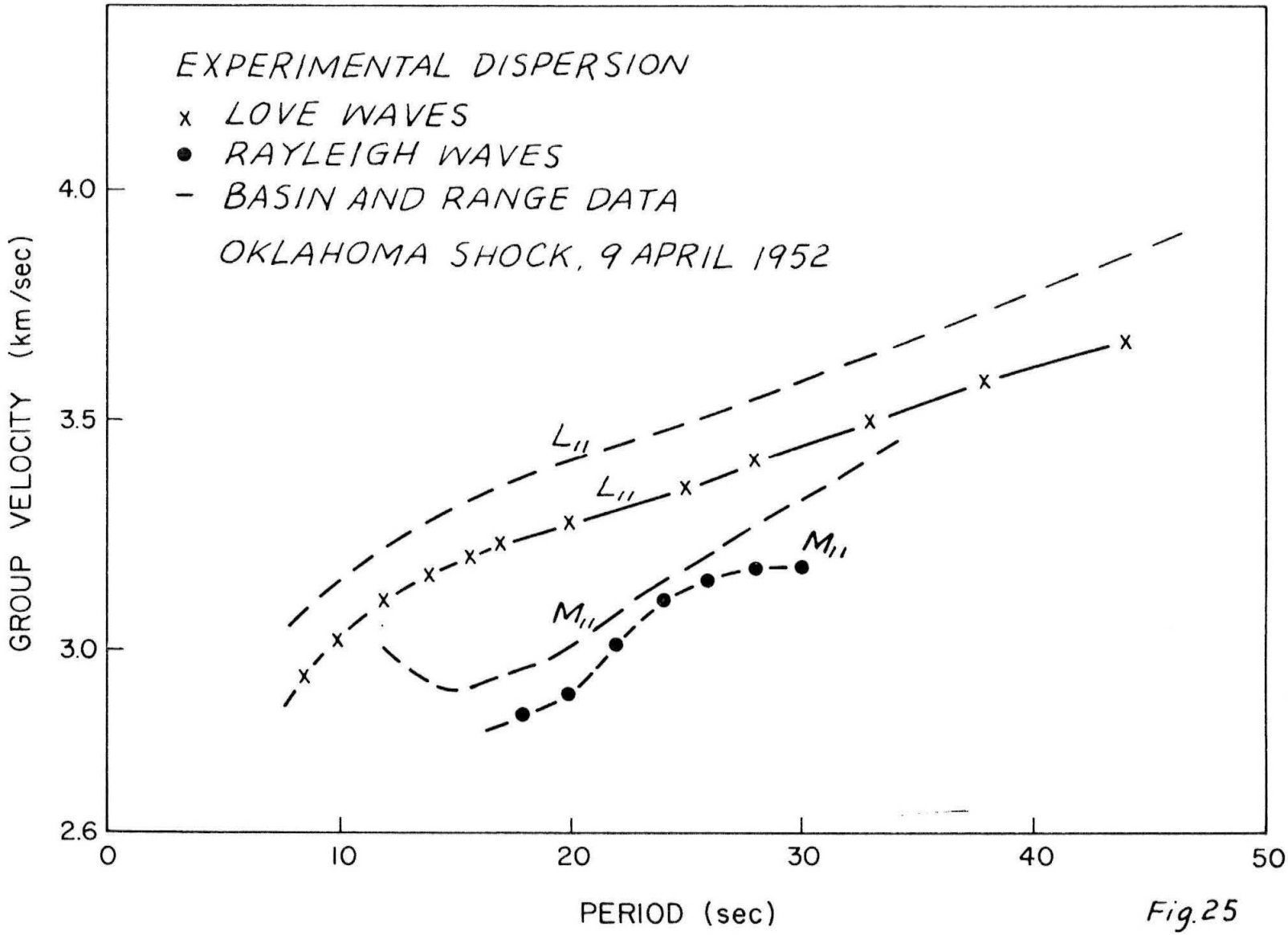
EXPERIMENTAL DISPERSION
x LOVE WAVES
● RAYLEIGH WAVES
– BASIN AND RANGE DATA
OKLAHOMA SHOCK, 9 APRIL 1952
GROUP VELOCITY (km/sec)
4.0
3.5
3.0
2.6
0
10
20
30
40
50
PERIOD (sec)
$L_{11}$
$L_{11}$
$M_{11}$
$M_{11}$

Fig. 25

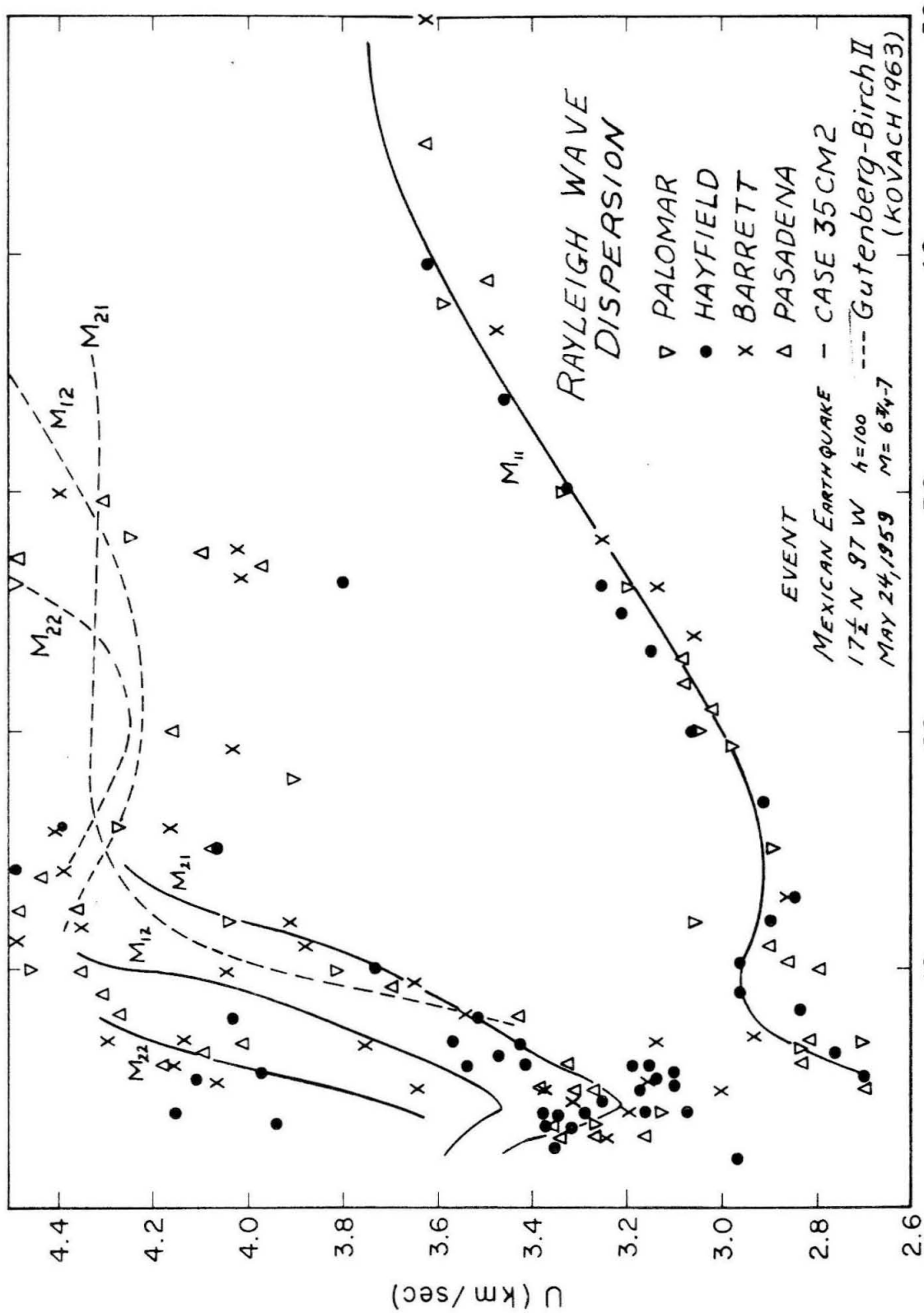
RAYLEIGH WAVE
DISPERSION
PALOMAR
HAYFIELD
BARRETT
PASADENA
EVENT
MEXICAN EARTHQUAKE - CASE 35CM2
17½ N 97 W h=100 ---Gutenberg-Birch II
MAY 24, 1959 M=6¾-7 (KOVACH 1963)
PERIOD (sec)
C (km/sec)
M11
M12
M21
M22

Fig. 26

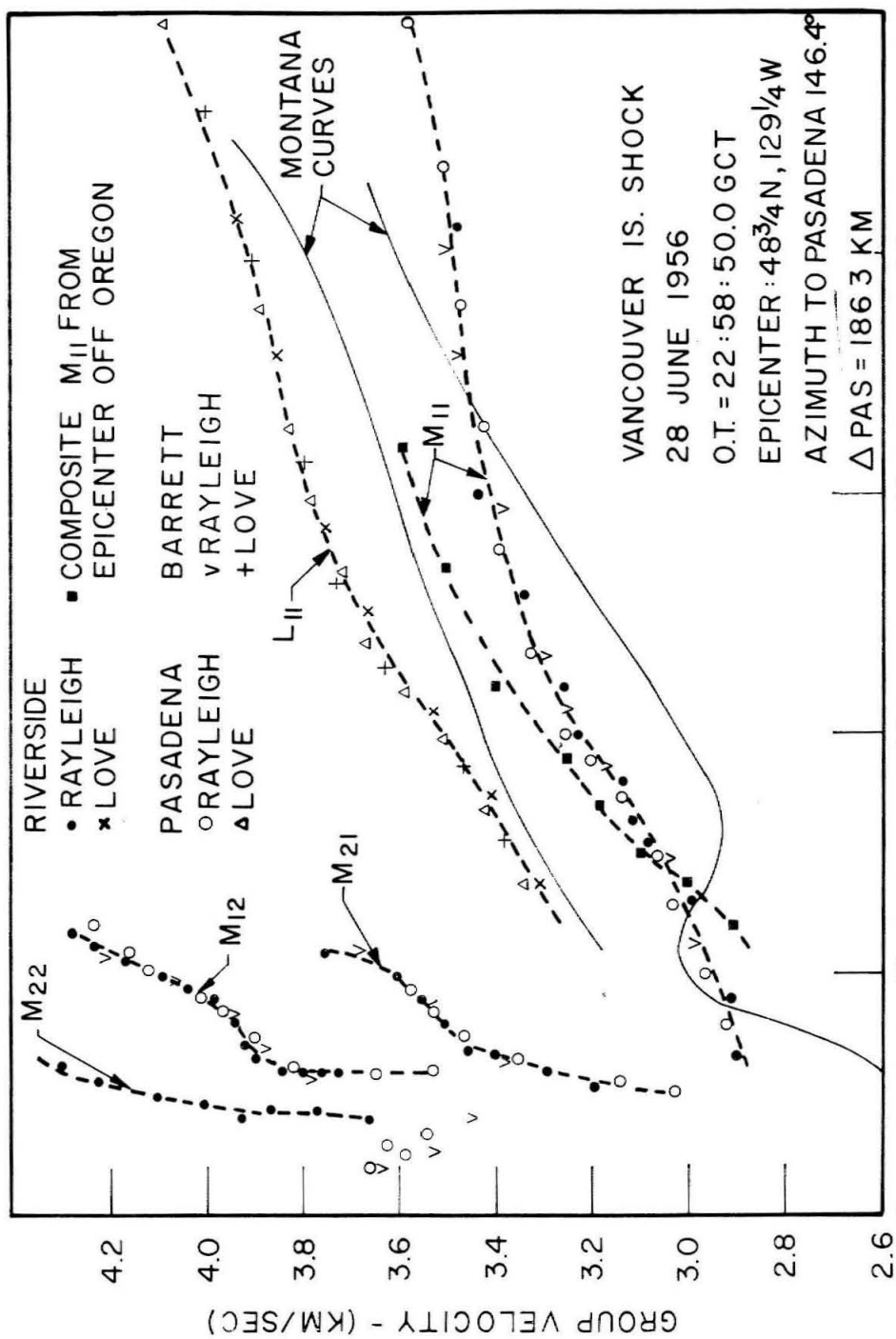
EXPERIMENTAL DISPERSION
RIVERSIDE
• RAYLEIGH
× LOVE
PASADENA
○ RAYLEIGH
△ LOVE
■ COMPOSITE M11 FROM EPICENTER OFF OREGON
BARRETT
v RAYLEIGH
+ LOVE
MONTANA CURVES
M22
M12
M21
M11
L11
VANCOUVER IS. SHOCK
28 JUNE 1956
O.T. = 22:58:50.0 GCT
EPICENTER: 48¾N, 129¼W
AZIMUTH TO PASADENA 146.4°
Δ PAS = 1863 KM
GROUP VELOCITY - (KM/SEC)
4.2
4.0
3.8
3.6
3.4
3.2
3.0
2.8
2.6
0
10
20
30
40
50

Fig. 27

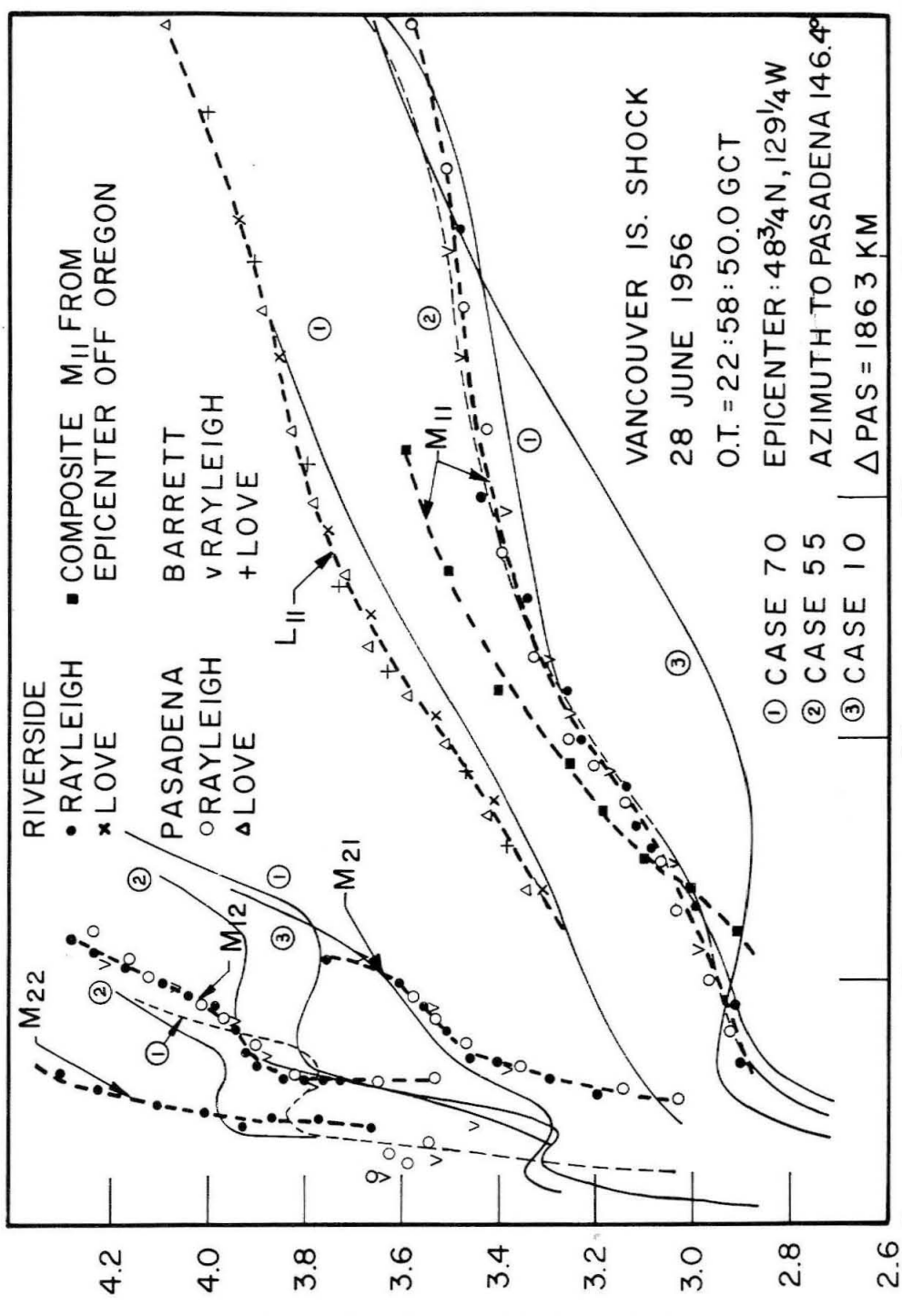
EXPERIMENTAL DISPERSION
RIVERSIDE
• RAYLEIGH
× LOVE
PASADENA
○ RAYLEIGH
△ LOVE
■ COMPOSITE $M_{II}$ FROM EPICENTER OFF OREGON
BARRETT
v RAYLEIGH
+ LOVE
$M_{22}$
$M_{12}$
$M_{21}$
$L_{II}$
$M_{II}$
① CASE 70
② CASE 55
③ CASE 10
VANCOUVER IS. SHOCK
28 JUNE 1956
O.T. = 22:58:50.0 GCT
EPICENTER: 48¾N, 129¼W
AZIMUTH TO PASADENA 146.4°
Δ PAS = 186 3 KM
GROUP VELOCITY - (KM/SEC)
4.2
4.0
3.8
3.6
3.4
3.2
3.0
2.8
2.6
0
10
20
30
40
50

Fig. 28

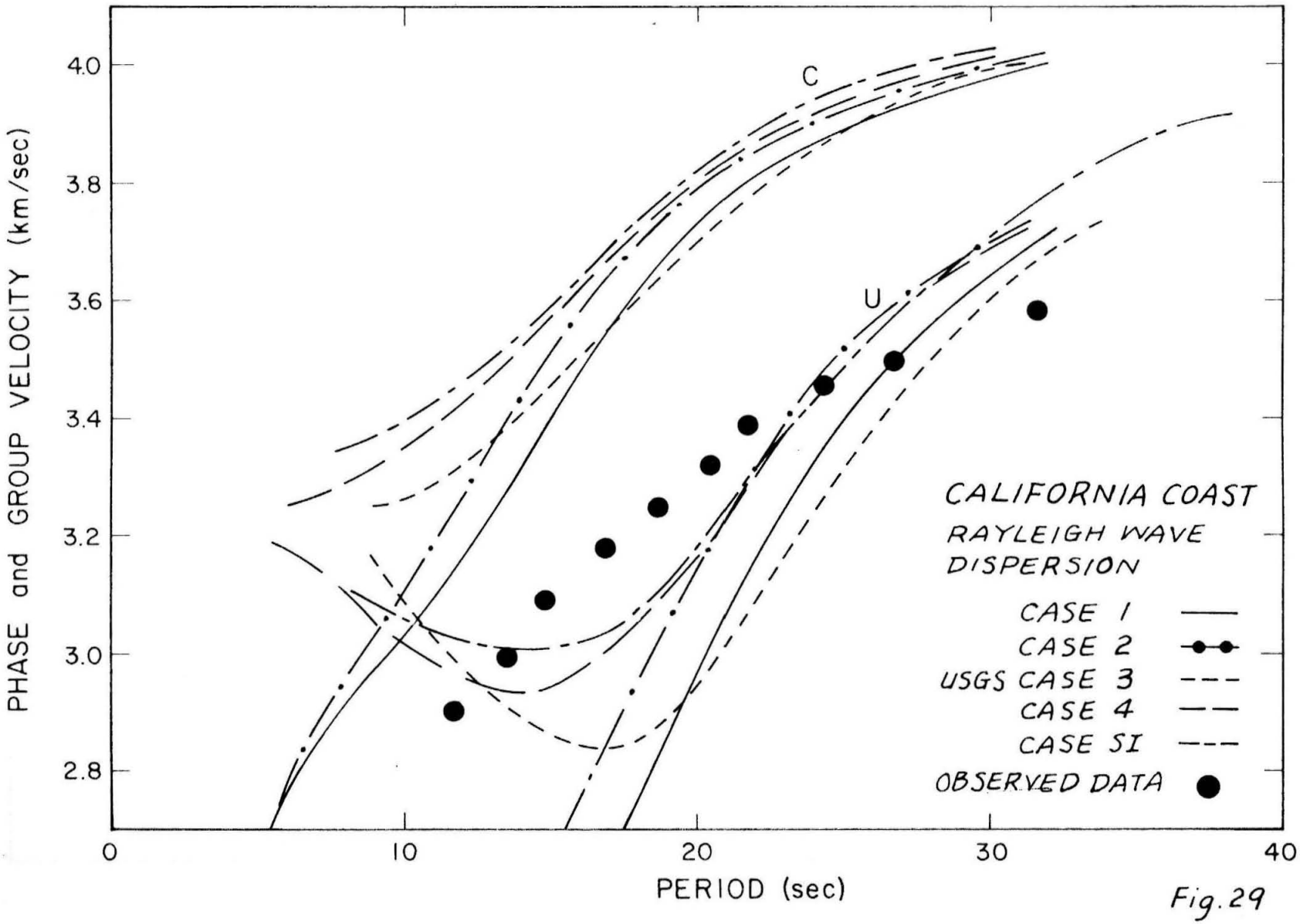
PHASE and GROUP VELOCITY (km/sec)
4.0
3.8
3.6
3.4
3.2
3.0
2.8
0
10
20
30
40
PERIOD (sec)
C
U
CALIFORNIA COAST
RAYLEIGH WAVE
DISPERSION
CASE 1
CASE 2
USGS CASE 3
CASE 4
CASE SI
OBSERVED DATA

Fig. 29

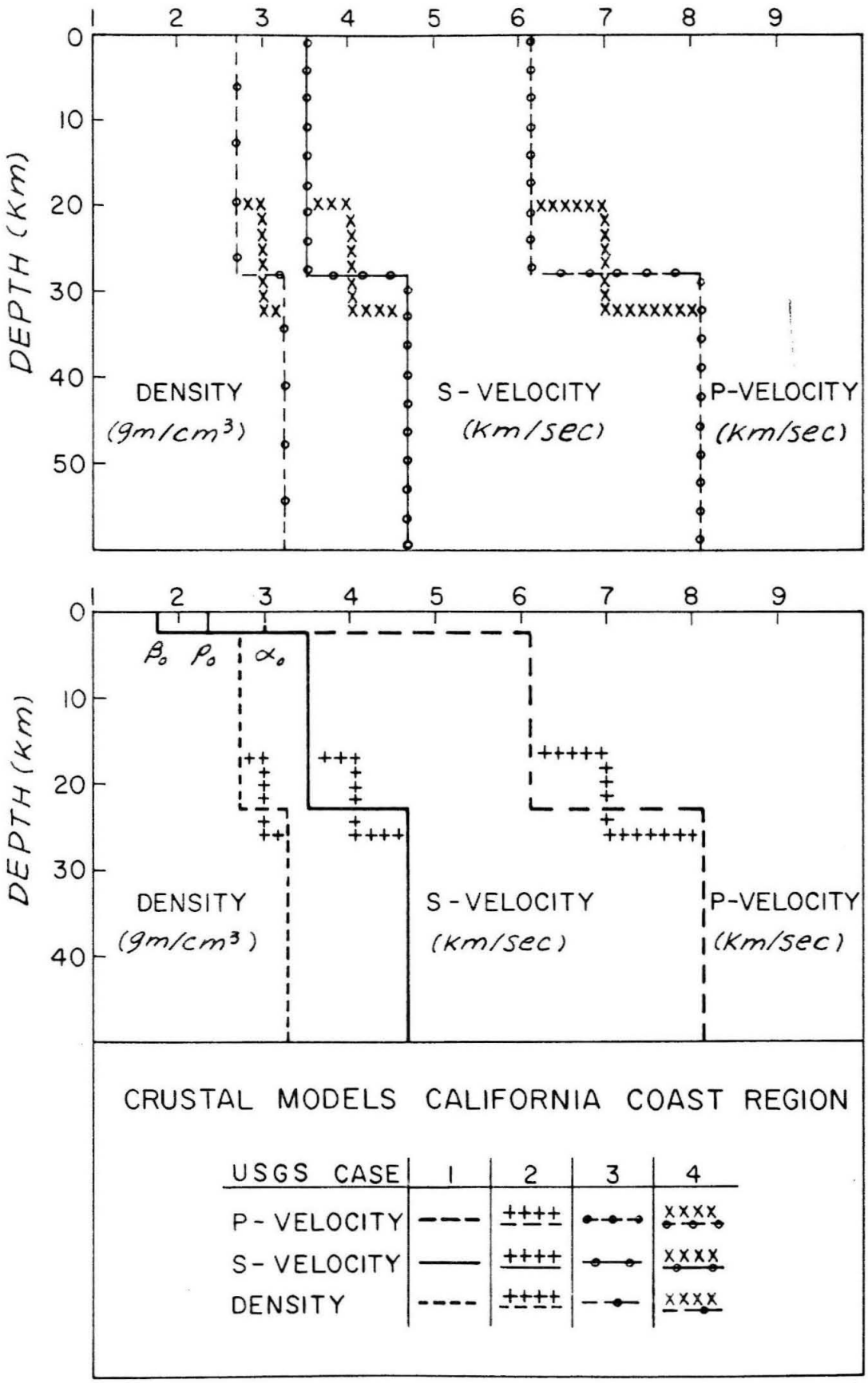
DEPTH (Km)
DENSITY (gm/cm³)
S-VELOCITY (km/sec)
P-VELOCITY (km/sec)
$\beta_o$ $\rho_o$ $\alpha_o$
CRUSTAL MODELS CALIFORNIA COAST REGION
USGS CASE 1 2 3 4
P-VELOCITY
S-VELOCITY
DENSITY

Fig. 30

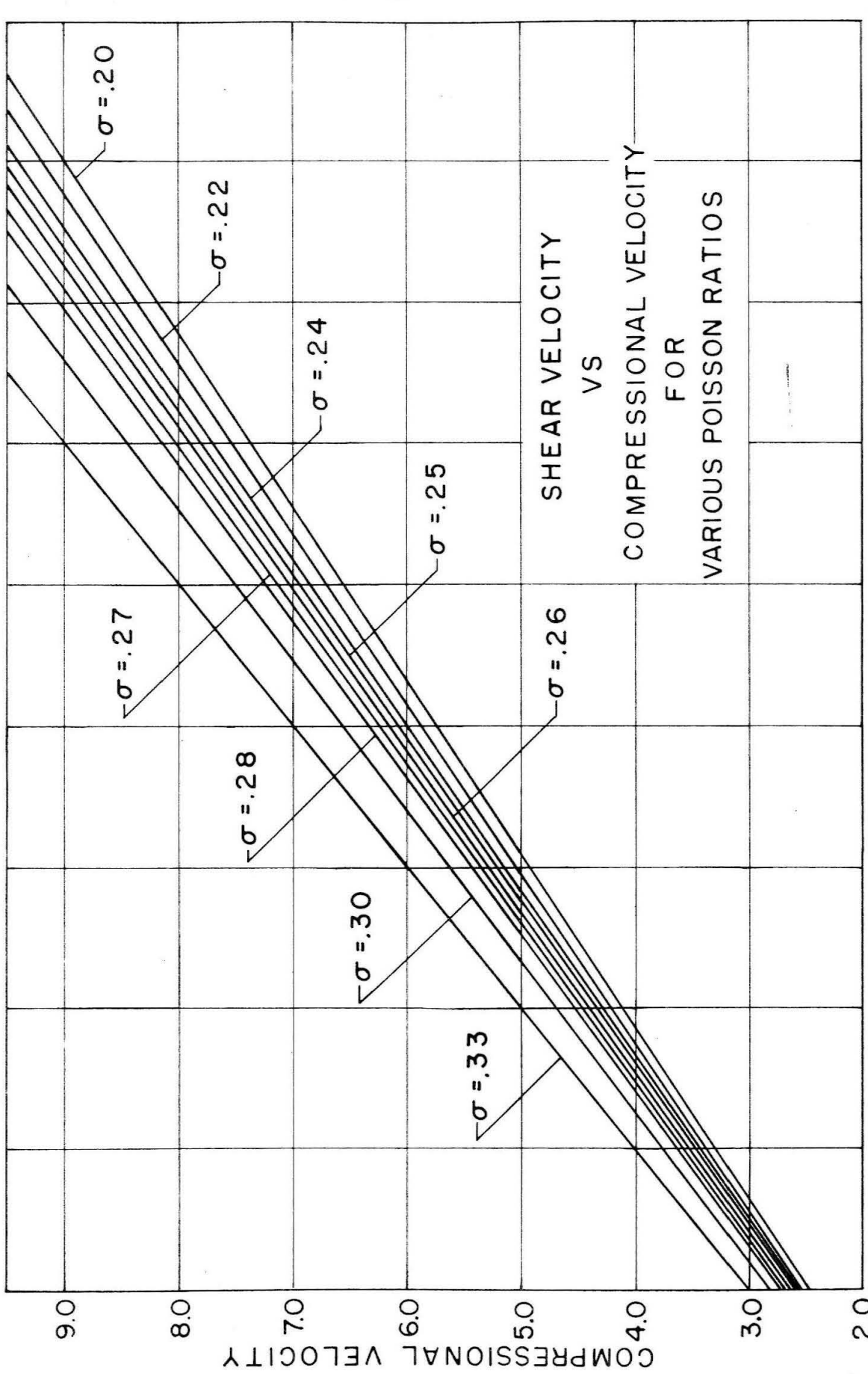
SHEAR VELOCITY
VS
COMPRESSIONAL VELOCITY
FOR
VARIOUS POISSON RATIOS
σ = .20
σ = .22
σ = .24
σ = .25
σ = .26
σ = .27
σ = .28
σ = .30
σ = .33
SHEAR VELOCITY
COMPRESSIONAL VELOCITY
1.5
2.0
2.5
3.0
3.5
4.0
4.5
5.0
5.5
6.0
2.0
3.0
4.0
5.0
6.0
7.0
8.0
9.0

Fig. 31

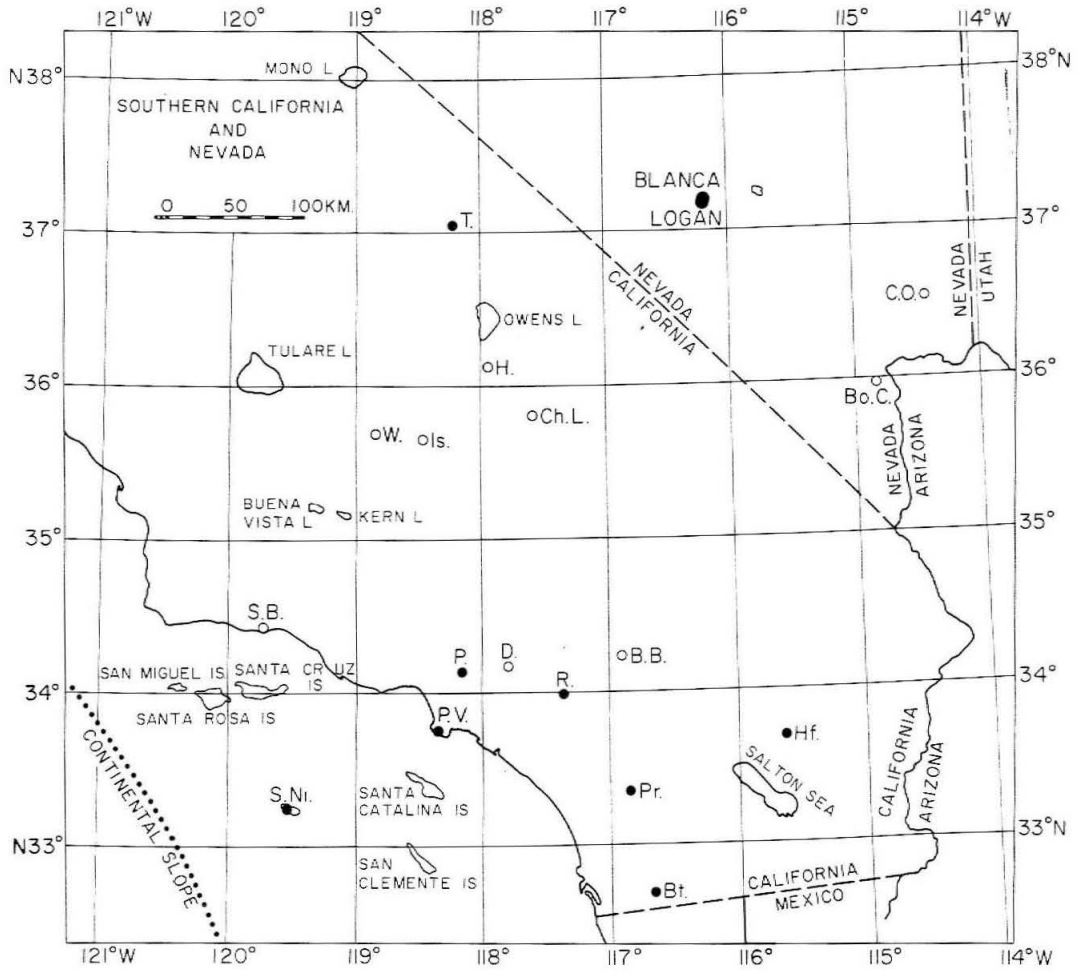
121°W
120°
119°
118°
117°
116°
115°
114°W
N38°
38°N
37°
36°
35°
34°
N33°
33°N
MONO L
SOUTHERN CALIFORNIA AND NEVADA
0 50 100KM.
T.
BLANCA
LOGAN
NEVADA
CALIFORNIA
C.O.o
NEVADA
UTAH
OWENS L
TULARE L
oH.
Bo.C.
oCh.L.
oW. Ols.
NEVADA
ARIZONA
BUENA VISTA L
KERN L
S.B.
P.
D.
oB.B.
R.
SAN MIGUEL IS
SANTA CRUZ IS
SANTA ROSA IS
P.V.
Hf.
SALTON SEA
CALIFORNIA
ARIZONA
CONTINENTAL SLOPE
S.Ni.
SANTA CATALINA IS
Pr.
SAN CLEMENTE IS
Bt.
CALIFORNIA
MEXICO

Fig. 32

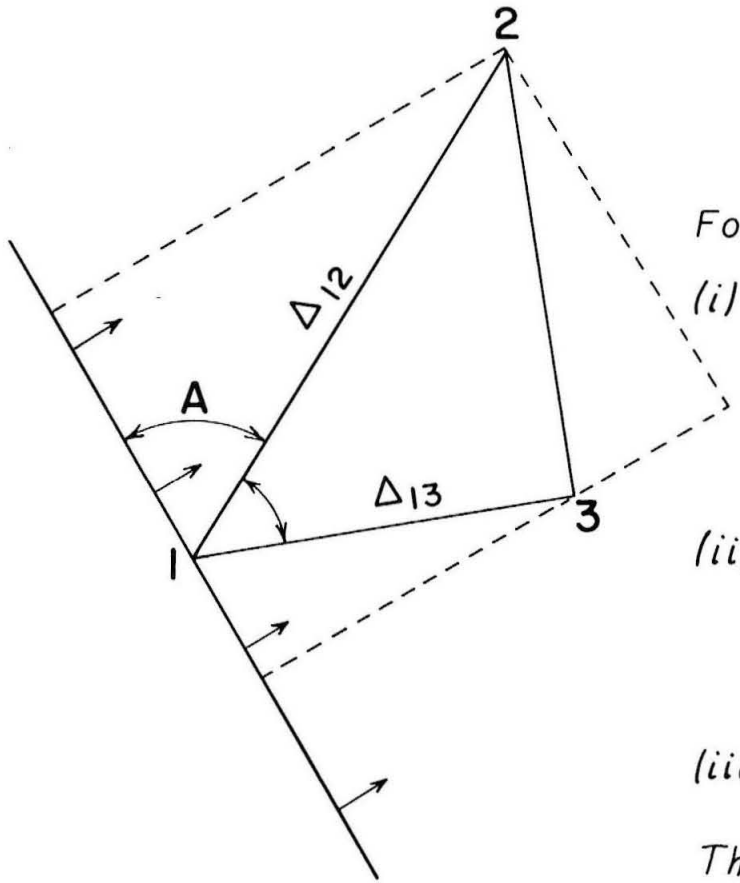


## PRESS' TRIPARTITE METHOD

For the $k^{th}$ peak across the array

(i) $$C_k = \frac{\Delta_{12} \sin A_k}{{}_k\tau_{12}} = \frac{\Delta_{13} \sin (A_k + \alpha)}{{}_k\tau_{13}}$$

${}_k\tau_{ij}$ = travel time from $i^{th}$ to $j^{th}$ station

(ii) $$A_k = \tan^{-1}\left[\frac{\sin\alpha}{\frac{{}_k\tau_{12}\,\Delta_{13}}{{}_k\tau_{13}\,\Delta_{12}} - \cos\alpha}\right]$$

(iii) Average period = $\overline{T}_k = \sum_{j=1}^{3} T_{kj} / 3$

Then from (i), (ii), and (iii)

Phase Velocity = $C_k = C(\overline{T}_k)$

Direction of Propagation = $A_k = A(\overline{T}_k)$

Fig. 33

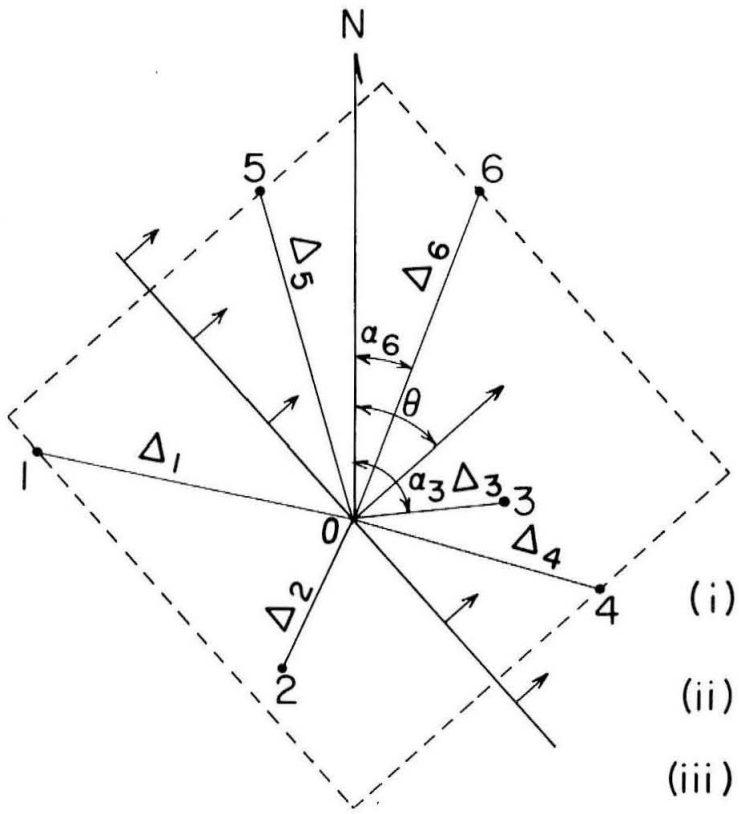


## LEAST SQUARES METHOD

For $k^{th}$ peak at $i^{th}$ station

$$\tau_{ik} = \Delta_i \cos\alpha_i \frac{\cos\theta_k}{C_k} + \Delta_i \sin\alpha_i \frac{\sin\theta_k}{C_k} + \tau_{ok}$$

$$= a_i x_k + b_i y_k + c_i z_k$$

where $x_k = \frac{\cos\theta_k}{C_k}, y_k = \frac{\sin\theta_k}{C_k}, z_k = \tau_{ok}$

$a_i$, $b_i$, $c_i$, $\tau_{ik}$ are known

Find $x_k, y_k, z_k$ by least squares

Then

(i) $C_k = (x_k^2 + y_k^2)^{-1} \pm (x_k^2 + y_k^2)^{-\frac{3}{2}} (x_k^2 \sigma_x^2 + y_k^2 \sigma_y^2)^{\frac{1}{2}}$

(ii) $\theta_k = \tan^{-1}\left(\frac{y_k}{x_k}\right) \pm (x_k^2 + y_k^2)^{-1} (y_k^2 \sigma_x^2 + x_k^2 \sigma_y^2)^{\frac{1}{2}}$

(iii) $\bar{T}_k = \sum_{i=1}^{N} T_{ik}/N$ = Average Period

So (i), (ii), (iii) give:

Phase Velocity = $C_k = C(\bar{T}_k)$

Direction of Propagation = $\theta_k = \theta(\bar{T}_k)$

Predicted Arrival Time at O = $\tau_{ok}$

Fig. 34

# FOURIER TRANSFORM TRIPARTITE METHOD

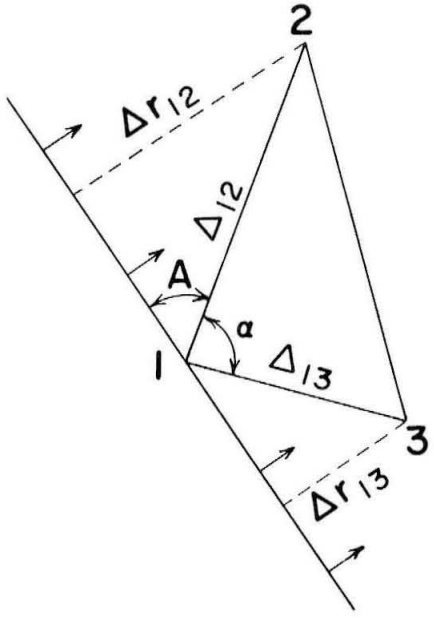


$$C = \frac{\Delta r_{12}}{\tau_{12} + T(\Delta\phi_{12} \pm m)} = F'_{12}$$

$$= \frac{\Delta r_{13}}{\tau_{13} + T(\Delta\phi_{13} \pm n)} = F_{13}$$

Choose pairs $(m,n)_i$ such that $F_{12} - F_{13} \leq \epsilon$

Then use TRIPARTITE METHOD:

$$A_i(T) = \tan^{-1}\left[\frac{\sin \alpha}{\frac{\Delta_{12}(\tau_{13} + T(\Delta\phi_{13} \pm n_i))}{\Delta_{13}(\tau_{12} + T(\Delta\phi_{12} \pm m_i))} - \cos\alpha}\right]$$

$$C_i(T) = \frac{\Delta_{12} \sin A_i(T)}{\tau_{12} + T(\Delta\phi_{12} \pm m_i)} = \frac{\Delta_{13} \sin (A_i(T) + \alpha)}{\tau_{13} + T(\Delta\phi_{13} \pm n_i)}$$

Consider only the Phase Velocities, $C_i(T)$, for which $A_i(T) - \frac{\pi}{2}$ agrees with the azimuth from the center of the array to the source

*Fig. 35*

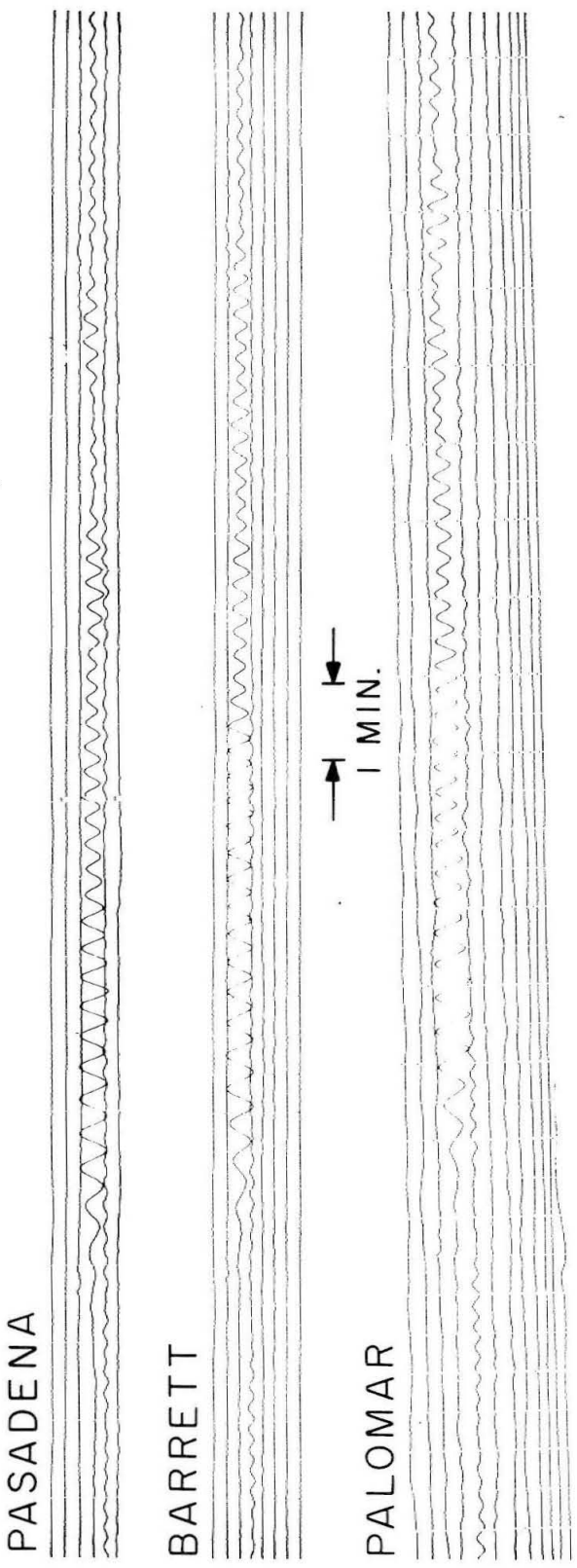


Fig. 36

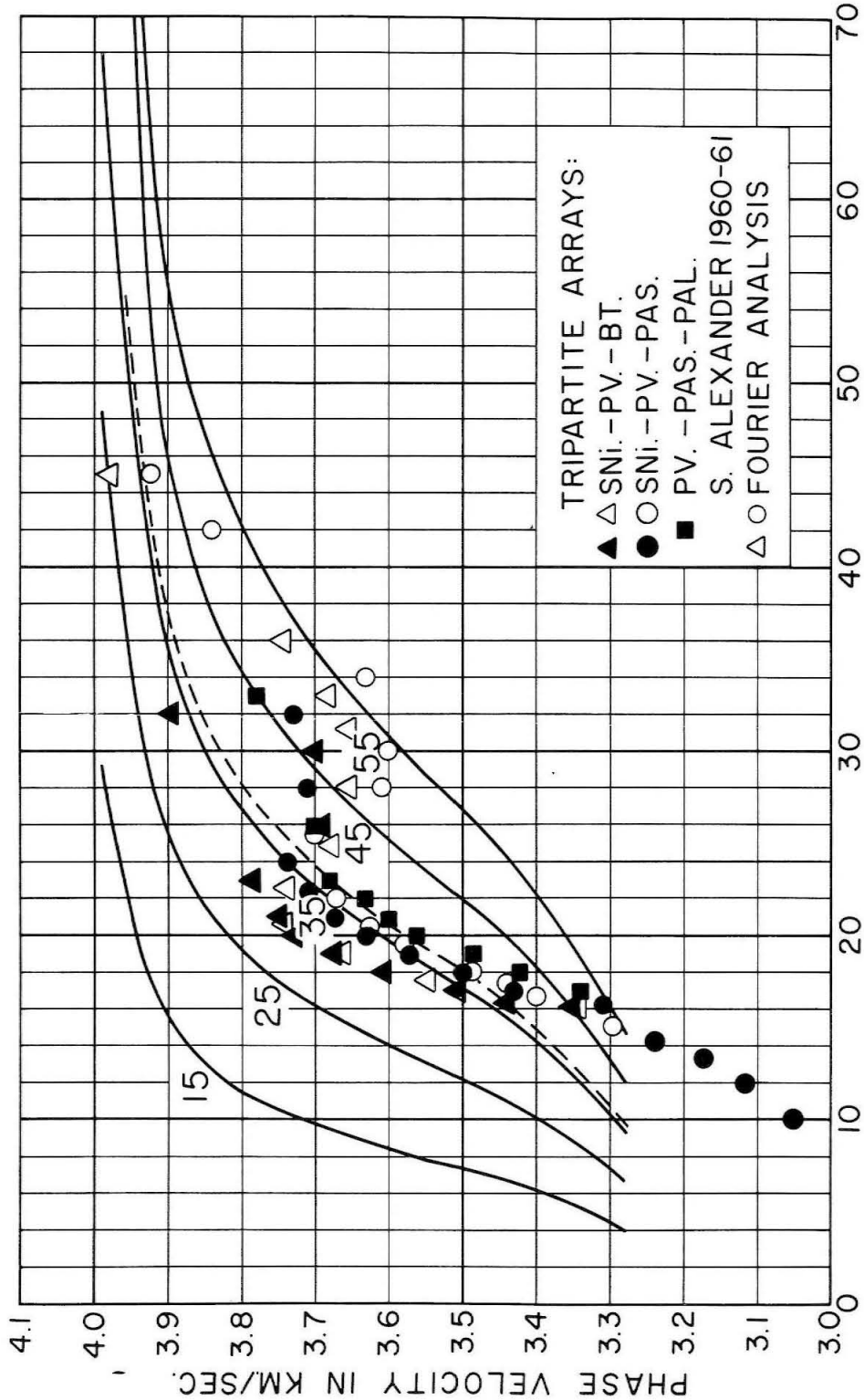


PHASE VELOCITY VS. PERIOD FOR COASTAL REGION OF SOUTHERN-CALIFORNIA

Fig. 37

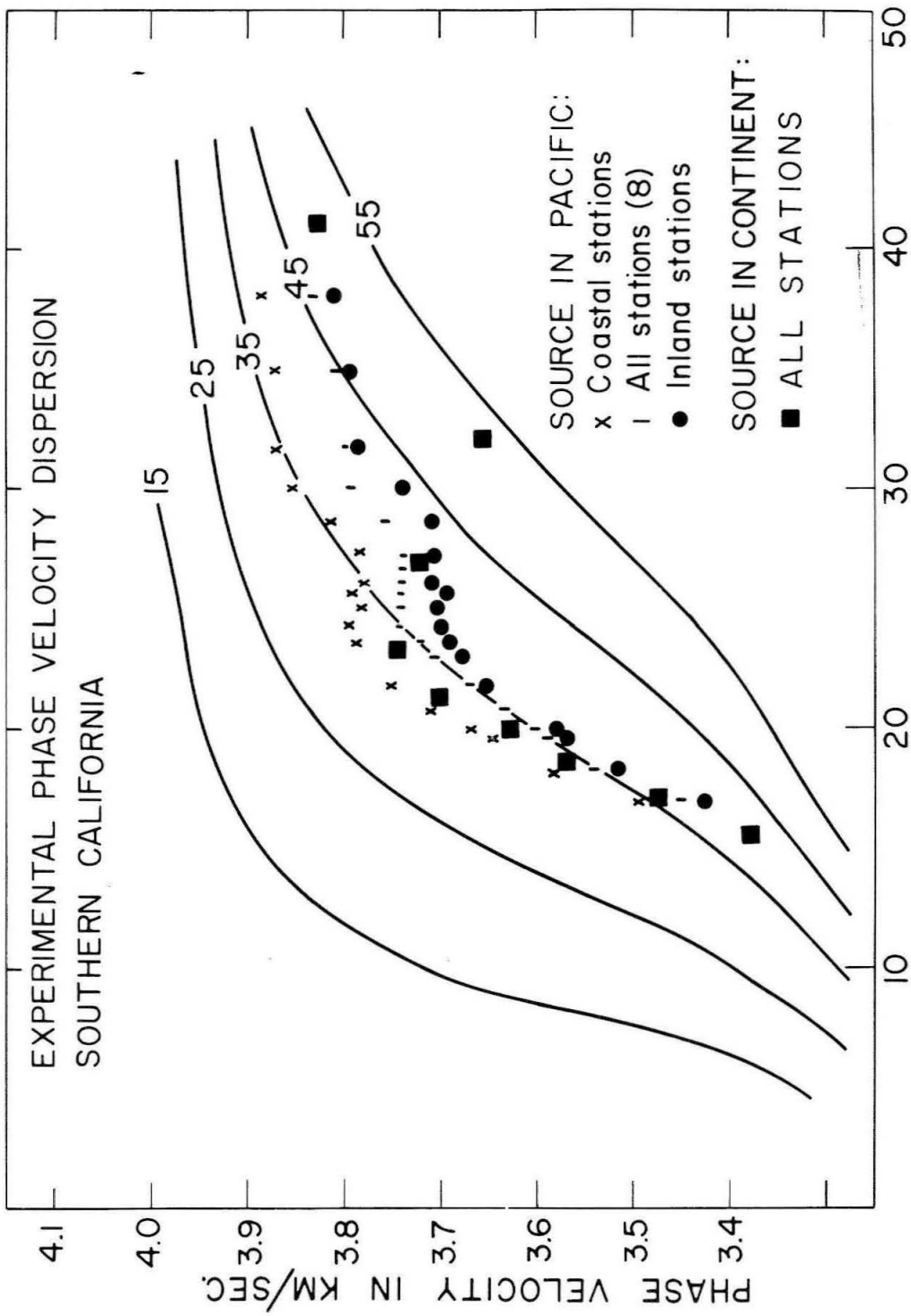
EXPERIMENTAL PHASE VELOCITY DISPERSION
SOUTHERN CALIFORNIA
15
25
35
45
55
SOURCE IN PACIFIC:
x Coastal stations
I All stations (8)
● Inland stations
SOURCE IN CONTINENT:
■ ALL STATIONS
PHASE VELOCITY IN KM/SEC.
4.1
4.0
3.9
3.8
3.7
3.6
3.5
3.4
10
20
30
40
50
PERIOD IN SECONDS

Fig. 38

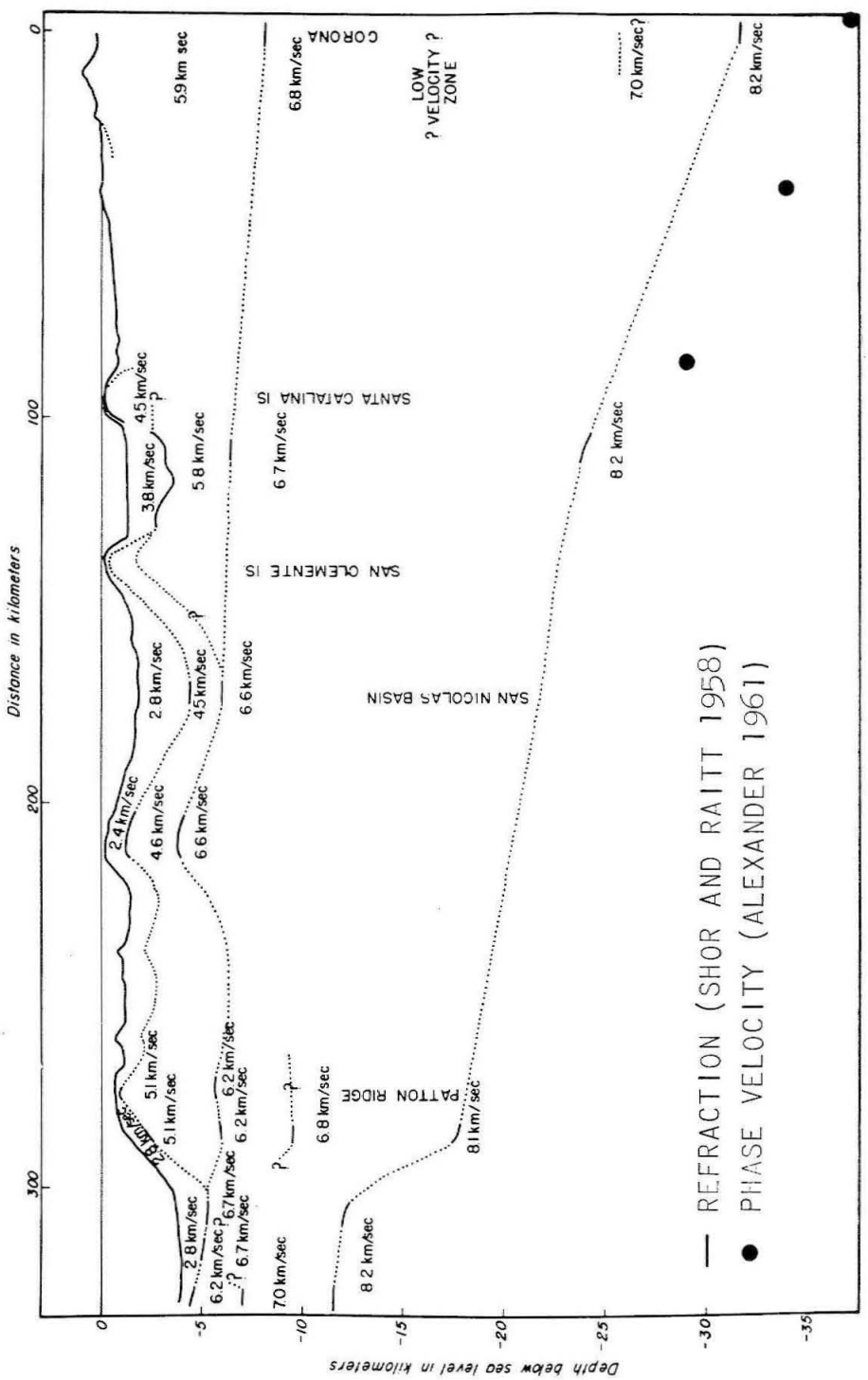


STRUCTURAL SECTION FROM THE PACIFIC OCEAN BASIN (LEFT) TO PENINSULAR RANGES (RIGHT). DOTTED LINES INDICATE AREAS WHERE DATA ARE LACKING.

Fig. 39

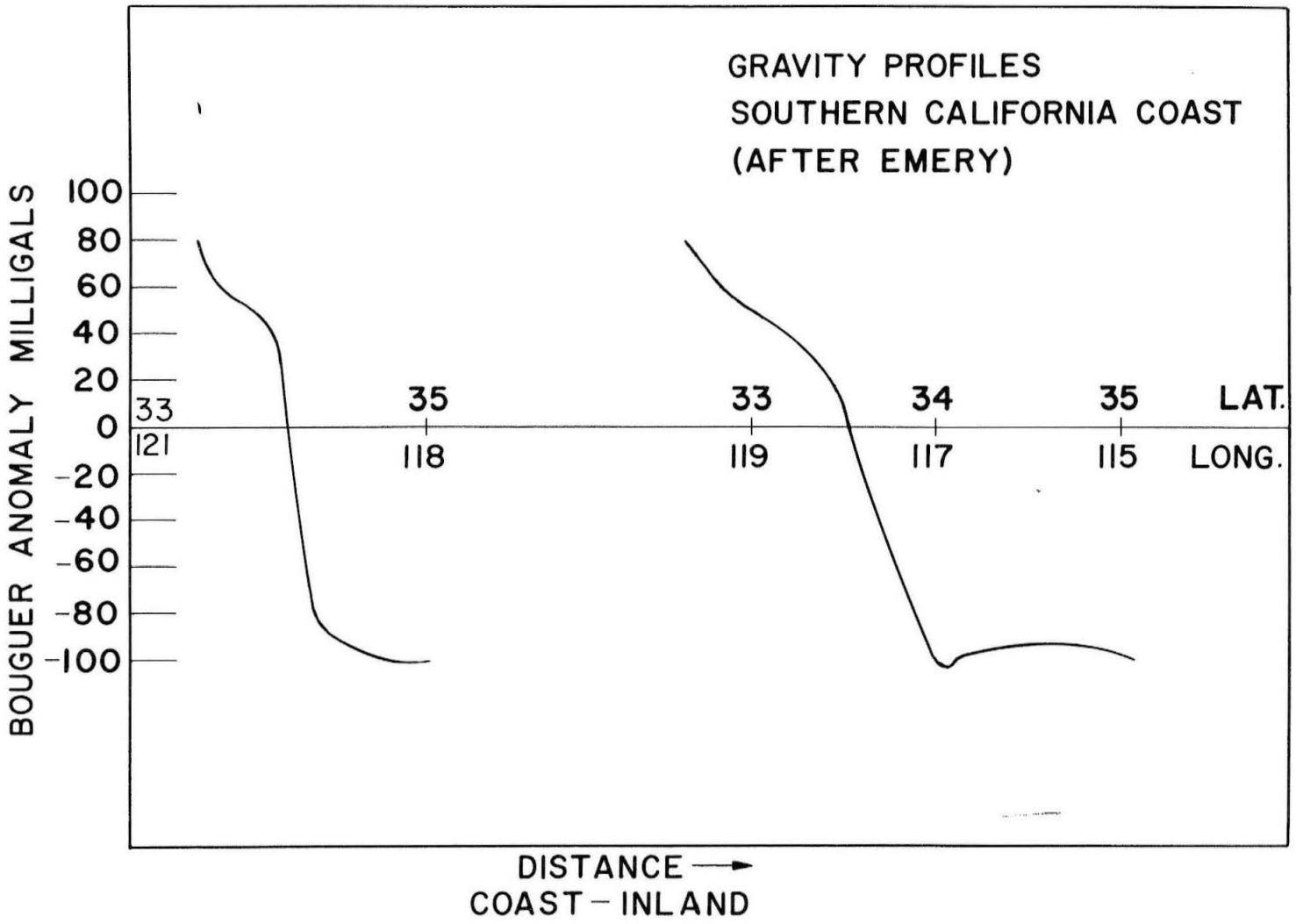
GRAVITY PROFILES
SOUTHERN CALIFORNIA COAST
(AFTER EMERY)
BOUGUER ANOMALY MILLIGALS
100
80
60
40
20
0
-20
-40
-60
-80
-100
33
121
35
118
33
119
34
117
35
115
LAT.
LONG.
DISTANCE →
COAST – INLAND

Fig. 40

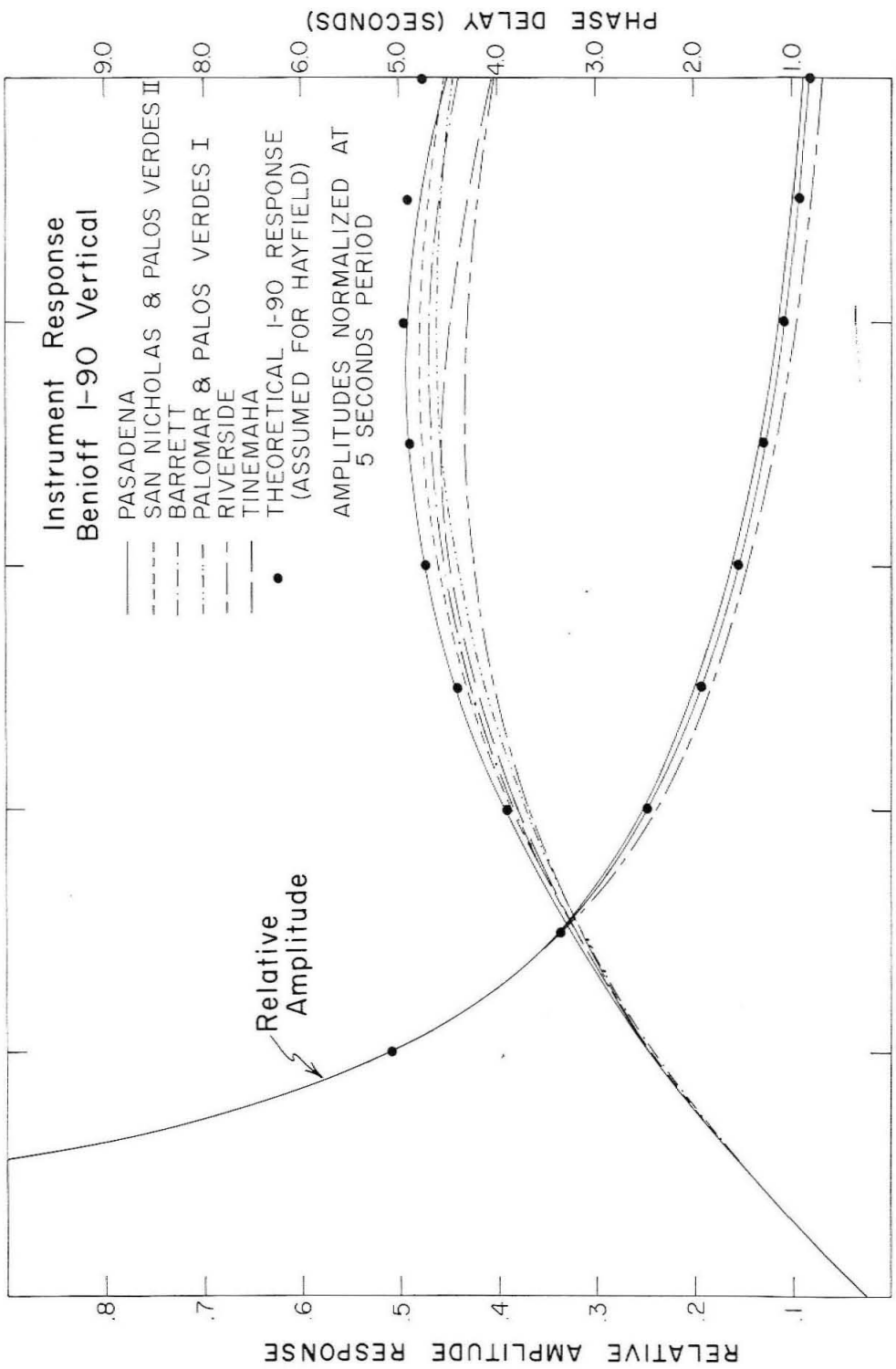
Instrument Response
Benioff I-90 Vertical
PASADENA
SAN NICHOLAS & PALOS VERDES II
BARRETT
PALOMAR & PALOS VERDES I
RIVERSIDE
TINEMAHA
THEORETICAL I-90 RESPONSE
(ASSUMED FOR HAYFIELD)
AMPLITUDES NORMALIZED AT
5 SECONDS PERIOD
Relative
Amplitude
RELATIVE AMPLITUDE RESPONSE
PHASE DELAY (SECONDS)
Period (sec)
0
10
20
30
40
50
.1
.2
.3
.4
.5
.6
.7
.8
1.0
2.0
3.0
4.0
5.0
6.0
8.0
9.0

Fig.41

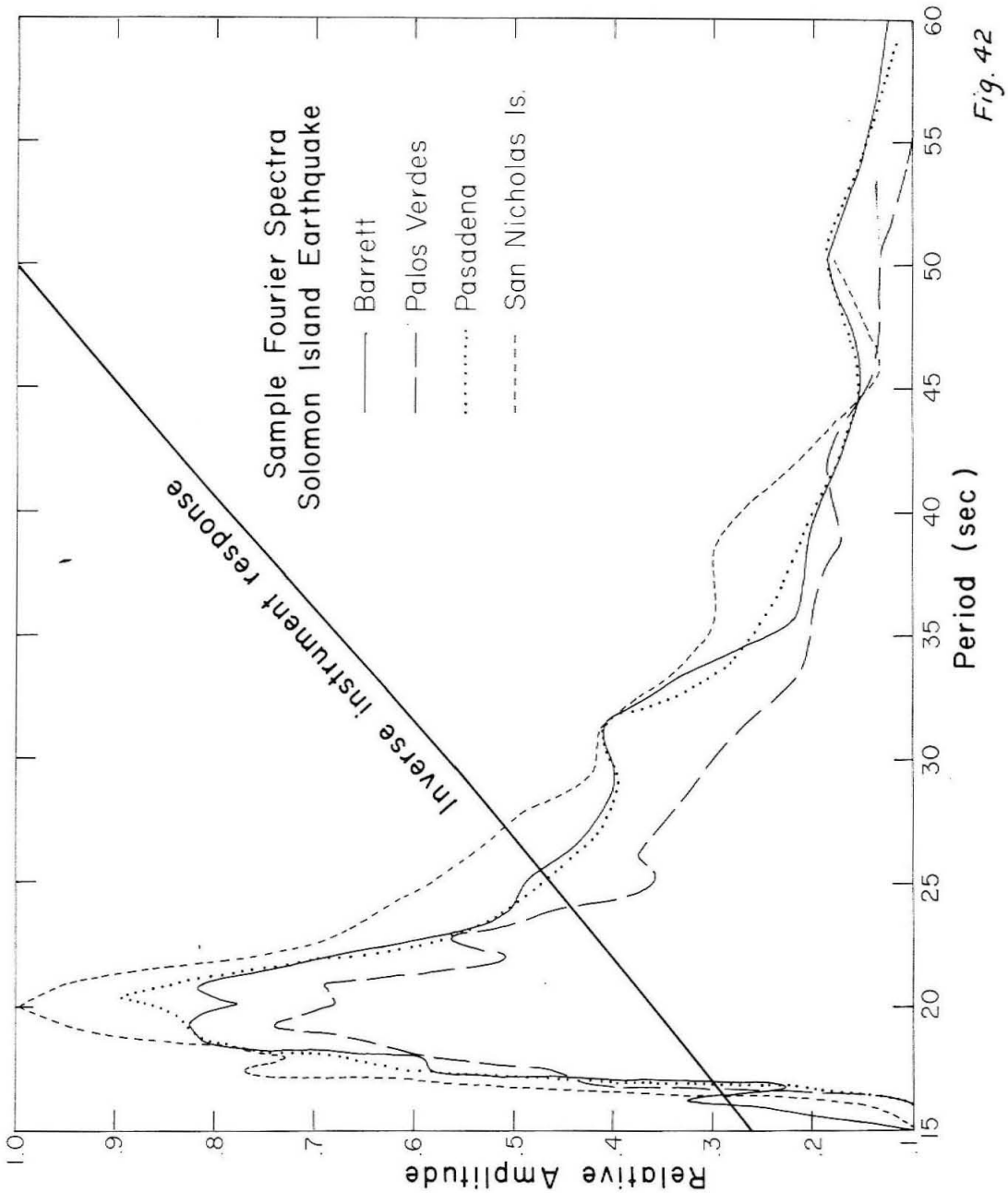
Sample Fourier Spectra
Solomon Island Earthquake
Barrett
Palos Verdes
Pasadena
San Nicholas Is.
Inverse Instrument response
Relative Amplitude
Period (sec)
1.0
.9
.8
.7
.6
.5
.4
.3
.2
.1
15
20
25
30
35
40
45
50
55
60

Fig. 42

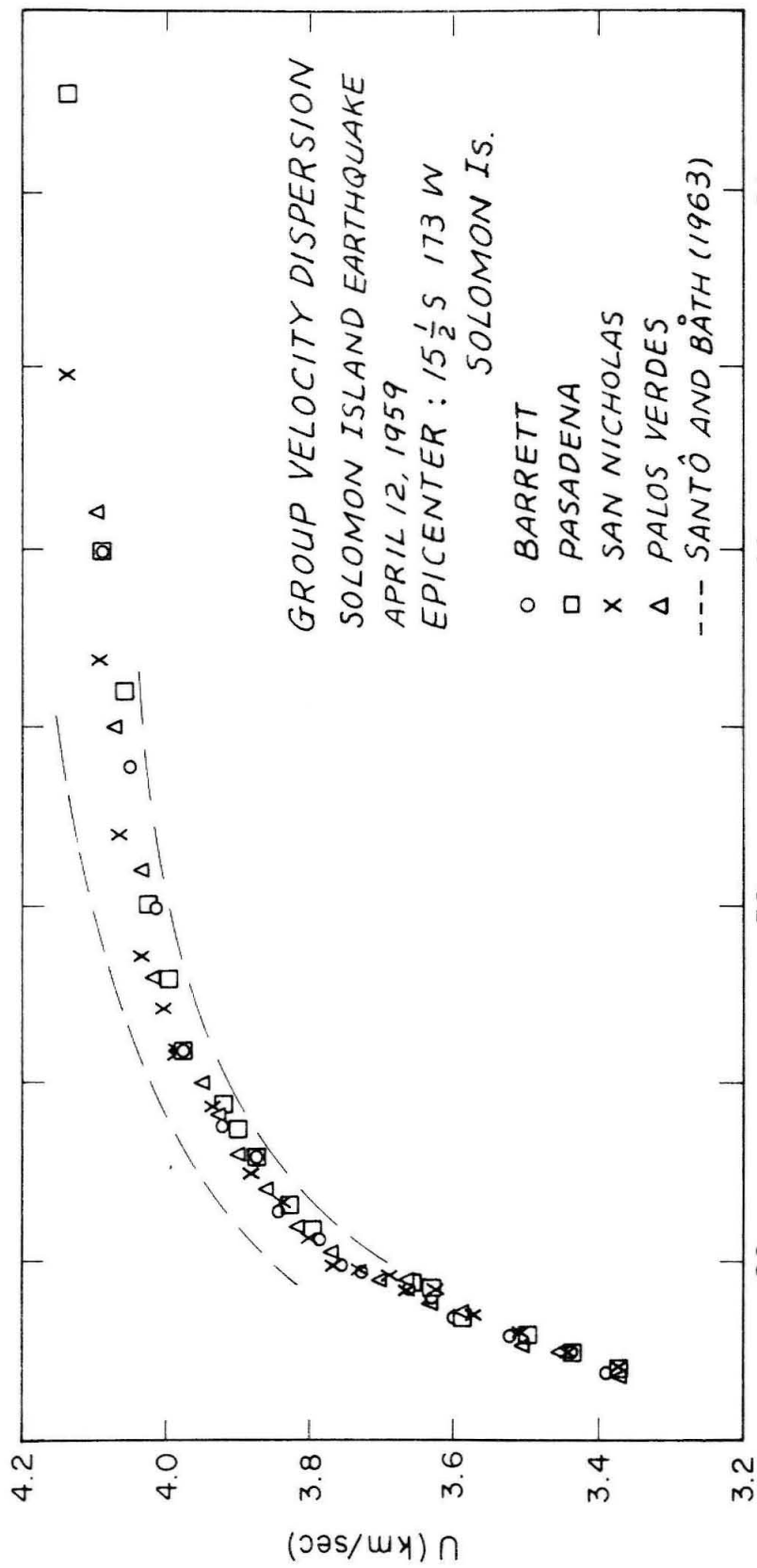
GROUP VELOCITY DISPERSION
SOLOMON ISLAND EARTHQUAKE
APRIL 12, 1959
EPICENTER : 15½ S 173 W
SOLOMON Is.
○ BARRETT
□ PASADENA
× SAN NICHOLAS
△ PALOS VERDES
--- SANTÔ AND BÅTH (1963)
C (km/sec)
PERIOD (sec)
4.2
4.0
3.8
3.6
3.4
3.2
20
30
40
50

Fig. 43

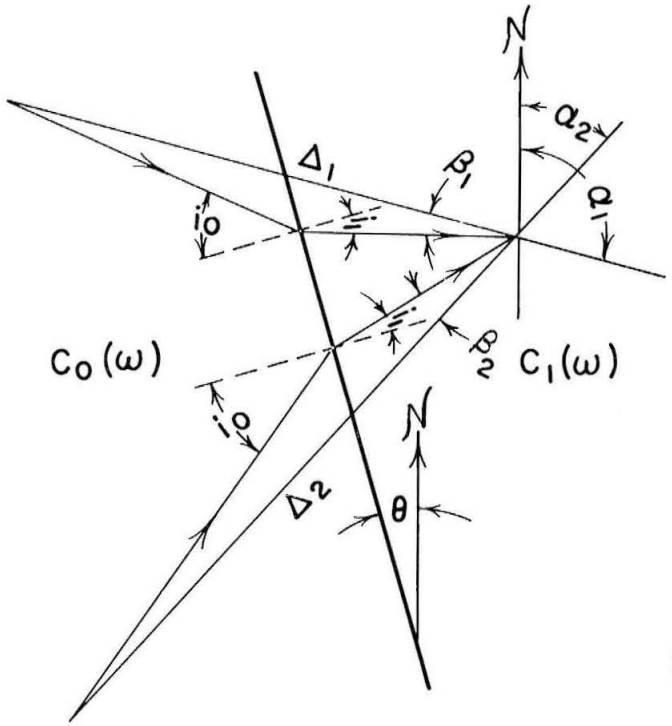


STRIKE OF LINEAR FEATURES

PLOT $\alpha_i(\omega)$ vs $\beta_i(\omega)$ FOR N EVENTS ACROSS THE ARRAY.

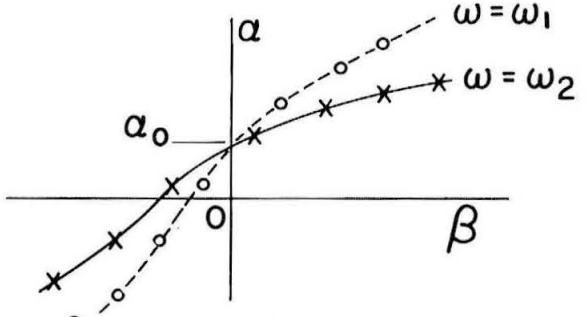


SO, $\theta = \alpha_0 - \pi/2$ STRIKE

NOW $C_1/C_0 = \text{SIN}\, i_1 / \text{SIN}\, i_0$

KNOWING $\theta$ OBTAIN $i_1$; THEN

$C_0(\omega) \geq C_1(\omega) \text{SIN}\, i_1(\omega) / \text{COS}(\alpha - \theta)$

GIVES A LOWER BOUND FOR $C_0(\omega)$.

*Fig. 44*

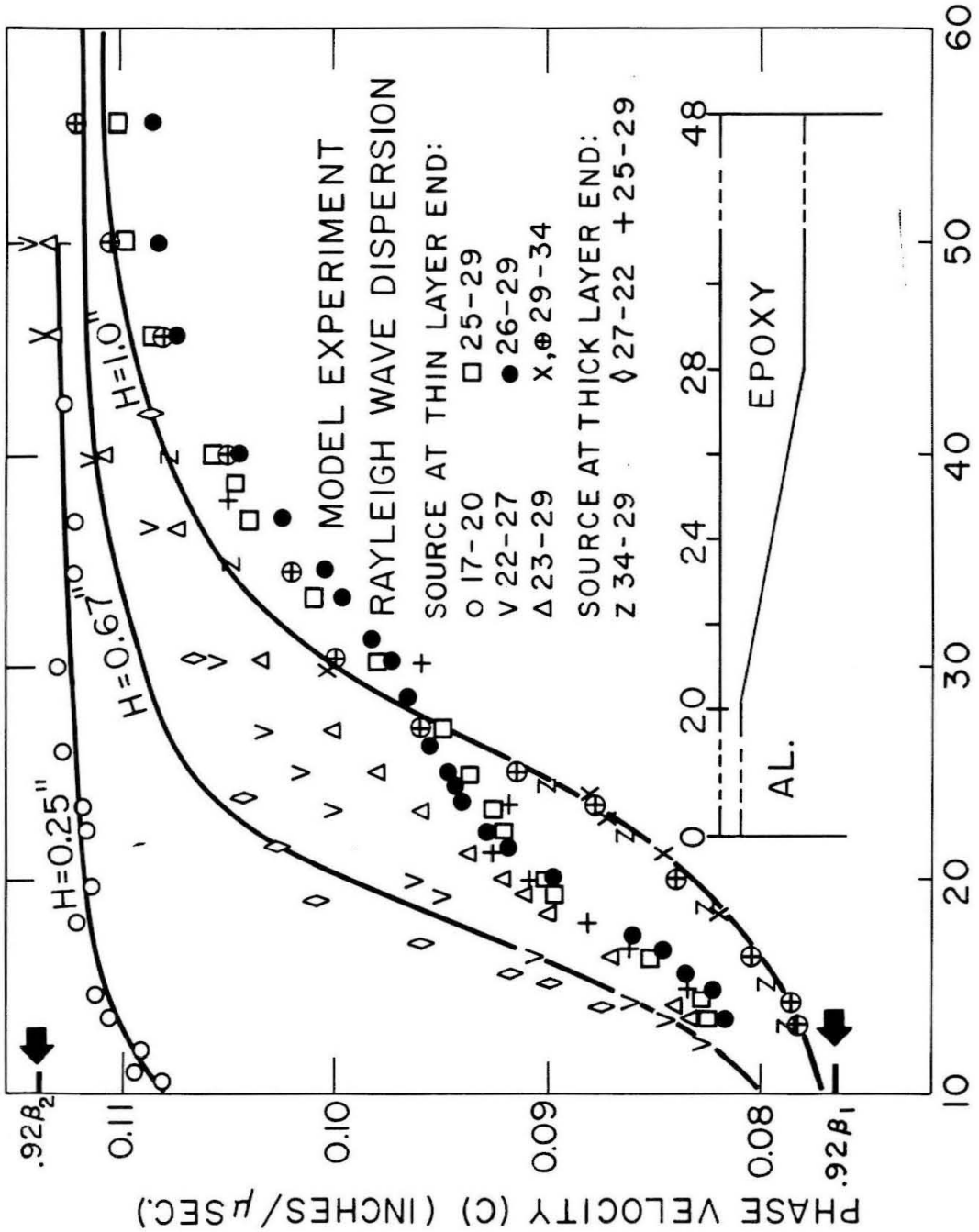
PHASE VELOCITY (C) (INCHES/μSEC.)
PERIOD IN μSEC.
.92β2
.92β1
0.11
0.10
0.09
0.08
10
20
30
40
50
60
H=0.25"
H=0.67"
H=1.0"
MODEL EXPERIMENT
RAYLEIGH WAVE DISPERSION
SOURCE AT THIN LAYER END:
○ 17-20
□ 25-29
▽ 22-27
● 26-29
Δ 23-29
x,⊕ 29-34
SOURCE AT THICK LAYER END:
Z 34-29
◊ 27-22
+ 25-29
EPOXY
AL.
0
20
24
28
48

Fig. 45

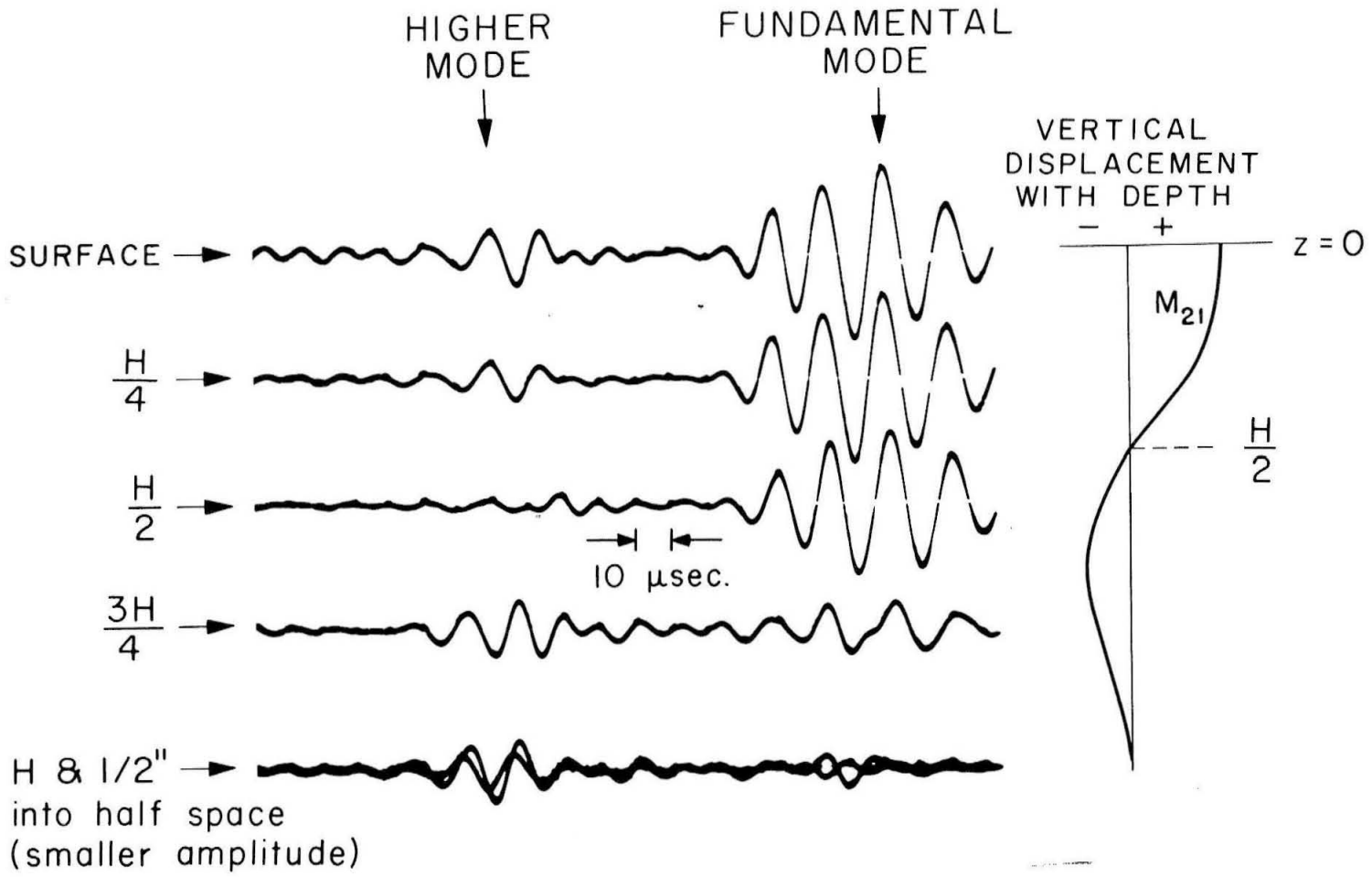


VERTICAL COMPONENT WITH DEPTH AT Sta. 27

Fig. 46

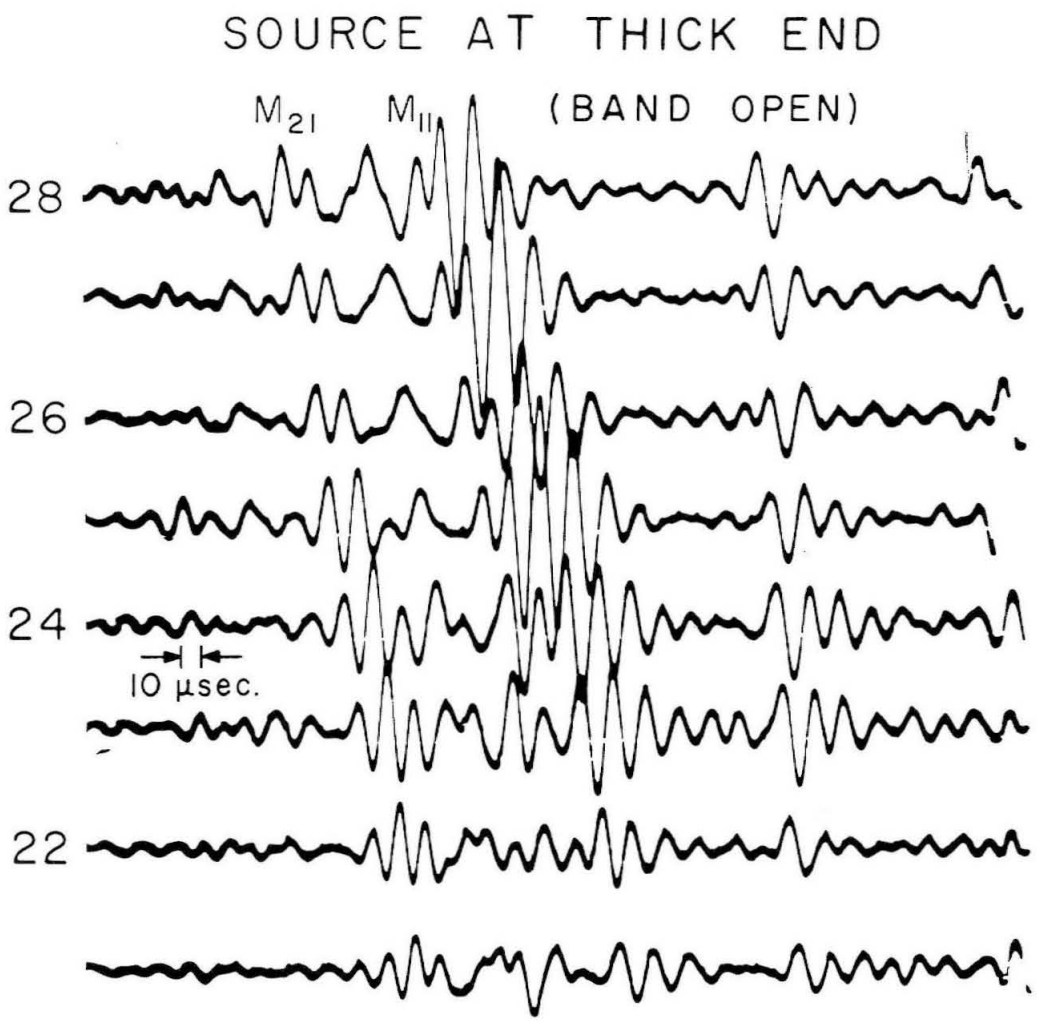


Fig. 47

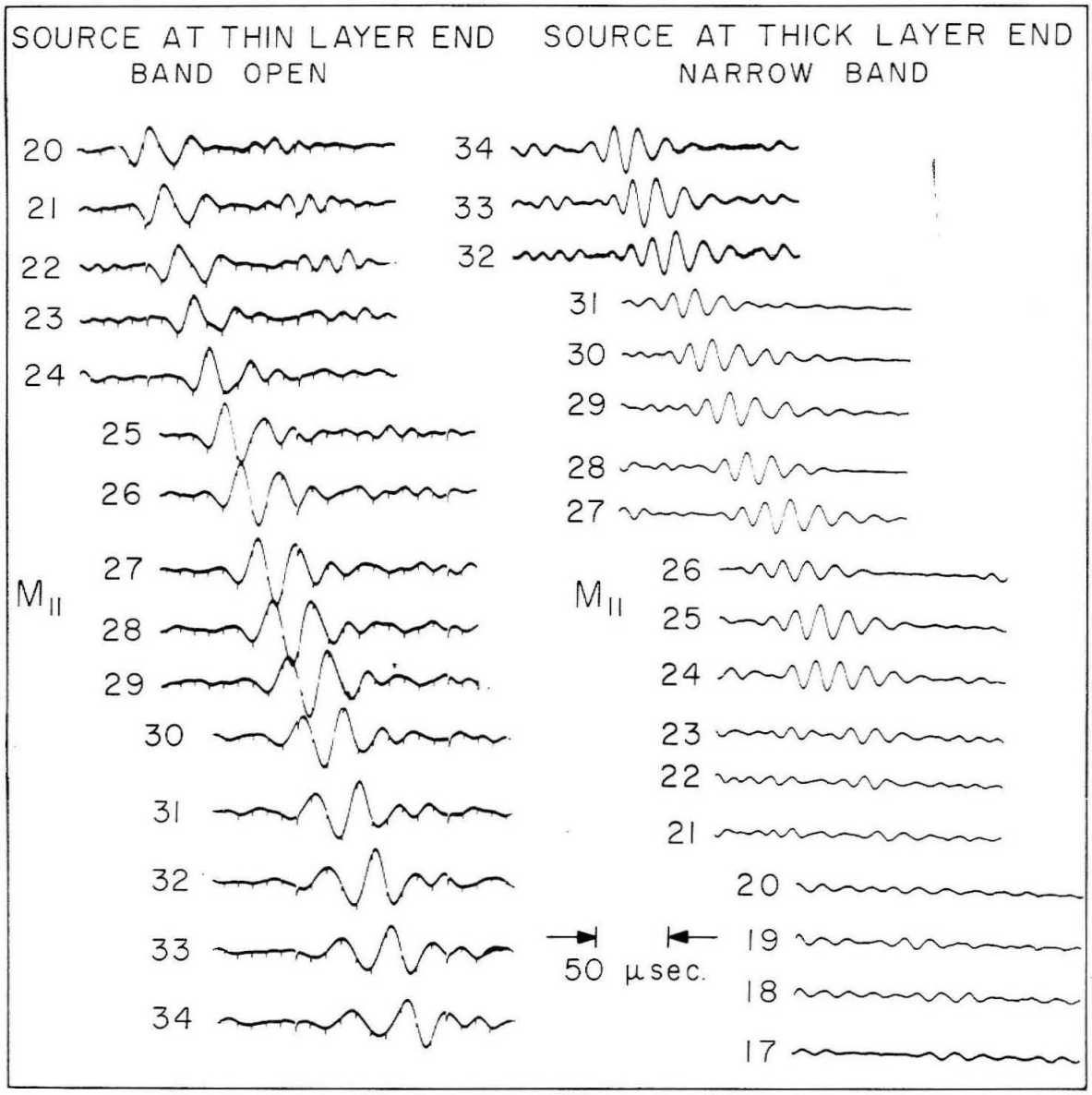
SOURCE AT THIN LAYER END
BAND OPEN
SOURCE AT THICK LAYER END
NARROW BAND
20
21
22
23
24
25
26
27
28
29
30
31
32
33
34
$M_{II}$
34
33
32
31
30
29
28
27
26
25
24
23
22
21
20
19
18
17
$M_{II}$
50 μsec.

Fig. 48